CHAPTER 32

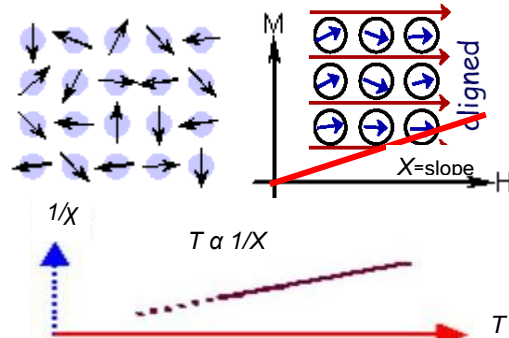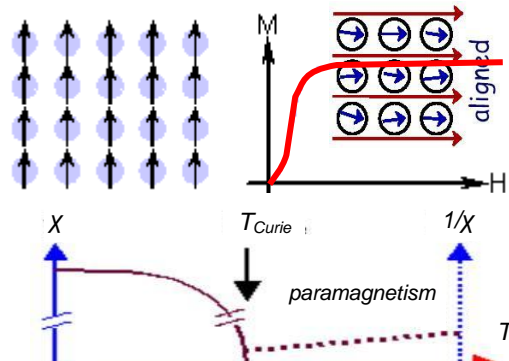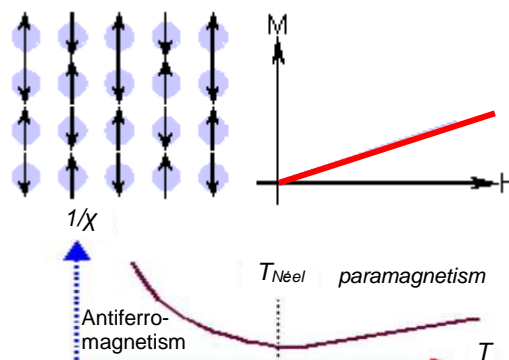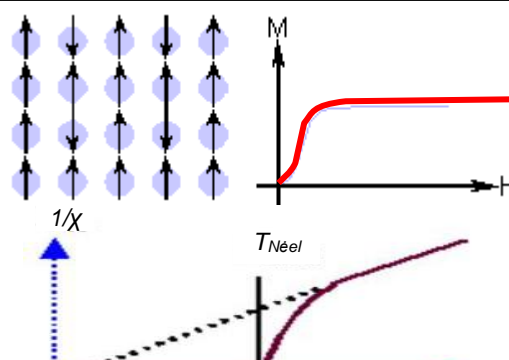# Hard Magnetic Materials - Permanent Magnets

All materials can be classified in terms of their magnetic behaviour, falling into one of five categories depending on their bulk magnetic susceptibility (permeability). The two most common types of magnetism are diamagnetism and paramagnetism, which account for the magnetic properties of most of the periodic table of elements at room temperature, as indicated in figure 32.1. The diamagnetic elements are usually referred to as non-magnetic, while those that are referred to as magnetic are classified as ferromagnetic. The only other type of magnetism observed in pure elements at room temperature is antiferromagnetism, as with Cr. Magnetic materials (as opposed to elements) can also be classified as ferrimagnetic although this is not observed in any pure element but is found in compounds, such as the mixed oxides, known as ferrites, from which ferrimagnetism derives its name. Magnetic susceptible falls into a particular range of values for each of the five material types as shown in Table 32.1, with some examples, with the five categories shown in figure 32.2.

Figure 32.1. *Periodic table, classifying the type of magnetic behaviour of each element at room temperature.*

Table 32.1. Magnetic behaviour of five different types of materials ($\mu_r = \chi + 1$, $B = \mu_o(H+M) = (1+\chi)\mu_o H = \mu_r \mu_o H$)

Type of Magnetism	Susceptibility	Atomic (*H*=0) / Magnetic Behaviour *M(H)*		Example/ Susceptibility *χ*	
Diamagnetism	Small and negative $\chi < 0$ M= χ H No temperature dependence	Atoms have no magnetic moment		Bi Au Cu H_2O SiO_2 $CaCO_3$ Super Con-ductor	-166 x10⁻⁶ -34.7x10⁻⁶ -9.63x10⁻⁶ -9.2x10⁻⁶ -6.2x10⁻⁶ -4.8x10⁻⁶ ≈10⁵
Paramagnetism	Small and positive 1 » χ > 0 M= χ H $1/\chi$(T) linear (weak)	Atoms have randomly oriented magnetic moments		Aℓ β-Sn Pt Mn Air O_2	21.1x10⁻⁶ 22.7x10⁻⁶ 257x10⁻⁶ 904x10⁻⁶ 0.36x10⁻⁶ 2.1x10⁻⁶
Ferromagnetism	Large and positive, function of applied field, microstructure dependent χ >0, |χ| » 1	Atoms have parallel aligned magnetic moments		Fe Ni Co SiFe	~80,000 7x10⁴
Antiferromagnetism	Small and positive χ >0	Atoms have mixed parallel and anti-parallel aligned magnetic moments		Cr FeMn NiO MnO	318x10⁻⁶
Ferrimagnetism	Large and positive, function of applied field, microstructure dependent χ » 1	Atoms have anti-parallel aligned magnetic moments		Ba-ferrite Fe_3O_4	~3000 100

i. Diamagnetism

Diamagnetic metals have a weak, negative susceptibility to magnetic fields. In a diamagnetic material, there are no unpaired electrons and all the orbital shells are filled, hence no net magnetic moment. The intrinsic electron magnetic moments cannot produce any bulk effect, thus magnetization arises from electron orbital motion. Under the influence of an applied field, H, the spinning electrons precess and this motion, which is a type of electric current, produces a weak internal magnetisation, $M (=\chi H = (\mu_r - 1) \times H = J / \mu_o)$, that opposes the externally applied magnetic field, thus causing a repulsive effect. The cause of this interaction is in accordance with Lenz's Law by which small, localized currents generated in the material created magnetic fields in opposition to the applied changing field. All materials have a diamagnetic effect, which is often masked by a larger paramagnetic or ferromagnetic component. Although diamagnetism is generally a weak effect in most materials, superconductors exhibit a strong effect, thus repel magnetic fields from their bulk. The dimensionless volumetric susceptibility value χ ($\mu_r = \chi + 1$) is independent of temperature.

Most elements in the periodic table, including copper, silver, gold, and helium are diamagnetic. The strongest diamagnetic elements are bismuth and carbon graphite, as highlighted in Table 32.1.
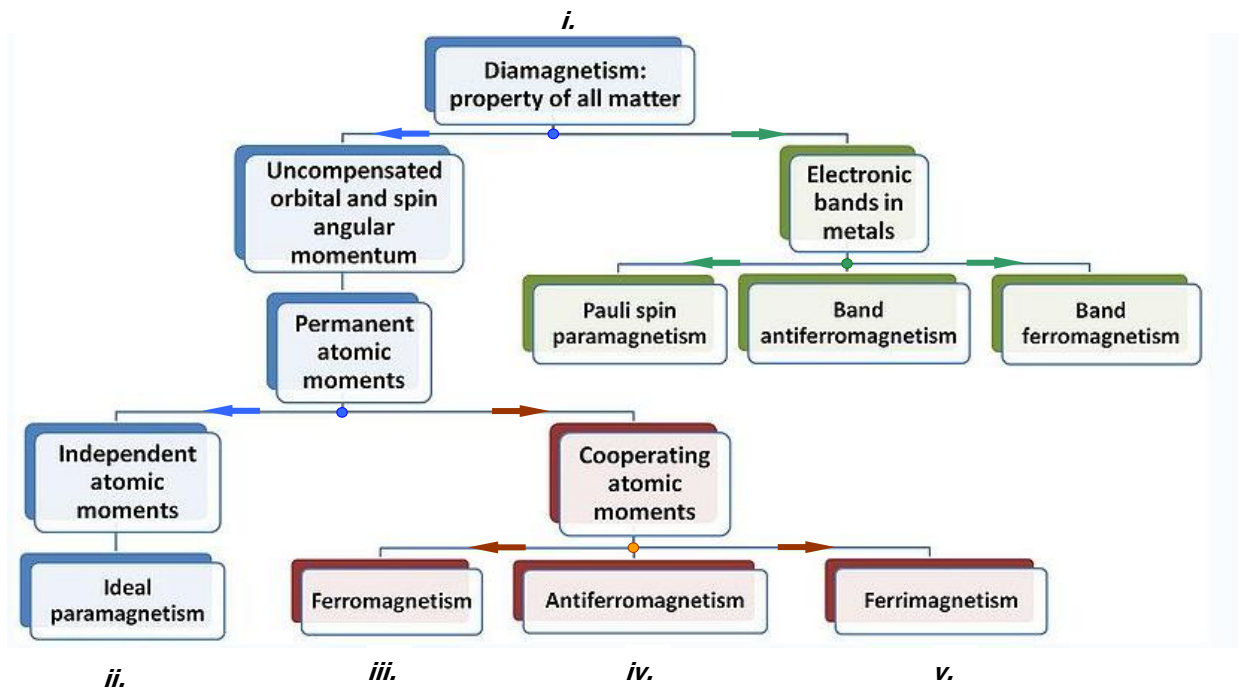

Figure 32.2. *Types of natural magnetism.*

ii. Paramagnetism

Paramagnetic metals have a small, positive susceptibility to magnetic fields. They become magnetized in the same direction as the applied magnetic field and the magnetization magnitude is proportional to the applied magnetic field. In a paramagnetic material there are unpaired electrons, specifically, atomic or molecular orbitals with exactly one electron in them. While paired electrons are required by the Pauli exclusion principle to have their intrinsic (spin) magnetic moments pointing in opposite directions, causing their magnetic fields to cancel out, an unpaired electron is free to align its magnetic moment in any direction. When an external magnetic field, H, is applied, these magnetic moments tend to align in the same direction as the applied field, thus reinforcing it.

Paramagnetic materials are attracted to magnetic fields, hence have a relative magnetic permeability slightly greater than one (that is, a positive magnetic susceptibility, $\chi > 0$). The force of attraction generated by the applied field is linear and weak. Unlike ferromagnets, paramagnets do not retain any magnetization in the absence of an externally applied magnetic field, because thermal motion causes the spins to return to a random orientation. Thus the total magnetization decreases to zero when the applied field is removed. Even in the presence of a H field, the induced magnetization is small because only a small fraction of the spins are oriented by the field. This small fraction is linearly proportional to the field strength, H.

The randomly oriented moments result from thermal agitation. A magnetic field slightly aligns these moments whence low magnetisation results, aligned with the applied field. As the temperature increases, the thermal agitation increases and it becomes harder to align the atomic magnetic moments, hence the magnetic susceptibility, χ, decreases. This behaviour is known as the *Curie law*, as shown in equation (32.1), where C is a material-specific constant called the Curie constant.

$$M = H \times \chi = H \times \frac{C}{T} \qquad \left(= H \times (\mu_r - 1) \right) \tag{32.1}$$

M is the resultant magnetism (with reference to the permeability of a vacuum), *T* is absolute temperature, K, and *H* is the externally produced magnetic field, A/m.

This law indicates that the susceptibility χ of paramagnetic materials is inversely proportional to temperature. Curie's law is only valid under low magnetisation conditions, since it does not consider magnetisation saturation that occurs when the atomic dipoles are all aligned in parallel. After complete alignment, increasing the external field will not increase the total magnetisation since there can be no further alignment. However, such saturation typically requires extremely strong magnetic fields.

The Curie law is a special case of the more general Curie-Weiss law, equation (32.2), which incorporates a temperature constant, T_C, and derives from Weiss theory, proposed for ferromagnetic materials, that incorporates the interaction between magnetic moments.

$$\chi = \frac{C}{T - T_C} \tag{32.2}$$

In equation (32.2), T_C, in degrees Kelvin, K, can be positive, negative or zero. When $T_C = 0$, the Curie-Weiss law equates to the Curie law. A non-zero T_C indicates that there is interaction between neighbouring magnetic moments and the material is only paramagnetic above a certain transition temperature. If T_C is positive then the material is ferromagnetic below the transition temperature and the value of T_C corresponds to the transition temperature, the Curie temperature, T_C. If T_C is negative then the material is antiferromagnetic below the transition temperature, the Néel temperature, T_N, however the value of T_C does not relate to T_N. Equation (32.2) is only valid for a paramagnetic material state and is not valid for many metals, as the electrons contributing to the magnetic moment are not localised. However, the law does apply to some metals, for example, the rare-earth elements shown in figure 32.1, where the 4f electrons, that create the magnetic moment, are closely bound.
Paramagnetic materials include magnesium, molybdenum, lithium, sodium, and tantalum. Paramagnetic materials like aluminium, uranium, and platinum become more magnetic when they are very cold.

iii. Ferromagnetism
Ferromagnetic materials have a large positive susceptibility to an external magnetic field. Ferromagnetism is the term for the basic mechanism by which specific materials (such as iron) form permanent magnets and/or exhibit strong magnetic interaction with magnets.
A paramagnetic substance has unpaired electrons, but additionally ferromagnetism is only possible when atoms are arranged in a lattice and the atomic magnetic moments can interact to align parallel to each other. The effect is due to the presence of a molecular field within the ferromagnetic material, which is sufficient to magnetise the material to saturation, $H = \lambda M$. This creates a net internal magnetic field much greater than the applied field. Even when the applied external field is removed, the electrons in the material maintain each other orientated in the same direction.
Magnetic domains within the material are the regions of atomic magnetic moments that are aligned. The movement of these domains determines how the material responds to a magnetic field and consequently the susceptible is a function of the applied magnetic field. Therefore, ferromagnetic materials are usually compared in terms of saturation magnetisation (magnetisation when all domains are aligned) rather than susceptibility.
In the elemental periodic table, only the three consecutive elements Fe, Co and Ni are ferromagnetic at and above room temperature. As ferromagnetic materials are heated, thermal agitation of the atoms decreases the degree of alignment of the atomic magnetic moments, hence saturation magnetisation decreases. Eventually the thermally agitated disorder overwhelms the energy lowering due to ferromagnetic order and the material becomes paramagnetic; the temperature of this critical transition is the Curie temperature, T_C (Fe: $T_C = 770°C$, Co: $T_C = 1131°C$, and Ni: $T_C = 358°C$). Above T_C, susceptibility varies according to equation (32.2).

iv. Antiferromagnetism
Antiferromagnetic materials are similar to ferromagnetic materials but the exchange interaction between valance electrons of neighbouring atoms leads to the anti-parallel alignment (as opposed to parallel alignment) of the atomic magnetic moments. Therefore the magnetic field cancels out and the material appears to behave like a paramagnetic material. It is difficult to magnetize such materials in the direction of the applied field but they still demonstrate a relative permeability slightly greater than 1. The magnetic susceptibility of an antiferromagnetic material is typically a maximum at the Néel temperature. Like ferromagnetic materials, these materials become paramagnetic above a transition temperature, the Néel temperature, T_N, where equation (32.2) is applicable. The Néel temperature is similar to the Curie temperature in ferromagnetism. In the periodic table, the only element exhibiting antiferromagnetism at near room temperature is chromium (Cr: $T_N = 37°C$).
Alloys such as iron manganese (FeMn), and oxides such as nickel oxide (NiO), manganese oxide, and iron oxide (FeO), exhibit antiferromagnetism.
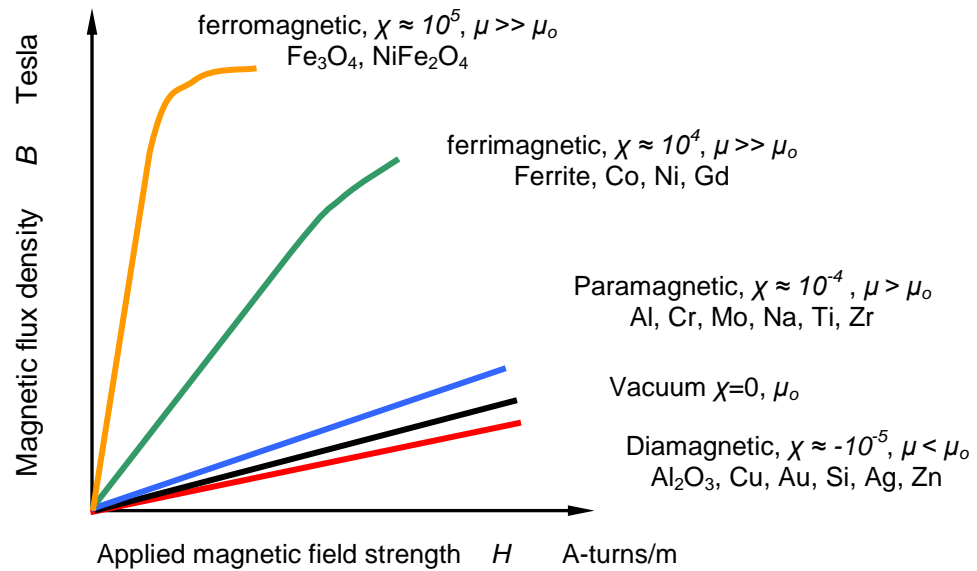
ferromagnetic, $\chi \approx 10^5$, $\mu \gg \mu_o$
Fe_3O_4, $NiFe_2O_4$

ferrimagnetic, $\chi \approx 10^4$, $\mu \gg \mu_o$
Ferrite, Co, Ni, Gd

Paramagnetic, $\chi \approx 10^{-4}$, $\mu > \mu_o$
Al, Cr, Mo, Na, Ti, Zr

Vacuum $\chi = 0$, μ_o

Diamagnetic, $\chi \approx -10^{-5}$, $\mu < \mu_o$
Al_2O_3, Cu, Au, Si, Ag, Zn

Applied magnetic field strength   *H*   A-turns/m

Figure 32.3. *Relative susceptibility χ (= μ_r - 1) of different materials.*

v. Ferrimagnetism

Ferrimagnetism is only observed in compounds that have more complex crystal structures than pure elements. Within such materials, the exchange interactions lead to parallel alignment of atoms in some of the crystal sites and anti-parallel alignment of others. The material devolves into magnetic domains, just like a ferromagnetic material and the magnetic behaviour is also similar, although ferrimagnetic materials usually have lower saturation magnetisations. In an optimal geometrical arrangement, there are more magnetic moments from the sublattices of electrons which point in one direction, than from the sublattices which point in the opposite direction. Both ferrimagnetic and ferromagnetic materials retain spontaneous magnetization below the Curie temperature, and show no magnetic order (are paramagnetic) above this temperature. However, there may be a temperature below the Curie temperature at which the two sub-lattices have equal (but opposite polarity) moments, resulting in a net magnetic moment of zero; this is called the *magnetization compensation point*.
Examples of ferrimagnetic materials are iron oxide (Fe_3O_4) and ferrite - $MO^.Fe_2O_3$.

The different magnetic types are summarised in figure 32.3 in terms of relative susceptibility. There are other types of magnetism, such as spin glass, superparamagnetism, superdiamagnetism, and metamagnetism.

32.1   Magnetic properties

The intrinsic properties of a magnetic material are those properties that are characteristic of the material and are unaffected by the microstructure (for example, grain size or crystal orientation of grains). These properties include Curie temperature, saturation magnetisation, and magneto-crystalline anisotropy.

i. Saturation Magnetisation

Saturation magnetisation, M_S, is a measure of the maximum field that can be generated by a material. It depends on the strength of the dipole moments on the atoms that make up the material and how densely they are packed. The atomic dipole moment is affected by the nature of the atom and the overall electronic structure within the compound. The packing density of the atomic moments is determined by the crystal structure (that is, the spacing of the moments) and the presence of any non-magnetic elements within the structure.
For ferromagnetic materials, M_S also depends on how well the moments are aligned, as thermal vibration of the atoms causes moment misalignment and a reduction in M_S. For ferrimagnetic materials not all of the moments align parallel, even at zero degree Kelvin, hence M_S depends on the relative alignment of the moments as well as the temperature. In the case of a single magnetic domain, its saturation magnetisation is referred to as the spontaneous magnetisation.
Table 32.2 gives examples of the saturation polarisation, J_S, (=$\mu_o M_S$) and Curie temperature, T_C, of commonly used magnetic materials.

ii. Magnetic Anisotropy

In a crystalline magnetic material, magnetic properties vary depending on the crystallographic direction in which the magnetic dipoles are aligned.

A measure of *magnetocrystalline anisotropy* in the easy direction of magnetisation, is the anisotropy field, H_a, which is the field required to rotate all the moments by 90° in a saturated single crystal.

Temperature dependant anisotropy is caused by a coupling of the electron orbitals to the lattice, and in the easy direction of magnetisation, this coupling creates orbitals in the lowest energy state.

The easy direction of magnetisation for a permanent magnet, based on ferrite or the rare earth alloys, is uniaxial. However, it is also possible to have materials with multiple easy axes or where the easy direction can lie anywhere on a certain plane or cone surface. The fact that a permanent magnet has uniaxial anisotropy means that it is difficult to demagnetise since it is resistant to rotation from the magnetisation direction. When no preferred crystallographic direction exists within a material, shape anisotropy may arise if there are non-spherical particles present within the material. The long axis of such particles is the preferred axis of magnetization, as with Alnico magnets.

In addition to magnetocrystalline anisotropy, there is another effect related to spin-orbit coupling called stress anisotropy or *magnetostriction*. Magnetostriction (which is temperature dependant) arises from the strain dependence of the anisotropy constants. Upon magnetization, a previously demagnetized crystal experiences a strain that can be measured as a function of the applied field along the principal crystallographic axes. A magnetic material will therefore change its dimension when magnetized. The inverse affect or magnetization change with stress, also occurs. A uniaxial stress can produce a unique easy axis of magnetization if the stress is sufficient to overcome all other anisotropies.

The third type of anisotropy is due to the shape of a grain. A magnetized body will produce magnetic charges or poles at its surface. This surface charge distribution, acting in isolation, is itself a magnetic field source, and is a demagnetizing field, opposing the magnetization that produced it. Anisotropy is temperature dependent, decreasing and vanishing at the Curie temperature.

iii. Magnetoresistance

Magnetoresistance (MR) is the effect by which the electrical resistance of a magnetic material changes depending on the relative direction of the current and the magnetisation. In most cases the electrical resistance is highest when the current and magnetisation are parallel and lowest when they are perpendicular. The level of magnetoresistance shown by a material is usually expressed in terms of the percentage change in resistance from the highest to the lowest resistance and is usually of the order of a few percent. The main application for MR sensors is in the read heads of hard disk drives.

Table 32.2. The saturation polarisation, B_S, and Curie temperature, T_C, of a range of magnetic materials.

Material	Magnetic Structure	J_S at 298K $J_S = \mu_o M_S$	T_C Curie temperature	reversible coefficient	
				α (B_r)	β (H_{ci})
		Tesla	ºC	%/ºC	%/ºC
Fe	Ferro	2.15	770		
Co	Ferro	1.80	1121		
Ni	Ferro	0.62	368		
Alnico 5/8	Ferro	1.08/0.80	900/860	-0.02	-0.03
$Nd_2Fe_{14}B$	Ferro	1.59	312	-0.11	-0.060
$SmCo_5$	Ferro	1.14	720	-0.04	-0.3
Sm_2Co_{17}	Ferro	1.25	820	-0.03	-0.3
FeCrCo	Ferro	1.35	630	-0.03	-0.04
Fe, 3wt% Si	Ferro	2.00	740		
Fe, 35wt% Co	Ferro	2.43	940		
Fe, 78wt% Ni	Ferro	0.70	580		
Fe 50wt% Ni	Ferro	1.55	500		
$Ba0.6Fe_2O_3$	Ferri	0.48	450	-0.19	0.40
$Sr0.6Fe_2O_3$	Ferri	0.48	450	-0.19	0.40
$MnO\text{-}Fe_2O_3$	Ferri	0.51	300	-0.19	0.40

| 32.2 | **Classification of magnetic materials** |

Magnetic materials can be classified as either *hard* or *soft*.

Magnetically soft materials can be readily magnetized, but the magnetism induced is only temporary. An alloy of iron with 4% silicon is used to make the cores of electromagnets and transformers. Stroking a magnet along a steel pin from one end to the other will weakly magnetize the steel pin. This is because large numbers of iron atoms (domains) of the steel become aligned in the same direction. Such materials typically have an intrinsic coercivity of less than 1000Am^{-1} and are primarily used to enhance and/or channel the flux produced by an electric current. A parameter often used as a figure of merit for soft magnetic materials is the relative permeability, μ_r, where $\mu_r = B/\mu_o H$, which is a measure of how readily the material responds to an applied magnetic field, H. Other important parameters are coercivity, saturation magnetisation, and electrical conductivity, plus a small hysteresis loop area.

Magnetically hard materials can be permanently magnetized by a strong magnetic field. Steel and special alloys, which contain various amounts of aluminium, nickel, cobalt, and copper, are used to make permanent magnets. Their magnetic properties are due to their atomic structure. The electrons in the outer orbit of an iron atom behave as an electric charge and produce a strong magnetic field. In magnetized iron, millions of individual iron atoms, called a domain, are aligned in the same direction. Each domain has a north and a south (seeking) pole. Iron is an example of a natural hard magnetic material. The strongest energy permanent magnets are NdFeB, made in a vacuum and at high temperature from powders of various alloy grains.

Hard magnets, also referred to as permanent magnets, are of magnetic materials that retain their magnetism after being magnetised, when the inducing field energy source has been removed. Practically, this occurs with materials that have an intrinsic coercivity of greater than ~10kAm^{-1}. The hysteresis loop area should be large, corresponding to a high stored energy. Saturation, coercive force, and remanence should also be large. Figure 32.4 shows this intrinsic coercivity, H_c, variation difference between hard and soft magnetic materials.
The development progress time-lines of hard magnetic materials is shown in figure 32.5.
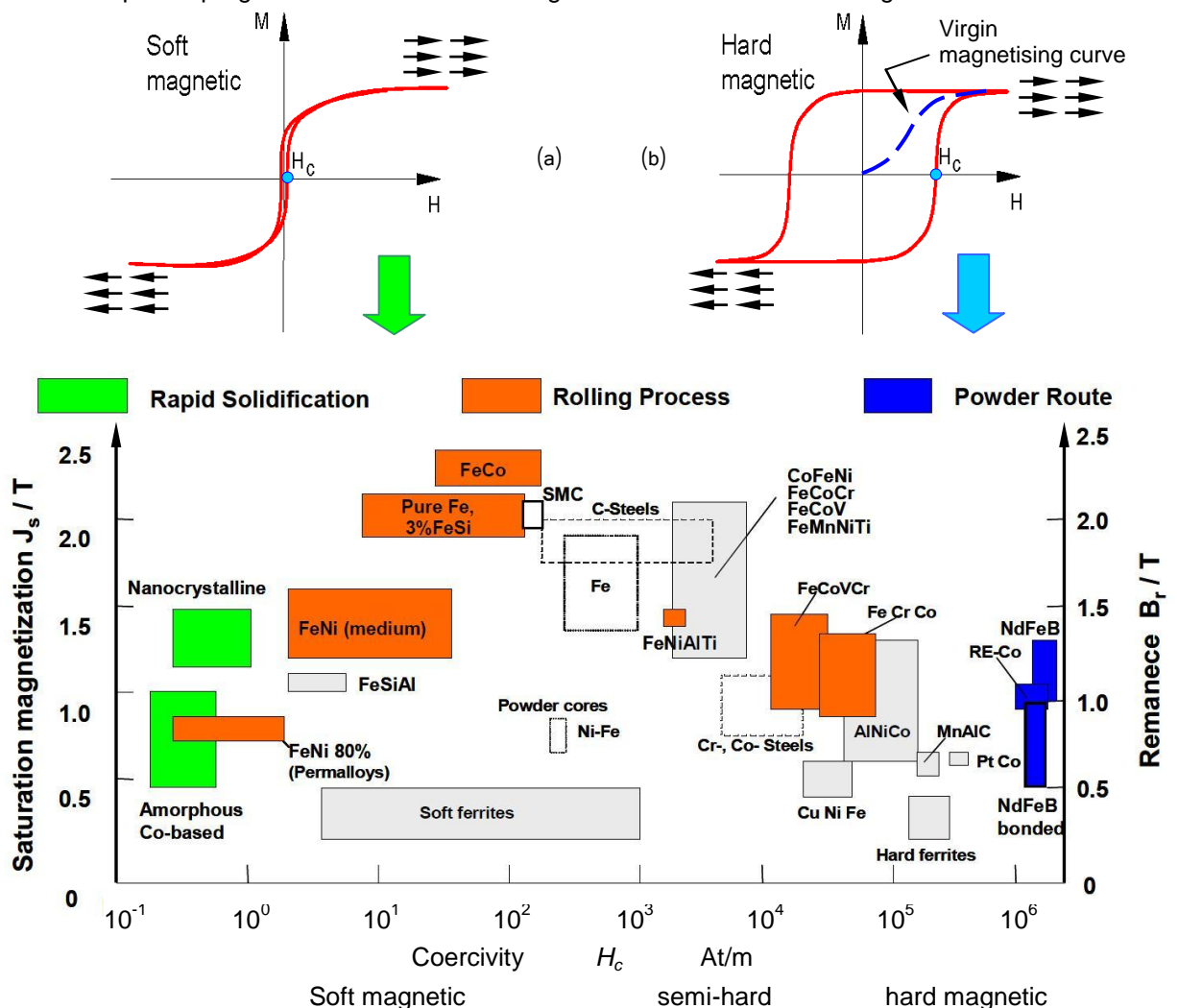

Figure 32.4. *Typical hysteresis loop and intrinsic coercivity H_c for:*
(a) soft, (b) hard magnetic materials, and (c) an overview of magnetic metals, alloys, and materials.

Hard magnetic materials can be divided into four categories: hard magnetic alloy material, hard magnetic ceramic material, bonded hard magnetic material, and flexible (or rubber) hard magnetic material, which in turn have the following subcategories:

1.   Hard magnetic alloy material:
         AℓNiCoTi
         FeCrCo
         FeCoVCr (RE - rare earth)
         RE Cobalt
         RE FeB, REFeN
         PtCo
         CuNiFe

2.   Hard magnetic ceramic material:
         Hard magnetic ceramic material ($M.nFe_2O_3$; M refers to Barium, Strontium and Plumbum; while *n* is within the range 4.5 to 6.5)

3.   Bonded hard magnetic material:
         bonded NiCoFeTi
         bonded RE Cobalt
         bonded NdFeB
         bonded ferrite

4.   Flexible hard magnetic material:
         Individually or mixed ferrite and neodymium magnetic powders
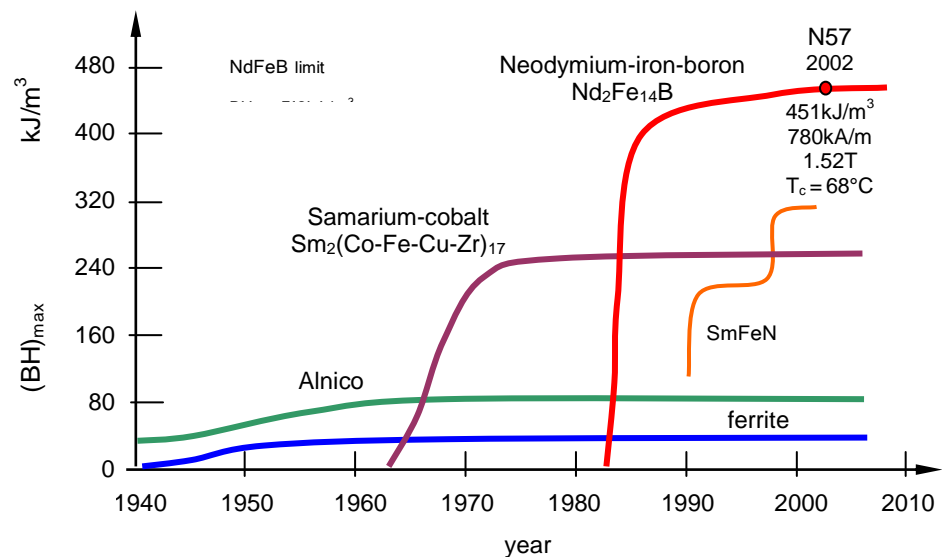

Figure 32.5. *The progressive development of permanent magnets.*

Magnet alloys that utilize elements from the Lanthanide series of the periodic table shown in figure 32.1 are commonly referred to as Rare Earth (RE) magnets. Specific magnetic materials containing rare earth elements, plus transitional elements (TE), are Neodymium Iron Boron (NdFeB) and Samarium Cobalt (SmCo) magnets, as shown in figure 32.6.

32.2.1 Alloys

i. Nickel-iron alloys

Nickel-iron alloys, known as permalloy, are versatile and are composed of a wide range of magnetic material, from 30 to 80wt%Ni. Widely varying properties result and the optimum composition is selected for a particular application. High Ni content alloys have high permeability; around 50wt%Ni gives high saturation magnetisation while a low Ni content produces a high electrical resistance (low ac losses). Some Ni-Fe alloys have zero magnetostriction and zero magnetic anisotropy, such as mumetal which is produced by a specific heat treatment (dry hydrogen atmosphere furnace with a dewpoint of < -40°C at 1100-1180°C for 2-4 hours). Such alloys have extremely high relative permeability, up to 300,000, and an intrinsic coercivity as low as 0.4Am[-1].

Chemical composition:

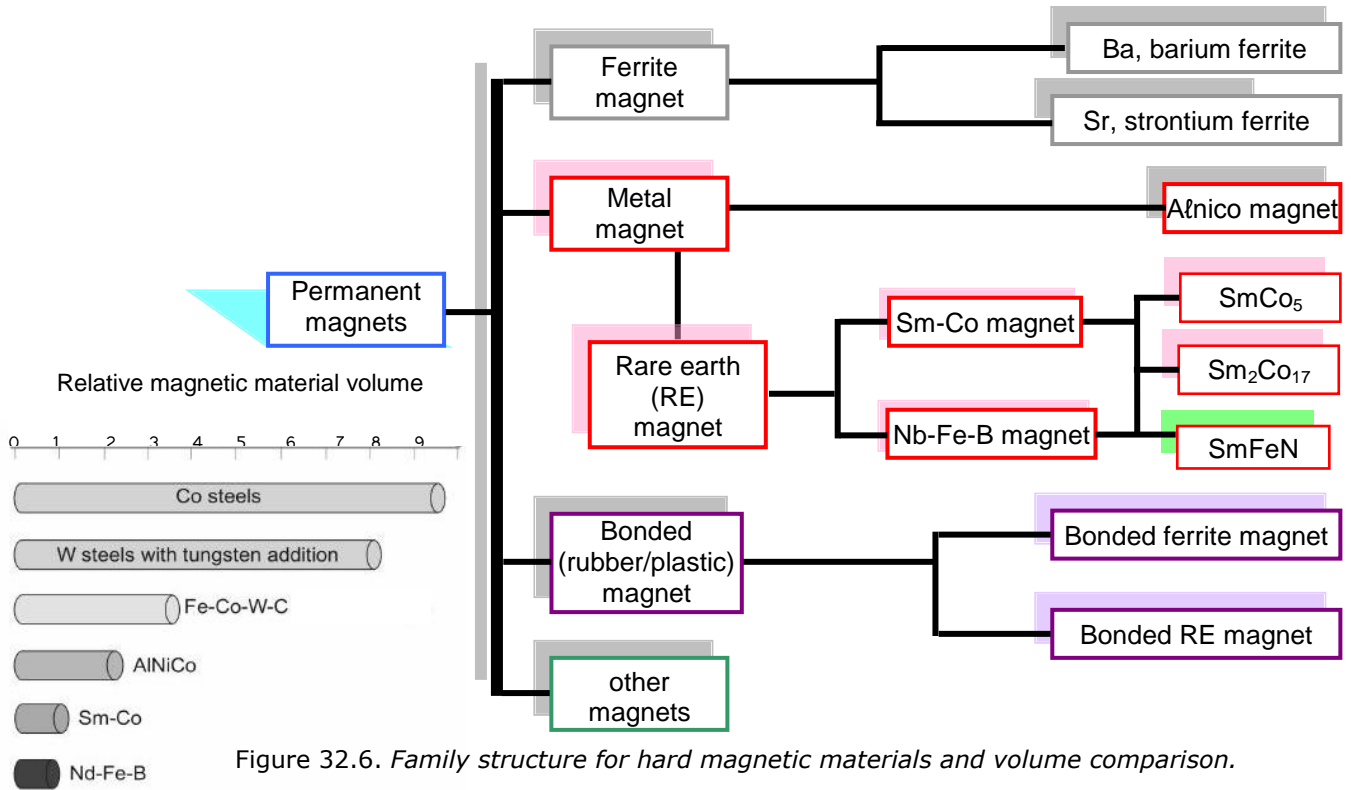| Wt %	Ni	Cu	Cr	S	P	Si	Mn	C	Mo	Fe
Comp 1	79 - 80.6			< 0.008	< 0.02	0.42	0.95	< 0.03	3.8 - 5	balance
Comp 2	75 - 77	4-6	> 3	< 0.02	< 0.02	> 0.5	> 1.8	< 0.05		

Figure 32.6. *Family structure for hard magnetic materials and volume comparison.*

ii. Cobalt alloys

(a) Aℓnico hard magnet material: (alloys based on Al, Ni, and Co)

Chemical composition:

Wt %	Al	Ni	Co	Cu	Ti	Nb	Si	Fe
AℓNiCo	6 - 13.5	12 - 28	0 - 42	2 - 6	0 - 9	0 - 3	0 - 0.8	balance

A hard magnet that incorporates aluminium, nickel, cobalt, ferrum, and titanium, is called an AℓNiCo magnet. Typical weight% is: Fe-35, Co-35, Ni-15, Aℓ-7, Cu-4, Ti-4.

This group of magnets offer far more magnetic hardness than magnetic steels. Their properties rely on the shape anisotropy improvement associated with the two-phase nanostructure comprised of ferromagnetic Fe-Co needles in a matrix of non-magnetic Aℓ-Ni. Due to their high Curie temperature, ~850°C, they have more stable properties around room temperature than some other alloys. This material has the lowest temperature coefficient (-0.02% per degree centigrade) of all permanent magnets, thus producing a constant field over a wide temperature range (-270°C to +500°C).

Alnico is classified as either an isotropic or anisotropic hard magnetic material. Aℓnico 2, 3 and 4 are unoriented – magnetic properties are isotropic and equal in all directions. Grades 5 to 9 are anisotropic.

There are two manufacturing techniques for AℓNiCo hard magnet, namely casting and powder metallurgy (sintering for smaller magnets). If the cobalt content is more than 15%, the introduction of an external magnetic field during heat treatment at 1260°C in a hydrogen (or inert gas or a vacuum) atmosphere creates anisotropy for the sintered magnet, allowing the magnetic property to be increased in the preferred direction. For column crystal or monocrystalline shaped material, a strong external magnetic field parallel to the column crystal axis during heat treatment (annealing), produces optimal properties for the cast (and sintered) hard magnetic material.

Disadvantages of the Aℓnico materials are relatively low coercivity and mechanical brittleness.

Anisotropic columnar Aℓnico 9, has an energy product of ~80kJm^{-3}. However, although having a relative high B_r, its main disadvantage is low intrinsic coercivity (H_c ~50kAm^{-1}) thus it must be made in the form of horseshoes or long thin cylinders/rods, which cannot be exposed to significant demagnetising fields.
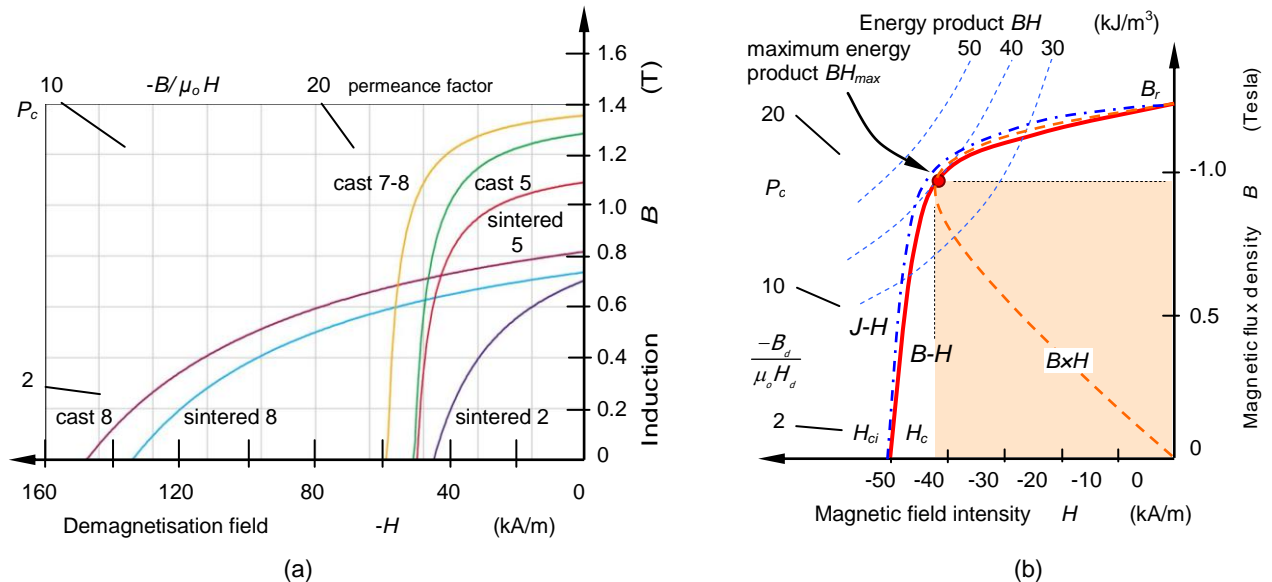
Figure 32.7. *Second quadrant hysteresis loop for: (a) Aℓnico family and (b) Aℓnico 5.*

(b) CrFeCo hard magnet material

Chemical composition:

Wt %	Cr	Co	Si, Ti, Mo, Al, V	Fe
CrFeCo	25 - 35	7 - 25	0.1 - 3	balance

CrFeCo can be classified into isotropic and anisotropic hard magnetic materials.
There are two production techniques for CrFeCo hard magnet alloy: casting and powder metallurgy. The material is ductile (good machinability) and can be easily hot rolled or cold rolled into strip or drawn into bar shapes, or, after punching, turning or drilling, can be made into the required shape and still maintain its magnetic properties. It has a low coercivity, and is relatively high in cost. Although mostly iron, which is inexpensive, there is significant cobalt and chrome content which is considerably more expensive. Typically strong, hard, tough, but brittle. It is hydrogen resistant.
[B_r=1.35T, BH_{max}=52kJ/m^3, H_c= 49kA/m, α=-0.03%/°C, β=-0.04%/°C, T_C=640°C, T_{op}=500°C and μ_{rc} = 2.5]

(c) FeCoVCr hard magnetic material

Chemical composition:

Wt %	Co	V+Cr	Fe
FeCoVCr	49 - 54	4 - 13	balance

FeCoVCr hard magnetic anisotropic alloy is produced using a casting process, and can be hot rolled or cool rolled into strip or drawn into wire shapes. Cool deformation (80% to 95%) and subsequent annealing heat treatment at 500 to 600°C is a necessary processing step to obtain the required anisotropic magnetic properties.
[B_r = 0.85T, BH_{max} = 15kJ/m^3, H_{ci} H_c = 28kA/m, α=-0.01%/°C, β=0%/°C, T_C=720°C, T_{op}=500°C, and μ_{rc}= 5]

iii. Samarium Cobalt alloys

Chemical composition, typically:

Wt %	Sm	Co	Fe and Cu
SmCo	35	60	balance

This alloy group combines cobalt, iron (transition metals - TM) and a light rare earth (RE) element to exhibit permanent magnetic properties. They exhibit high-energy hard-magnetic behaviour, but are costly. These magnets have good thermal stability, thus are used where magnets are exposed to high temperatures (>150°C) or low temperatures (<100K). They are brittle and hard to machine.

The combination of a rare earth and a transition metal is ideal as the rare earth provides the anisotropy to the phase and the transition metal provides a high magnetisation and Curie temperature. By varying the percentages of the composition and changing the sintering and heat treatment cycles, two grades are produced, namely $SmCo_5$ termed 1:5 and Sm_2Co_{17} termed 2:17. They differ in energy product, temperature coefficient, and magnetisation force required to saturate. In the case of $SmCo_5$

$$Sm_2O_3 + 10\,Co + 3\,Ca \rightarrow 3\,CaO + 2\,SmCo_5$$
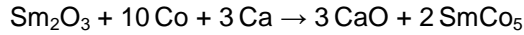
The reaction takes place at 1100°C for 1 to 4 hours in a hydrogen (or inert gas) atmosphere or a vacuum. Usually excess Ca is added, typically 20 to 40%, to assure that the reaction goes to completion. $SmCo_5$ sintered magnets have energy products of ~160kJm^{-3}. These magnets have excess Sm that forms a smoothing grain boundary phase and coercivity is achieved by preventing the nucleation of reverse domains.

The maximum energy product is increased to 240kJm^{-3}, with a Sm_2Co_{17} based alloy. The theoretical limits are 230kJ/m^3 and 270kJ/m^3 for $SmCo_5$ and Sm_2Co_{17}, respective. These materials are based on the composition $Sm_2(Co,Fe,Cu,Zr)_{17}$ and achieve permanent magnetic properties by control of the microstructure. The 2:17 magnets are produced by powder metallurgy and are solution treated at ~1100ºC, where they are single phase, then heat treated at 500ºC to 800ºC. This homogenising stage is followed by aging treatments at lower temperature where a cellular microstructure is formed. The cells are based on the Sm_2Co_{17} type phase, which is enriched in Fe and the cell boundaries comprise a layer of $SmCo_5$ type phase, which is enriched in Cu. The intrinsic magnetic properties of the cells and their boundaries vary such that the magnetic domain wall energy is greatly reduced within the cell boundary and hence pin the domain walls, leading to permanent magnetic properties. They can operate at high temperature, ~500ºC, when small quantities of zirconium, hafnium, etc. are added to give better heat treatment response.
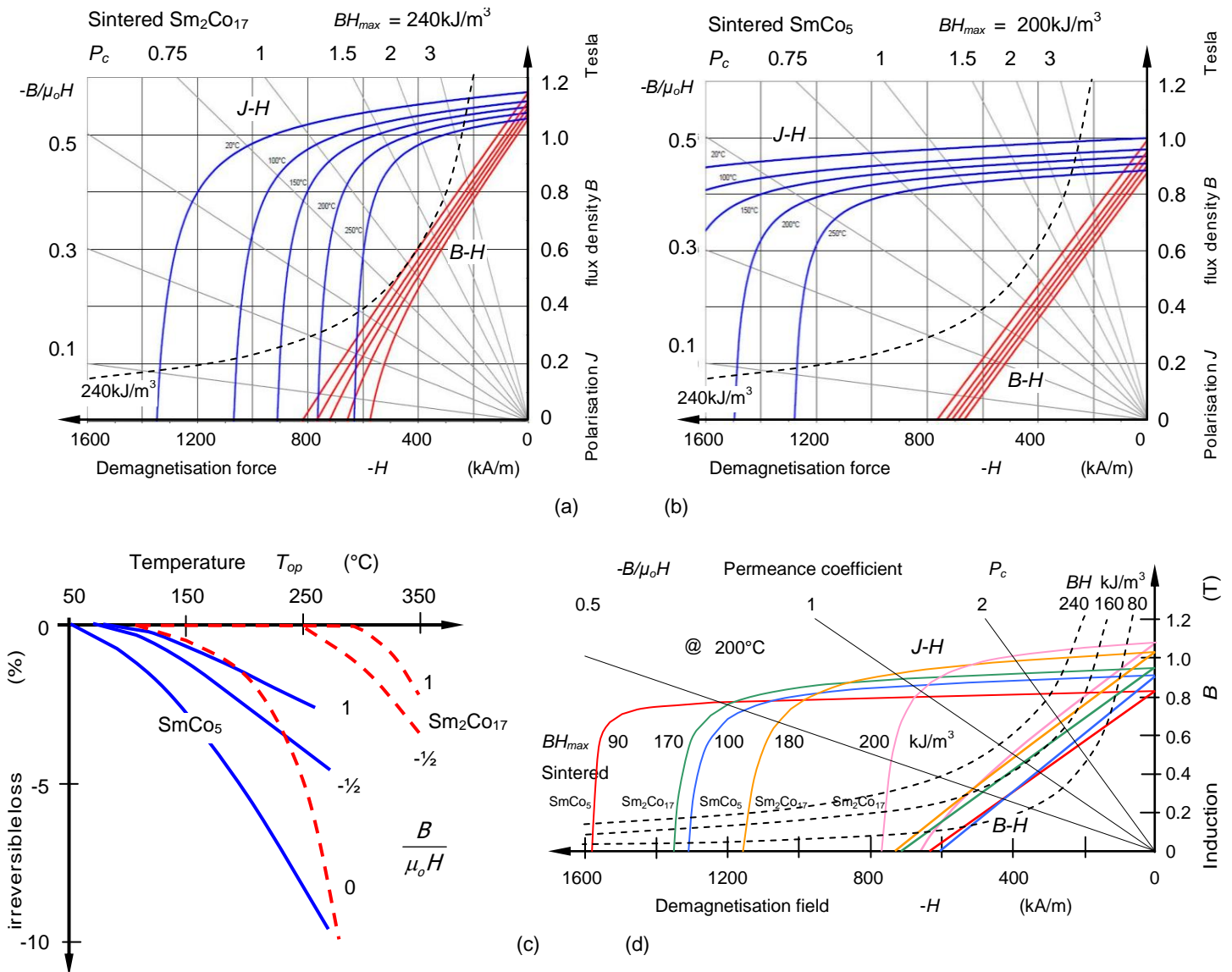
Figure 32.8. *Second quadrant hysteresis loop for samarium cobalt alloys:*
(a) Sm_2Co_{17}, (b) $SmCo_5$, (c) characteristics at 200°C (with constant energy contours shown), and
(d) temperature dependant irreversible losses as a function load line slope.

Both grades exhibit excellent energy, temperature, and corrosion resistant properties, applicable when a compact high energy field is required at temperatures of over 100°C or in hostile environments. These alloys have the best reversible temperature coefficient of all rare earth alloys, typically -0.03%/°C, as shown in Table 32.2. SmCo requires large magnetizing fields (in excess of 28MAt/m) to saturate and under operational conditions, are difficult to de-magnetise.

A problem with Sm/Co based magnets is the expense of the raw materials. Samarium is much less abundant than other light rare-earth elements, such as La, Ce, Pr, and Nd, which account for over 90% of rare-earth metals in typical rare-earth ores.

Samarium-cobalt magnets are manufactured by similar routes as ferrites, being formed into either a fully dense sintered magnet, or a compression - or injection-moulded bonded magnet. Because both samarium and cobalt are relatively expensive elements, anisotropic magnets are usually produced with optimized properties along a pre-determined axis.

Rare-earth magnets have a rather more complicated domain wall mechanism than that for pure magnetocrystalline anisotropy, such that the best magnetic properties are only achieved with the powder milled to a grain size which is an order of magnitude larger than the single domain size. This means that, not only can domain walls exist, but also they can move relatively freely within a grain. While this allows saturation magnetization to be achieved with only a modest applied field, a high intrinsic coercivity will depend upon the grains' ability to resist the formation of a reverse domain when a demagnetizing field is applied. This property is therefore controlled by the grain boundaries, which are composed of deviations from the primary composition that provides a strong pinning of the domain walls at these sites. This mechanism, known as *nucleation*, where a grain undergoing nucleation, occurs in $SmCo_5$ magnets.

Sm_2Co_{17} differs from $SmCo_5$ in that its grains contain a fine cell structure. Heat treatment of this compound promotes the formation of Sm_2Co_{17} cells, separated by thin walls of $SmCo_5$ which can provide pinning of the domain walls (rather than the grain boundaries). Pinning, rather than nucleation, is therefore the controlling mechanism in Sm_2Co_{17} magnets, and this requires that a much greater field be applied to initially magnetize it into saturation.

Whether it is a nucleation-type $SmCo_5$ or a pinning-type Sm_2Co_{17} magnet, that is, whether the domain walls are pinned at the grain or cell boundaries, they will move quite freely once these pinning forces are overcome, and M_{sat} will abruptly flip over into the opposite direction when an applied field of $-H_{ci}$ is reached. This effect is seen in the shape of the demagnetization curves for samarium-cobalt type magnets, figure 32.8. The change in H_{ci} with temperature is seen in figure 32.8a for Sm_2Co_{17} and largely for $SmCo_5$ in figure 32.8b.

The theoretical Sm_2Co_{17} limit is 270kJ/m^3, N34, with the single phase $SmCo_5$ limit is 230kJ/m^3, N28.8.

iv. Samarium Iron Nitride alloys

The rare earth alloy $Sm_2Fe_{17}N_3$ incorporates Fe rather than the more costly transition metal Co. While its magnetic properties can theoretically exceed those of $Nd_2Fe_{14}B$, its processing is more complex. Only bonded magnets (extrusion-flexible and injection-rigid) are made from $Sm_2Fe_{17}N_3$, (1 to 2μm powder) which are more easily made in isotropic form than anisotropic. Such permanent magnet alloys offer high resistance to demagnetisation, high magnetisation, lightweight, and increased resistance to corrosion and temperature, compared with neodymium iron boron. They oxidize readily, have high irreversible loss at high temperature and are expensive.

> [Extrusion moulded, flexible: B_r = 0.78T, BH_{max} = 111kJ/m^3, H_{ci} = 812kA/m, H_c = 520kA/m, $α$=-0.05%/°C, $β$ =-0.45%/°C, T_C = 498°C, T_{op} = 80°C, and $μ_{rc}$ = 1.15:
> Injected moulded, rigid: B_r = 0.81T, BH_{max} = 115kJ/m^3, H_{ci} = 756kA/m H_c = 533kA/m, $α$ = -0.05%/°C, $β$=-0.45%/°C, T_C = 498°C, T_{op} = 110°C, and $μ_{rc}$ = 1.15]

Explosion sintered $Sm_2Fe_{17}N_y$ yields a squarer BxH area, which is further improved, Curie temperature wise, with the addition of Ta. [B_r = 0.83T]

v. Neodymium Iron Boron alloys

Chemical composition:

Wt %	Nd	Fe	B	Al	Nb	Dy
NdFeB	29 - 32	64.2 - 68.5	1.0 - 1.2	0.2 - 0.4	0.5 -1	0.8 -1.2

NdFeB combines a high saturation magnetisation with good resistance to demagnetisation. The high cost of samarium and the price volatility of cobalt have lead to NdFeB magnets becoming the preferred material for applications requiring high-energy magnets. Despite the high energy-product, these magnets have a relatively low Curie temperature, typically 312°C, which prohibits their use in high temperature applications. Additions of Co/Tb and Dy improve temperature and coercivity characteristics but decrease the saturation polarisation and increases production costs. Co improves corrosion resistance. NdFeB is easier to machine than Alnico and SmCo magnets. NdFeB are materials based on the magnetic phase $Nd_2Fe_{14}B$, with two different powder metallurgy processing routes being employed.

Process route #1 *Sintering (orient-press-sinter)*

Powder NdFeB based sintered permanent magnets produce a maximum energy product of ~451kJm^{-3}, by accurate heat treatment, controlled processing, and with the use of iron rich compositions.

Sintered NdFeB based magnets achieve their coercivity by virtue of an Nd-rich phase at the grain boundaries, which acts to produce liquid phase sintering, smooth the boundaries, hence prevent nucleation of reverse magnetic domains.

The processing sequence for sintered NdFeB based magnets is shown in figure 32.9. The *as-cast* (untreated) ingot must first be broken into a powder. This is achieved most conveniently by exposing the ingot to hydrogen, which is absorbed at the surface. The hydrogen enters the material in the spaces between the atoms and causes the material to expand. The differential expansion generates stress in the ingot and the alloy breaks down into a fine powder, with an average grain size of 100µm. This process is known as *Hydrogen Decrepitation*, HD. The HD powder is then broken up further by a jet milling stage, which reduces the grain size to less than 5µm – the size of a few domains and therefore inherently anisotropic. When the alloy is in a powdered form, it is flammable, thus is handled under an inert gas.

Each particle of the broken down powder is a single crystal, 3 to 5µm, which can be aligned in a magnetic field; a few 10ms alternating pulses at 6.4MA/m. This alignment is held in place by pressing the powder into a green (unsintered) compact, which is about 60% dense. The compact is then heated in a vacuum (or inert gas) to ~1060ºC for 4 hours. During the heating stage, the hydrogen is driven out of the material and is pumped away. Sintering occurs and the compact densifies, with the assistance of a liquid formed by the melting of the Nd-rich phase. After sintering, then quenching, the magnets are heat-treated, annealed, at ~550ºC to 800ºC for 1 hour, thereby achieving optimum magnetic properties.

The magnet is then machined to the dimensions for the intended application. Due to the large degree of shrinkage that occurs during sintering, which is greater in the direction of alignment, it is not possible to press compacts that will shrink to the exact size required. Machining is an expensive operation and, particularly for small magnets, a large proportion of the material may need to be machined away.
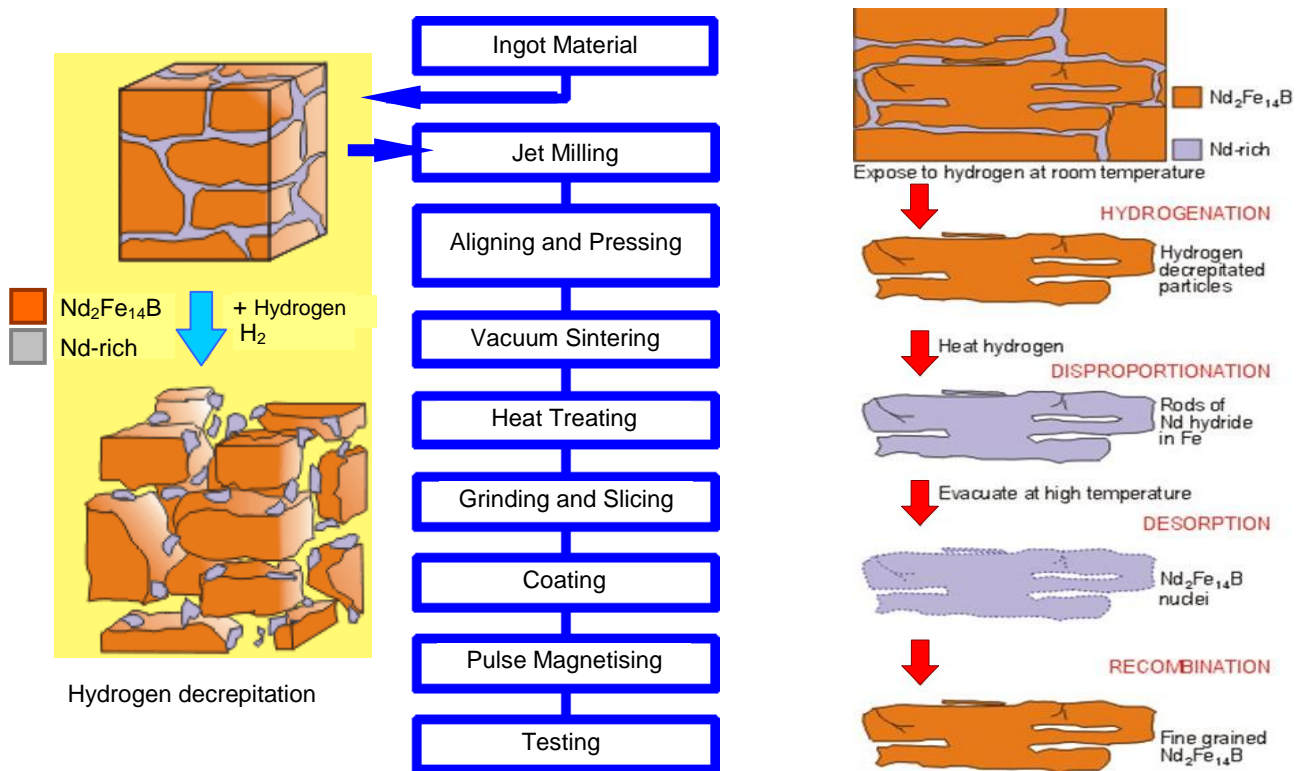
Figure 32.9. *The processing route for sintered NdFeB permanent magnets, left HD and right HDDR.*

Due to the highly reactive nature of the Nd-rich phase, the magnets tend to corrode rapidly, particularly in moist environments. Therefore, the next processing stage is to provide a protective barrier on the magnet surface, usually a nickel (plus copper) coating, although aluminium, zinc, and epoxy resins are also used. Finally, the magnet material is magnetised and tested.

An extension to the HD process is the *hydrogenation disproportionation desorption and recombination* (HDDR) process. Unlike the more straightforward HD-process, the HDDR route involves heating the bulk alloy in 1 bar of hydrogen to ~800°C. The first stage is the decrepitation of the alloy due to the initial

absorption of the hydrogen, as described previously. At ~700°C, the $Nd_2Fe_{14}B$ matrix phase disproportionates during an exothermic and reversible reaction involving hydrogen absorption

$$Nd_2Fe_{14}B + (2 \pm x)H_2 \Leftrightarrow 2NdH_{2\pm x} + 12Fe + Fe_2B + \Delta H$$
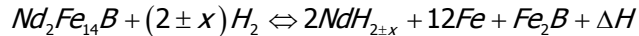
where x depends on temperature and pressure. Then desorption results in isolated 0.3um grains, which exhibit appreciable coercivity. Fully dense isotropic magnets are produced by hot pressing the powder mixed with thermosetting resins in a compression mould, at 750°C in an inert atmosphere.

In summary, neodymium-iron-boron magnets may be made from alloy powder, which is:

- sintered, nucleation-type;
- rapidly quenched, magnetocrystalline; then
- HDDR, magnetocrystallination.

Processing route #2 Melt Spinning

Melt-spinning is used to produce a ribbon like powdered material. Molten alloy is ejected onto the surface of a rotating water-cooled wheel, and cooling rates (rapid quenching) of the order of one million °C/s are achieved. The microstructure and magnetic properties of the NdFeB ribbons are sensitive to the quench rate, that is, the speed of the rotating wheel. High quench rates produce essentially amorphous ribbons (that is, no crystal grains) having negligible intrinsic coercivity. Optimum quench rates yield ribbons with high coercivities; they are comprised of roughly spherical $Nd_2Fe_{14}B$ grains (20 to 100 nm in diameter), which are single domain particles thus have a high coercivity, $\sim 1MAm^{-1}$. At wheel velocities below optimum, the slow cooling rate produces ribbons with larger grains and are characterised by low coercivities. This powder cannot be sintered to produce fully dense magnets without destroying the magnetic properties, but is utilised in one of three ways:

MQ-I

The melt spun ribbon (typically milled into thin platelets 200µm wide and 35µm thick) is blended with a resin to produce a bonded permanent magnet. The crystals of *MQ-I* material are randomly oriented so that the magnets are isotropic and can be magnetised along any axis to a BH_{max} of ~80 kJm^{-3}.

MQ- II

Improved densification of melt-spun ribbons can be achieved by hot pressing at ~750°C, without adversely effecting the coercivity of the powder. These *MQ-II* type magnets exhibit a slight degree of magnetic alignment, ~10%, and are 100% dense, that is, the magnetic properties are not diluted by a non-magnetic material, such as a resin. This gives *MQ-II* a higher BH_{max}, 100 - 120 kJm^{-3}, than *MQ-I*.

MQ-III /sintered

Substantially greater alignment (>75%), and hence greater maximum energy products, can be obtained by heating the *MQ-II* material to ~750°C in a die cavity having a larger diameter and then it is slowly deformed. This second hot press, termed die upset forging, produces plastic flow and a reorientation of the crystals. Such magnets, known as MQ-*III*, are 100% dense, and because of the alignment of crystals, have maximum energy products of ~400 kJm^{-3}.

NdFeB magnets made by rapid quenching, as opposed to sintering, require a much greater applied field to initially align the grains' magnetizations and magnetize this material to its saturation level. Neodymium-iron-boron magnets therefore exhibit similarly shaped demagnetization characteristics to the other classes described, with a well-defined *knee* (Cunic point) at which M_{sat} reverses as an applied field of $-H_{ci}$ is approached. As an example, figure 32.10b shows the demagnetization characteristics measured at different temperatures for one grade of fully dense anisotropic $Nd_2Fe_{14}B$. In all cases the higher the energy density, the lower the Curie temperature. $Nd_2Fe_{14}B$ with an energy density of 451kJ/m^3 must be operated at a temperature below 50°C. The theoretical maximum is 512kJ/m^3, N64.
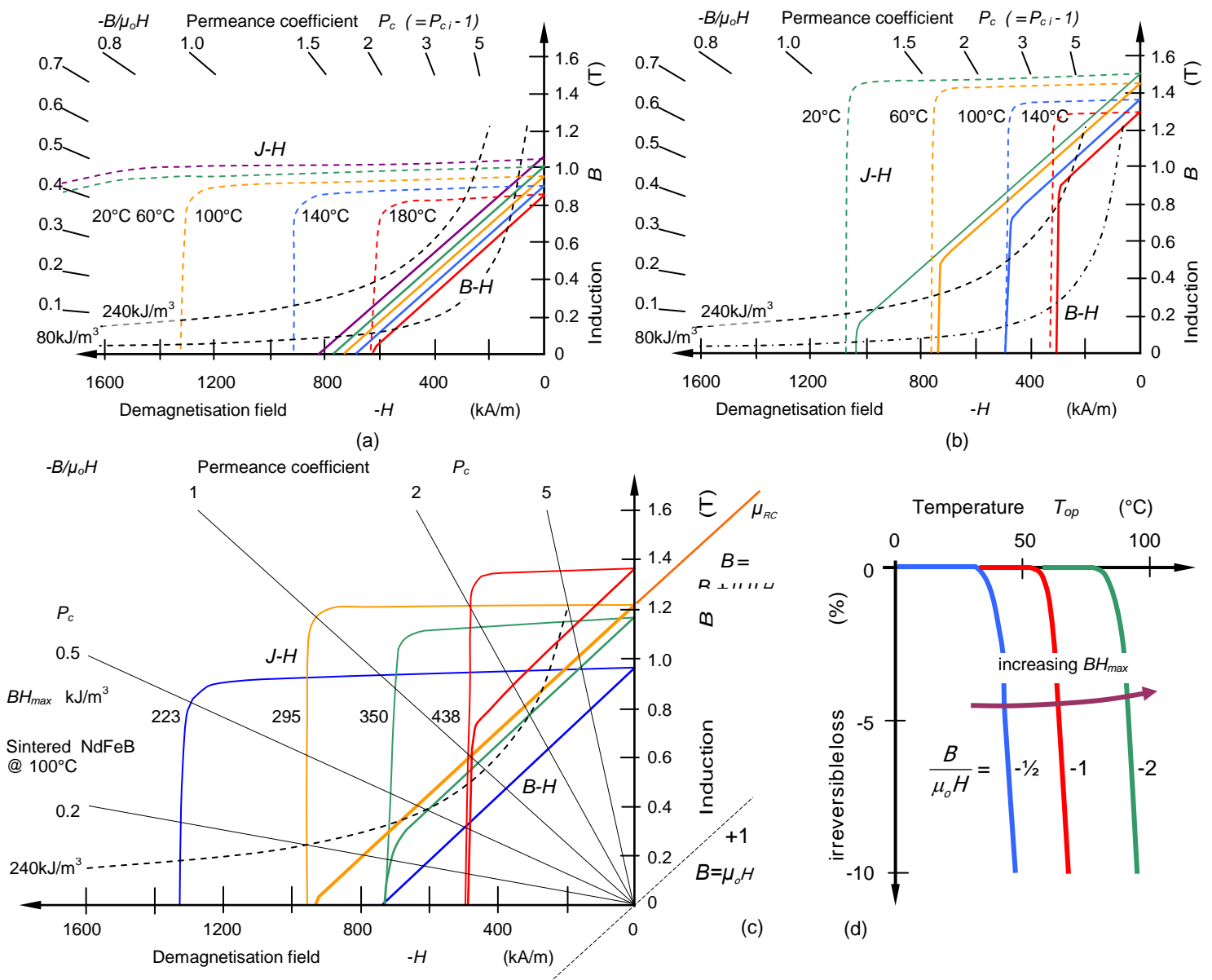
Figure 32.10. *Second quadrant hysteresis loop for sintered neodymium-iron-boron magnets: (a) N28, (b) N55, (c) characteristics at 100°C (with a constant energy contour shown), and (d) temperature dependant irreversible losses as a function load line, N55.*

Table 32.3.   NdFeB magnetic characteristics - sintering results in higher B_r than MQ processes

NdFeB Grade		Melt spin property (Magnequench)			sintered		
	symbol	*MQI*	*MQII*	*MQIII*	N28	N55	units
Maximum energy product	BH_{max}	68 – 88/ 9 - 11	111 – 119/ 15 - 15	255 – 335/ 32 - 42	223 / 28	438 / 55	kJ/m³ / MGOe
Residual induction	B_r	0.61 – 0.71	0.8 – 0.83	1.16 – 1.31	1.06	1.50	T
Coercive force	H_c	412 - 446	557 - 573	875 - 979	835	1082	kA/m
Intrinsic coercive force	H_{ci}	716 - 1353	1393 - >1433	1173 - >1593	2705	1074	kA/m
Rev. Temp. Coefficient	α - B_r	-0.105	-0.10	-0.09	-0.11	-0.11	%/°C
Rev. Temp. Coefficient	β - H_{ci}	-0.6	-0.6	-0.6	-0.55	-0.65	%/°C
Magnetising filed	H_s	1990 - 2785	3581	2785 - 3581	1000	1000	kA/m
Recoil relative permeability	μ_{rc}	1.15 – 2.31	1.14	1.05 – 1.09	1.05	1.05	pu
Maximum operating temperature	T_{op-max}	80 - 180	160 - 200	150 - 200	200	80	°C
Curie temperature	T_C	305 -470	325 - 370	325 - 370	365	310	°C

vi. Amorphous and Nano-Crystalline Alloys

These materials can be produced in the form of a tape by melt-spinning. The alloys consist of iron, nickel and/or cobalt with one or more of the following elements: boron, carbon, phosphorous, and silicon. They have extremely low coercivity, an order of magnitude less than standard Fe-Si, and consequently have lower hysteresis losses. However, they have a relatively low magnetisation and are not suitable for high current applications.

Instead of casting the alloy onto a rotating wheel to produce tapes, it is also possible to direct a stream of molten alloy into a bath of water or oil to produce amorphous wires of typically 50μm thick. These wires exhibit a square hysteresis loop with large changes in magnetisation at low fields, making them ideal for sensing and switching.

Nano-crystalline material is produced by annealing the amorphous material. These alloys can be single phase but are usually comprised of nano-sized grains, in the range 10 to 50nm, in an amorphous matrix. They have relatively high resistivity, low anisotropy, good mechanical strength, and are better suited for soft-magnetic applications.

32.2.2 Ceramics

Hard Ceramic hexaferrites: ($BaFe_{12}O_{19}$ or $SrFe_{12}O_{19}$)

Hard hexagonal ferrite materials, often referred to as ceramic magnets, are ferrimagnetic and considering the proportion of iron within the material, have a low remanence, ~400mT. The coercivity of these magnets is typically ~250kAm^{-1}. The low remanence means that the maximum energy product is only ~40kJm^{-3}, which is lower than the alnicos, but due to the high coercivity, these magnets can be made into thinner sections. The magnets can be exposed to moderate demagnetising fields, and coupled with good mechanical characteristics and low cost, are suitable for applications such as permanent magnet motors.

Ceramic ferrites are made using an iron oxide powder, to which either barium or strontium (carbonate) is added to improve alignment of the crystal lattice structure. The chemical formula is $M \cdot n(Fe_2O_3)$, where M is Ba or Sr and 5.8<n<6.0. After milling, which produces small grains, <1mm, which is essential for generating coercivity in ferrites, the powder is pressed in a die, with an orienting field applied through the cavity if desired, enhancing the remanence and the maximum energy product. If no field is applied, an isotropic magnet results with no preferred magnetic properties in any particular direction. If an orienting field is applied, an anisotropic magnet results having preferred magnetic properties along a specific axis. The compacted powder is then sintered at a temperature of 1100°C to 1300°C (hence the name *ceramic*) to achieve full densification, cooled at a rate of less than 90°C per hour to avoid thermal shock, and then diamond ground to the required final dimensions. There are no problems with oxidation of the powder during processing, as the material is a stable iron oxide. Alternatively, the powder may be blended with a polymer binder, and then either extruded or formed in a die by compression, or injection-moulding, thus producing a bonded ferrite magnet of near net shape; again, anisotropic properties may be achieved by applying an orienting field through the die cavity. Due to their anisotropic structure, ferrites exhibit relatively high coercivity, however, the energy product is low.
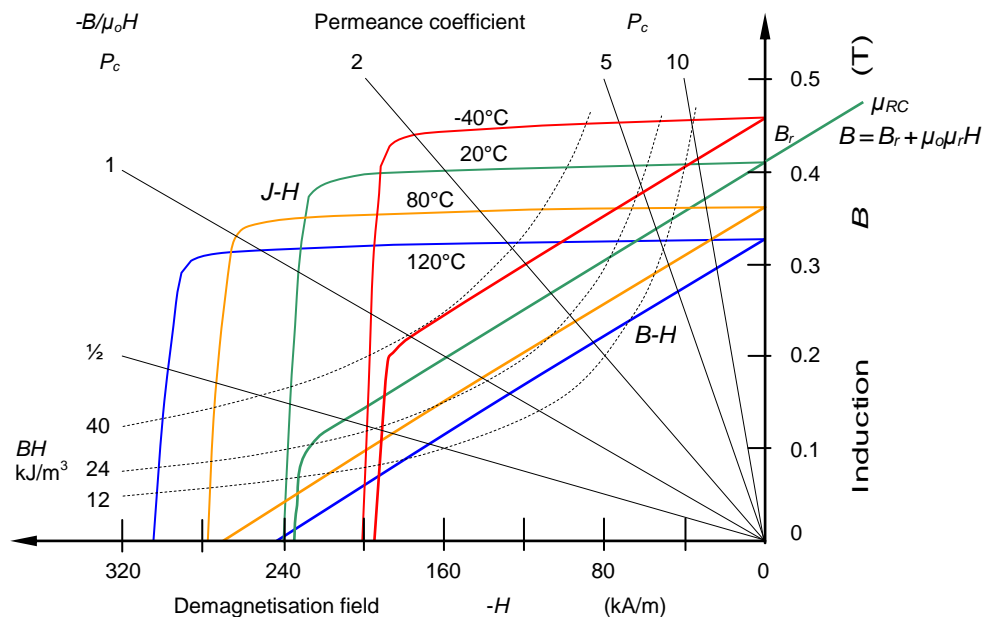

Figure 32.11. *Second quadrant hysteresis loop demagnetization characteristics measured at different temperatures for a sintered ceramic ferrite magnet (with constant energy contours shown).*

A hexagonal ferrite structure is found in both $BaO \cdot 6(Fe_2O_3)$ and $SrO \cdot 6(Fe_2O_3)$, with Sr ferrite having slightly superior magnetic properties.

Generally, magnet materials respond negatively to heat because thermal energy reduces the flux density and the ability of domains to remain aligned. Increased thermal energy increases the disorder present and at a particular temperature, the Curie point, the material loses its ferromagnetism. Excessive heating of a magnet may cause metallurgical changes to occur; in many magnets the safe operating temperature is well below the Curie point. The one exception is ferrites (ceramic magnets), which, due to their chemical nature, can withstand temperatures significantly past their Curie points. Ferrites also exhibit the unusual characteristic of increased coercivity with temperature, as shown in figure 32.11. Heat treatments during manufacturing are precisely controlled to precipitate desired phases and to control metallurgical changes.

The main advantage of ferrites is low cost, due to the ease of processing and the abundance, non-strategic, and low cost of raw materials, and complex shape possibilities. Ceramic magnet material (ferrite) has modest resistance to corrosion and can operate in moderate heat but demagnetise at low temperatures, typically, 20°C, as the knee moves up the characteristic line. Ferrites are brittle.

32.2.3 Bonded

Rigid bonded magnet materials can be made from Aℓnico, Ceramic, isotropic NdFeB (*MQ*), anisotropic NdFeB (HDDR), SmCo, SmFeN, or nano composite powders which are combined (forming a thermoset or thermoplastic) with a variety of plastic binders, a matrix with polyphenylene sulphide (PPS), chlorinated polyethylene (CPE) polyester, PVC, nylon (polyamide), duroplast or nitrile rubber. Rigid bonded magnets are processed by compression, injection, extrusion or calendaring shaping methods.
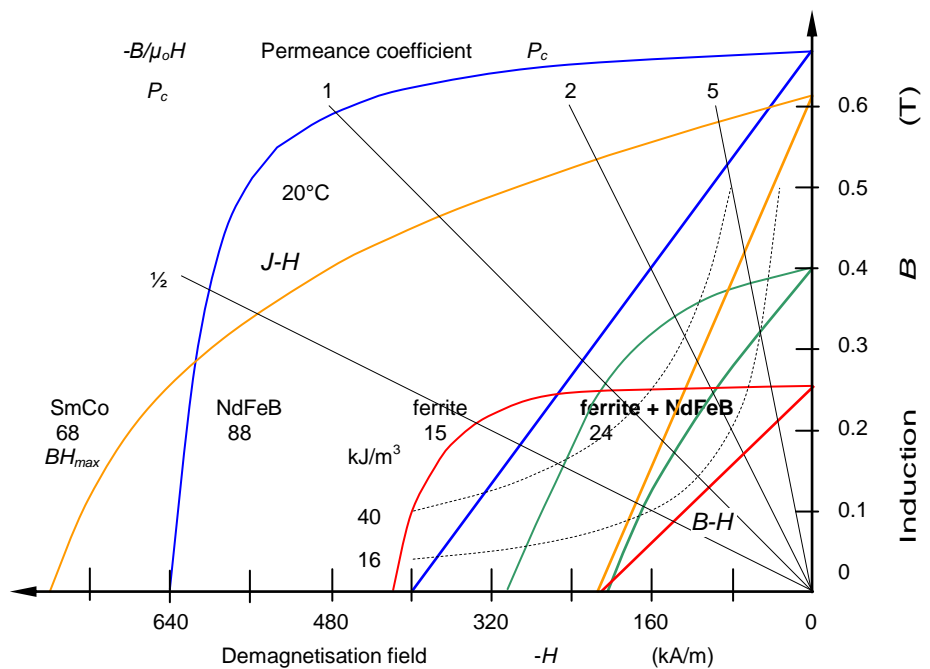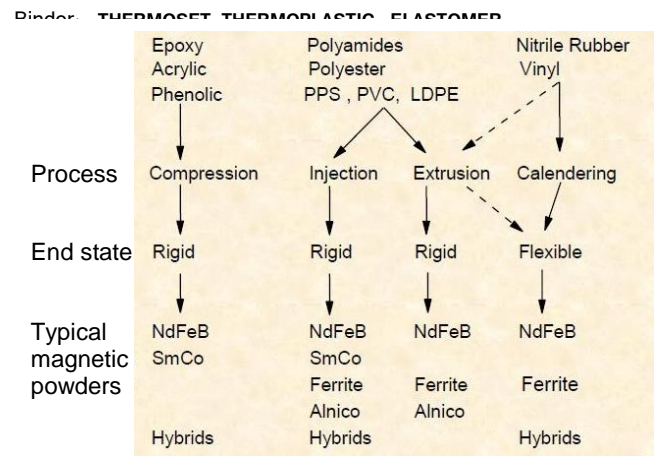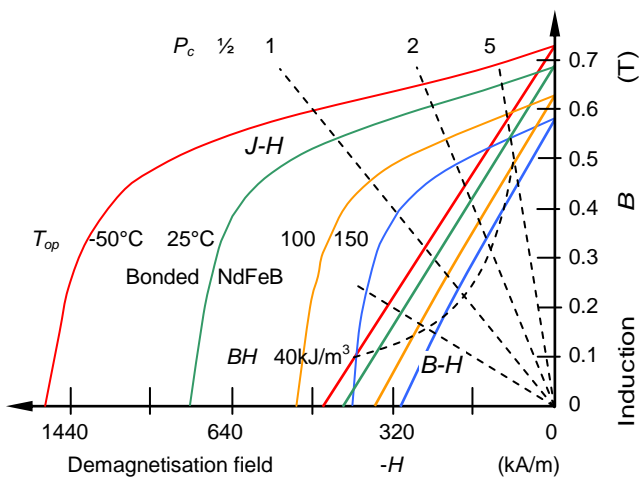

Figure 32.12. *Second quadrant hysteresis loop demagnetization characteristics measured at different temperatures for bonded magnets (with constant energy contours shown).*

They can be *injection moulded* thermoplastic bonded into mechanically-strong complex magnet shapes with accurate finished dimensions. Bonded magnet materials have a moderate resistance to corrosion and a low tolerance to heat, -40°C to 180°C, because of the binder material. The same bonder properties tends to make them chip and break resistant.

Bonded thermoset magnets can also be *compression bonded*, which offers a higher magnetic output (than injected moulded bonded magnets), due to a higher magnetic particle density than either NdFeB or SmCo powders, but are restricted to simpler geometries than injection moulded materials. The use of an epoxy binder and epoxy surface coating prevents oxidation and is resistant to normal industrial solvents and automotive fluids. Because of the compression bonding process, the tooling tolerances and mechanical strength properties are slight less than those materials that have been injection moulded.

In the case of NdFeB, the bonded material is isotropic, offering approximately 80kJ/m^3 or 30% of the energy produced by the sintered fully dense material, but can be magnetised in any direction. Typical of bonded magnets, the operating temperature range (specifically the upper limit) is restricted to -40°C to 165°C, with a poor temperature coefficient.
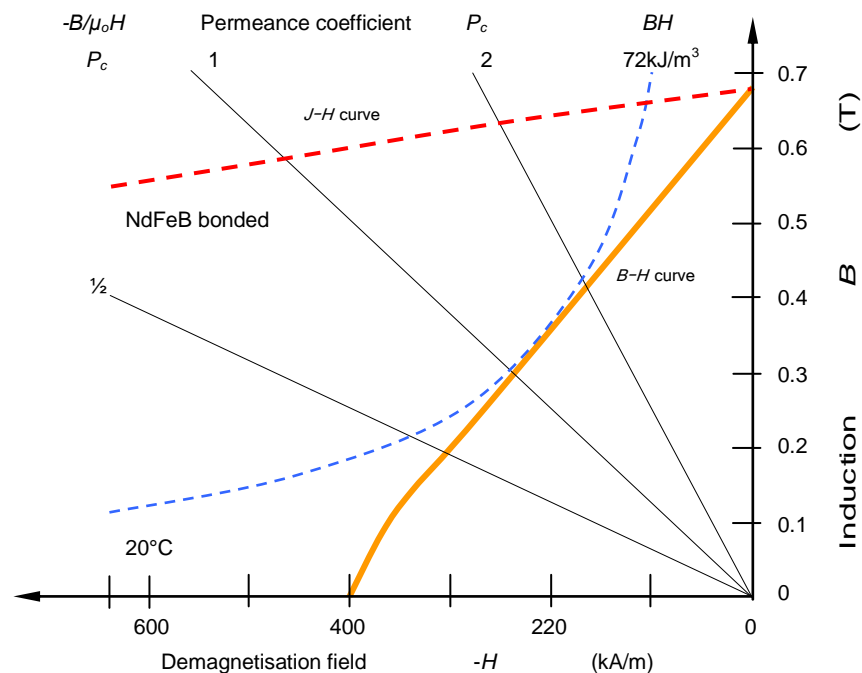
Figure 32.13. *Second quadrant hysteresis loop demagnetization characteristics for a flexible bonded magnet (with a constant energy contour shown).*

The energy product BH_{max} of bonded magnets is also lower than for a fully dense material. This is due to the magnetic material being diluted by the binder. Bonded samarium cobalt bonded materials are typically anisotropic with energy products of 40kJ/m^3 to 120kJ/m^3.

The polymer matrix associated with bonded magnets weakens magnetic properties and limits thermal properties. Their attribute is freedom of shape and design.

32.2.4 Flexible (rubber)

Flexible (rubber) magnets are manufactured by mixing (bonding) ferrite or neodymium magnet powders and synthetic or natural rubber (nitrile, vinyl, etc.) and resin elastomer binders. Flexible (rubber) magnets are manufactured by rolling (calendaring), injection or extrusion methods. Versatility, low cost, and ease of use are among the reasons to choose ferrite based flexible (rubber) magnets. Flexible magnets are usually manufactured in strip or sheet form. There are *isotropic* and *anisotropic* forms. The isotropic rubber magnet is normally magnetized with multipoles magnetization on one side only while the anisotropic form can have magnetics on both sides. The magnet material is low energy, as shown in figure 32.13, and does not usually replace fully dense magnet materials. Flexible neodymium material is higher in strength, but is made in limited quantities because the cost is high.

Table 32.4. Permanent magnet material features

Permanent magnet material	advantages	disadvantages
Alnico	Thermal stability	Brittle
	High service temperature	Low coercive force
	High flux density	Required thickness
	Complex shapes	Cost variability
	Easy to magnetise	
	Low tooling cost	
Hard ferrite	Low cost	Brittle
	High coercive force	Limited shape and tolerances
	Easy to magnetise/demagnetise	Low energy product
	Stability to oxidation	Performance varies – hi temperature dependency
		High tooling costs
Bonded ferrite	Flexible	Low energy product
	Easily shaped	Low service temperature
	Can build subassemblies	Performance varies – hi temperature dependency
	Requires little machining	
Samarium Cobalt	High energy product	Brittle
	High coercive force	High cost
	Compact	Difficult to magnetise/demagnetise
	High service temperature	Easy to oxidize
	Corrosion resistant	Powders pyrophoric – spontaneous ignition
	Thermal stability, low TC	
Neodymium-iron-boron	Highest energy product	Performance varies – medium temperature dependency
	High coercive force	Susceptible to corrosion
	Compact	Low service temperature
	Low energy cost	Difficult to magnetise
		May require coating
		Powders pyrophoric
Bonded Neodymium-iron-boron	High energy product	Performance varies – hi temperature dependency
	High coercive force	Susceptible to corrosion
	Low energy product cost	Low service temperature
	Easily shaped	
	Can build subassemblies	

32.3   Properties of hard magnetic materials

A permanent magnet is a material that when inserted, in a virgin form, into a strong magnetic field will not only begin to exhibit a magnetic field of its own, but also continues to exhibit a magnetic field once removed from the original magnetising field. Permanent-magnet materials are characterized by high values of remanent magnetization and coercivity. Such materials produce significant magnetic flux, even in magnetic circuits with air gaps.

A permanent magnet's magnetization M [the sum of the individual (unpaired electron spins) magnetic moments per unit volume] provides a magnetizing force H which establishes a flux density $B;$ these being related by $B = \mu_o(H + M) = \mu_o H + J$. This relationship can be used to convert the intrinsic M *versus H* magnetization characteristic into the usual B *versus H* magnetization characteristic shown in figure 32.12. The B *versus H* characteristic is more useful for practical magnet design since M exists only within the magnet while B 'flows' through the magnet and in the surrounding media.

The B within a magnet is indicative of the flux density it will deliver into the adjacent air gap, and the point at which a magnet operates on its demagnetization curve relates B to the *de*magnetizing force *-H* it

experiences. The demagnetization curve shows that as the magnitude of *-H* increases, the flux density delivered by the magnet falls, ultimately at $H = -H_{ci}$ to $B = 0$. However, an unconstructive phenomenon begins within the magnet before *-H$_{ci}$* is reached, because the *knee* (Cunic point) in the demagnetization curve represents the onset of a reversal of the material's *M* (that is, the threshold for irreversible loss, where the characteristic rapidly leaves the second quadrant and moves into the third quadrant). Thus it is desirable that the operating point of a permanent magnet always remain above the temperature dependant *knee* in the demagnetization curve.

The second quadrant of a hysteresis loop (the *demagnetization curve*) is usually employed for analyzing a permanent-magnet material. Residual flux density or remanent magnetization is B_r, while coercivity, H_c, is a measure of the magnitude of the mmf required to demagnetize the material, and the capability of the material to produce flux in a magnetic circuit that includes an air gap.

Magnets are characterized by the three main characteristics.
- Residual Induction or Remanent flux density (B_r, measured in Tesla).
  - An indication of how strong the magnet is capable of being.
- Coercive Force or Coercivity (H_c, measured in kA/m).
  - An indication of inherent stability and how difficult it is to demagnetize the magnet.
- Maximum Energy Product per unit volume (BH_{max}, measured in kJ/m^3).
  - An indication of the magnet material volume required to produce a given level of magnetic flux. It is where the magnetic field energy density into the air gap surrounding the magnet, is at a maximum, i.e., the operating point that minimises magnet volume.

The temperature dependence of residual induction and coercive force are modelled by

$$B_r\left(T\right) = B_{r\,20°C}\left(1 + \alpha\left(T - 20°C\right)\right)$$
$$H_{ci}\left(T\right) = H_{ci\,20°C}\left(1 + \beta\left(T - 20°C\right)\right)$$

(32.3)

where reversible temperature coefficient of B_r and H_{ci} (and H_c), specifically *α* and *β* respectively, are defined as

$$\alpha = \frac{\Delta B_r}{B_r} \times \frac{1}{\Delta T} \times 100\% \qquad\qquad \beta = \frac{\Delta H_{ci}}{H_{ci}} \times \frac{1}{\Delta T} \times 100\%$$

(32.4)

Behaviour of a permanent magnet is referenced to the second quadrant of its *B versus H* curve, where it is termed the *demagnetization curve*. The second quadrant of the curve (b-o-c), shown in figure 32.14c, can be used to demonstrate the demagnetisation characteristics of a permanent magnet material.

Most magnetic materials are classed as *anisotropic*, that is, a preferred magnetic axis is determined during manufacturing so that the magnets can only be magnetised in that predetermined direction. *Isotropic* materials may be magnetized in any direction, but generally have inferior performance than anisotropic grades.

- Remanence is the intercept of the *B versus H* curve on the positive *B* axis. For an *ideal* material, its value is $B_r = \mu_o M_{sat}$, but B_r is always the value of flux density for the condition when a magnet develops no magnetizing force ($H = 0$). Magnetization *M*, a bulk material property, is the sum of the magnetic dipole moments μ_m per unit volume [M_{sat} is saturation magnetisation, A/m]. B_r is coincident to both the intrinsic *J-H* curve and the normal *B-H* curve.
- Coercivity is the intercept of the *B versus H* curve on the negative *H* axis. Its value *-H$_c$* is the magnetizing force required to reduce the magnet's flux density *B* to zero, which on the *ideal* curve in figure 32.14c, is *-H$_c$ = M$_{sat}$*. There is no observable (external) field because the applied field *H* (specifically, *H$_c$*) is balanced out by the flux *M* of the magnet material. Because they are opposing, the net observable induction *B*, is zero. Notice that by comparing the *normal* and *intrinsic* characteristics, the values of *-H$_c$* and *-H$_{ci}$* are not the same, that is, the magnetizing force *H$_c$* required to make *B* = 0 may be less than that required to reduce the net observable flux density B to zero, namely *H$_{ci}$*, after which the material's magnetization direction is reversed.
- Maximum energy product *BH$_{max}$* is the point on the second quadrant *B versus H* curve at which the product of *B* and *H* for the magnet is a maximum. On the *ideal* curve in figure 32.14, it is located exactly halfway down the second quadrant line, with a value of *-BH$_{max}$ = μ_o(½M$_{sat}$)²*.

Generally $\mu_o M_s = J_s > B_r$, $B_r \geq \mu_o H_c$, $H_{ci} \geq H_c$, and $\frac{1}{4}B_r^2 \geq \mu_o BH_{max}$. The slope of the normal curve at the *B*-axis intercept is called the recoil permeability, $\mu_o \mu_{rc}$. The third and fourth quadrants are the same as the first and second quadrants, except have the 'opposite' polarities. The whole curve forms the hysteresis loop.
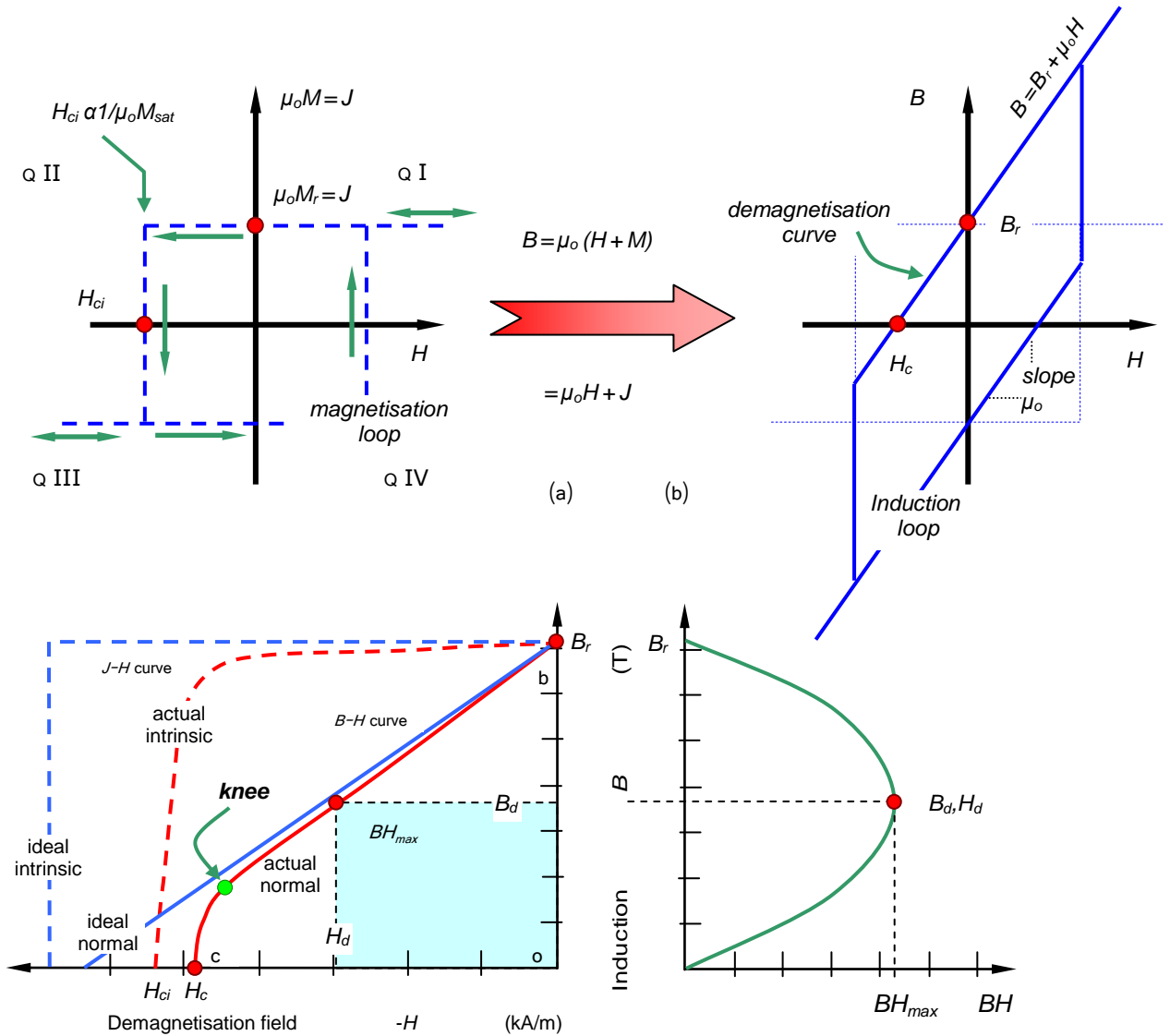
Figure 32.14. *Magnetic material curves: (a) ideal magnetisation loop, (b) ideal induction loop, and (c) second quadrant hysteresis loop for a sintered magnet.*

Several characteristics have to be taken into consideration when deciding which permanent magnetic material to use, namely:

- Flux related requirements of:
  - energy stored in the material;
  - flux density on the surface of the magnet; and
  - pull required to remove the magnet from a flat piece of steel.
- Maximum operating temperature.
- Cost.
- Availability.
- Degree of corrosion likely to be encountered.
- Magnetic stability required.
- Size and/or weight limitations.

General relative characteristics are shown in figure 32.15 and the following design points are related sequentially to the data columns in Table 32.5.

i. A method of comparing the magnetic performance or the capability of different types and grades of permanent magnet is to consider their maximum energy product BH_{max}. This is the operating point where the magnet will provide most energy for a minimum volume. When the permanent magnet behaves linearly with a constant recoil permeability μ_{rc} the maximum energy product can be expressed simply by:

$$BH_{max} = \frac{B_r^2}{4\mu_{rc}} \qquad \text{J/m}^3 \qquad (32.5)$$

A material with the largest available maximum energy product results in the smallest required magnet volume. Maximum energy products for various hard magnetic materials are shown in Table 32.5.
Ignoring leakage flux, for a permanent magnet with an air gap, the air gap flux density and mmf's are:

$$B_g = \frac{A_m}{A_g} B_m \tag{32.6}$$

$$\frac{H_m \ell_m}{H_g \ell_g} = -1 \tag{32.7}$$

Combining gives
$$B_g^2 = \mu_o \frac{\ell_m A_m}{\ell_g A_g} \left(-H_m B_m\right) = \mu_o \frac{Vol_{mag}}{Vol_{air-gap}} \left(-H_m B_m\right) \tag{32.8}$$

where $B_g = \mu_o H_g$. That is

$$Volume_{mag} = Volume_{air-gap} \frac{B_g^2}{\mu_o} \frac{1}{\left(-H_m B_m\right)} \tag{32.9}$$

Equation (32.9) indicates that, to achieve a desired flux density in the air gap, the required magnet volume can be minimized by operating the magnet at the point of maximum energy product.

ii. Table 32.5 shows typical pole face flux densities for the various hard magnetic materials when operating near their BH_{max} point. This point is not at the remanence B_r, which is the induction under closed magnetic circuit conditions.

iii. The attraction force F between a permanent magnet and a soft magnetic body depends on three factors:
> B = flux density on the pole face
> A = area of the pole face
> μ = permeability of the material being attracted

and the force is given by:

$$F = B^2 A\mu \tag{32.10}$$

iv. There are two distinct temperature related loss categories, namely reversible and irreversible losses.
The *reversible* changes with temperature are dependant on material composition and are unaffected by shape, size or working point on the demagnetisation curve. This loss vanishes without need for remagnetisation when the magnet returns to its initial temperature.
Irreversible losses do not occur until a certain temperature, the Curie temperature T_C, has been exceeded. Unrecoverable losses occur when excessive temperatures are reached and metallurgical changes occur within the magnet. This loss can also be limited by operating at a high as possible working point (well above the *knee*, near B_r).

v. The maximum working temperature, before irreversible losses commence, is dependant on the magnet working point in the magnetic circuit. The higher the working point up the *B-H* demagnetising characteristic curve, the higher the temperature at which the magnet can operate. Irreversible losses can be recovered by remagnetising the magnet.

vi. Each magnetic material has a maximum temperature, above the Curie temperature, where metallurgical changes occur within the magnet structure and where the individual magnetic domains randomise due to the high level of thermal agitation. Once these losses occur they cannot be reversed by remagnetising.

vii. The effects of low temperatures are different for each material group and are also related to the magnet shape and therefore its working point on its demagnetization curve.

viii. The temperature has a significant effect on magnet stability, but exposure to high external fields, *H*, influences magnets as follows:
- It is possible to ensure magnetic stability, by pre-exposing the magnet to possible detrimental influences by thermal cycling and controlled demagnetizing fields (ageing) techniques.
- Another cause of performance loss is total composition structural breakdown due to corrosion or in the case of NdFeB, exposure to hydrogen.

ix. There are many protective coatings used to help prevent corrosion in magnets.
Samarium cobalt, alnico, and ceramic materials are corrosion resistant, and typically do not require to be coated against corrosion.
Alnico is easily coating for cosmetic purposes with a powder coating or electroplating when required.

Ceramics may be coated to seal the surface, which will otherwise be covered by a thin film of ferrite powder, which does not create a problem in most applications.

Magnets using rare earth (non-precious) elements are highly reactive at elevated operating temperatures in the presence of moisture, due to their strong negative electrochemical standard potential, between -2.2V and -2.5V. Rare-earth-hydroxide is formed, releasing hydrogen, which then reacts with free rare earth metal, forming rare earth metal hydrides. With $SmCo_5$ or Sm_2Co_{17}, by adding cobalt, the reaction with water is suppressed.

In the case of NdFeB magnets, which are particularly susceptible to corrosion, the individual magnet grains are held together mechanically and fixed to each other by the so-called neodymium-rich phase, so the neodymium reacts with water to form neodymium hydroxide. Addition of cobalt to the neodymium-rich phase improves the corrosion behaviour by systematically stopping intergranular corrosion in a warm, humid atmosphere. The corrosion behaviour of such alloys is similar to that of pure iron materials (steel). In cases where the humidity turns to condensation, the materials gradually rust forming non-magnetic (antiferromagnetic) metal oxides or hydroxide, similarly to red rust in the case of iron. In applications with possible condensation, hard magnetic parts should be coated. Spray coatings are either metallic (galvanic nickel 10µm thick and/or tin 15 to 30µm thick, or 5µm of electrically isolating aluminium – aluminium chromate vacuum deposited) or organic (5µm and 40µm of epoxy resin, lacquer, parylene or polyxylylene polymers.

x. Shape, tolerances, and quantity influence the prices of specific magnets but the most significant factor is the cost of the basic raw material.

Other design factors include time (magnetic creepage, energy loss of typically less than 1×10^{-5} pu per annum at 20°C), radiation, shape, weight (for example, NdFeB magnets are about 13% lighter than SmCo magnets), and shock and vibration. All these are factors affecting magnet stability. Stability can be described as the repeated magnetic performance of a material under specific conditions over the life of the magnet.

Summary of 2nd quadrant demagnetisation characteristics of different hard magnetic materials

Table 32.5. Hard magnetic material characteristics and properties

Material	structure	Energy BH_{max}/ recoil μ_{rc}	fux density/ coercivity	pull	α_r	T_{op}	T_C	Low T_{op}	magnetic stability	corrosion resistant	cost relative
		kJm^{-3}	T / kA/m	kg/cm^2	% / °C 20°C - 150°C	°C	°C		Thermal α/B_r %/K		
Design sequence stage		i	ii.	iii.	iv	v	vi	vii	viii	ix	x
Ferrite	anisotropic	24/1.15	0.5/180 0.1T typ	0.26	- 0.19	250	460	Large irreversible losses below -60 °C	poor -0.2	excellent	low x1
Ferrite	bonded	3-8/1.1	0.2/130	0.06	- 0.2		450				
Alnico	anisotropic	40/3	1.0/120 0.13T typ	0.42	- 0.02	540	860	Permanent losses of no more than 10% are to be expected down to 4K	excellent -0.02	fair	medium x5
Alnico	casted	38/	0.7/100	0.42		540	850				
SmCo	Sintered 1:5	144/1.05	1.0/ 0.28T typ	1.50	- 0.04	250	700		excellent -0.035	excellent	
SmCo	Sintered 2:17	200/1.1	1.2/800 0.32mT typ	2.08	- 0.03	300	750	Minimal losses down to 4K	excellent -0.03	excellent	very high x20
SmCo	Bonded 1:5	55/1.1	0.7/750	0.60			870				
NdFeB	N38H	256/1.05	1.3/800 0.4T typ	3.06	- 0.12	50-200	320	No irreversible losses down to 77K	moderate -0.13	poor	high x10
NdFeB	bonded	110/1.1	1/800	1.20	- 0.08		310				
ferrite	flexible	5/	0.16/110		- 0.14	100					low
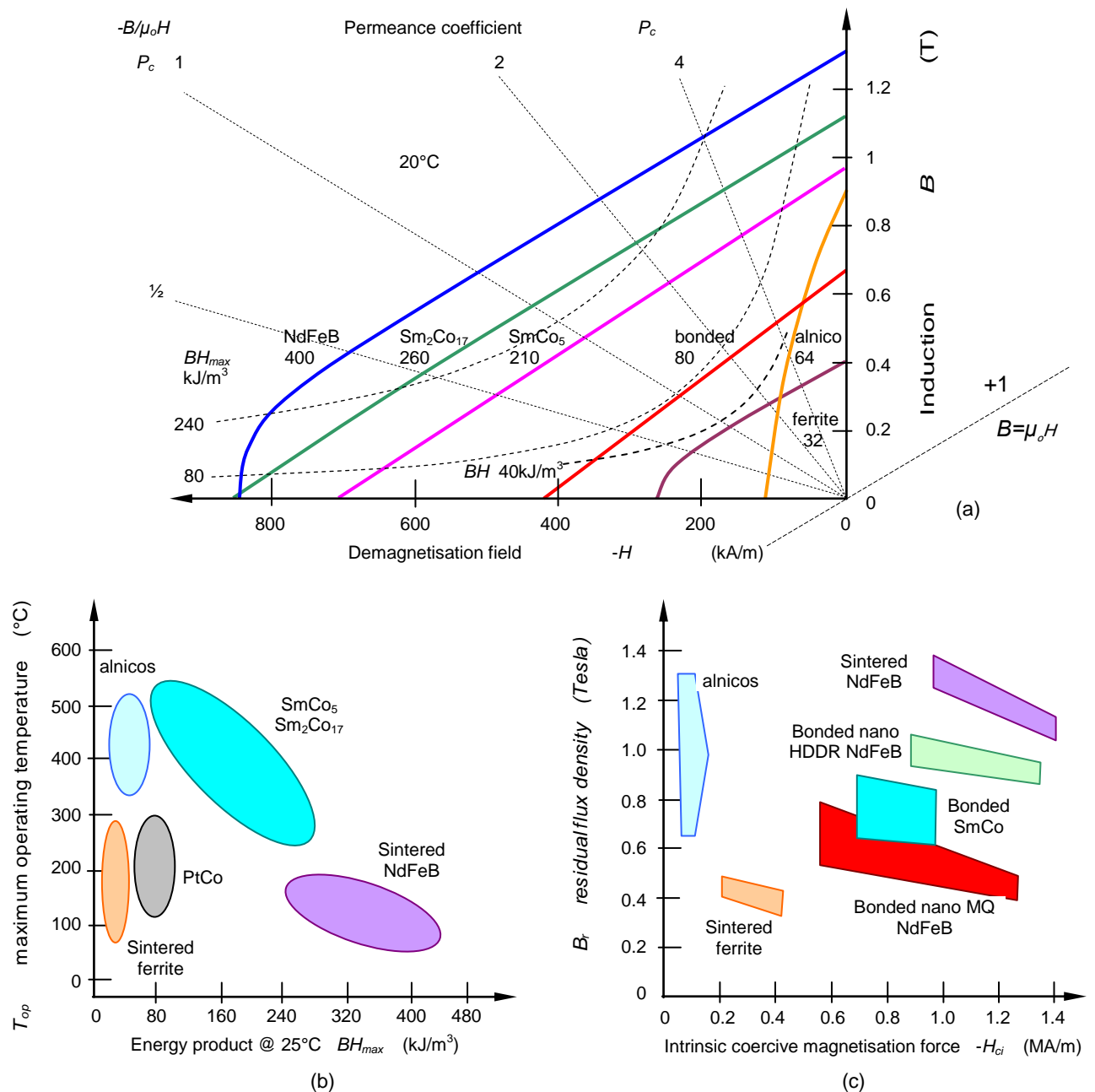
Figure 32.15. *Comparison of different magnetic materials: (a) second quadrant hysteresis loop demagnetization characteristics (with constant energy contours shown), (b) energy product versus maximum operating temperature, and (c) remanence versus intrinsic coercive force.*

32.4 **Permanent magnet magnetization curve (hysteresis loop) and recoil**

The magnetic circuit in figure 32.16a includes a section of un-magnetised hard magnetic material in a core of highly permeable soft magnetic material and an *N*-turns excitation winding. In figure 32.16c, it is assumed that the hard magnetic material is initially un-magnetized (corresponding to point *a*, the origin, in figures 32.16a and b) and current is applied to the excitation winding. Because the core is assumed to be of infinite permeability, the horizontal axis of figure 32.16c can be considered to be both a measure of the applied current $i = H\ell_m / N$ as well as the *H* field intensity in the magnetic material.

The magnetic circuit of figure 32.16a can be used to magnetize hard magnetic materials. The process requires a large excitation current be provided through the winding, thereby attaining point *b*, which is then reduced to zero, leaving the material with a remanent magnetization (or residual induction) B_r (point *c* in figure 32.16c).

With reference to figure 32.16c, the magnetization process progresses through four stages:

Stage 1. The permanent magnet starts in an initially unmagnetized state at field intensity $H = 0$ and flux density $B = 0$, point '*a*' in figure 32.16c.

Stage 2. As the current i in the coil is increased to a maximum, i_{max}, the B-H trajectory rises from point a in figure 32.16c to a maximum (H_{sat}, B_{sat}) at point b. It is assumed that driving the core well into saturation with field strength H_{sat} at point b, fully magnetizes the hard magnetic material.

Material	B_{sat} (T)	H_{sat} (kA/m)
Alnico5	0.3	300
Alnico8	0.8	500
Ferrite	1.0	900
$SmCo_5$	2-3	3000
Sm_2Co_{17}	2.5-3	3500
NdFeB	2.5-3	4000

Figure 32.16. *Magnetisation of a permanent magnet:*
(a) magnetic circuit incorporating a permanent magnet and an excitation winding,
(b) four quadrant B-H characteristics, and (c) portion of a B-H characteristic showing a minor loop, a recoil line and magnetic induction B_{sat} required to magnetise various permanent magnet materials.

Stage 3. Subsequently, when the coil current is decreased to zero (the external applied magnetising field intensity decreases to zero); the flux density from within the permanent magnet material also decreases. The *B-H* characteristic traverses part of a hysteresis loop, moving to point c at zero current. At point c, the applied field intensity H in the material is zero but the flux density B is at its remanent value B_r. Through hysteresis mechanisms, the magnet retains flux density B_r (retentivity if the magnetising force reached saturation - residual flux density if the magnetizing force did not reach saturation).

Stage 4. With the introduction of an air gap and/or an external demagnetizing field (current direction in the coil is reversed), the magnet operates within the second quadrant of the demagnetization curve, where H is negative and B is positive. The slope of the demagnetization curve in the second quadrant, as shown in figure 32.16c, is μ_m. Permeability μ_m is typically close to μ_o, the magnetic permeability of free space. With increased current, the intersection of the demagnetization curve with $B = 0$ occurs at $H = -H_c$, point g, where H_c is known as the coercivity (coercive force) of the magnetic material.

Assuming a linear demagnetising curve, the magnetic circuit second quadrant operating point conforms to the following mathematical relationship between flux density, B, and field intensity, H:

$$B = B_r + \mu_m H \tag{32.11}$$

The created (hysteresis) loops are a graphical representation of the relationship between an applied magnetic field and the resulting induced magnetization within a material. The field that is generated by the now magnetized material (orientated domains), B_i, when added to that of the applied field, H, is known as the normal induction, B_n, or simply B. This induction has two components (*normal* and *intrinsic* curves), and they are related by:

$$B_n = B = \mu_o M + \mu_o H = J + \mu_o H \tag{32.12}$$

The B versus H curve is known as the *normal* curve, while the J versus H curve is called the *intrinsic* curve (polarisation $J = \mu_o M$). These curves, also called hysteresis loops, are shown in figure 32.16b. The loops show the properties of the magnetic material as it is cycled between magnetization (saturated) and demagnetization (under the influence of an external magnetic field). The second (and third) quadrant of the loops display the magnetic properties as the magnet performs work.

When the current is reversed from zero to $-i_d$, the *B-H* characteristic operating point traverses along a hysteresis loop with a trajectory from point *c* to point *d*. If the current is maintained at $-i_d$, the magnet operating point is maintained at point *d*, where H_d, B_d generally denotes the operating point on the second quadrant demagnetising curve. This same operating point would be attained if the material were to start at point *c*, and with zero current excitation, from equation (32.8), an air gap of length $\ell_g = \ell_m (A_g / A_m)(-\mu_o H_d / B_d)$ were introduced into the core. If the current becomes more negative, the trajectory continues to trace out the hysteresis loop toward point *e*. If instead of increasing the current magnitude, it is reduced from $-i_d$ to zero, the trajectory does not retrace the hysteresis loop toward point *c*. Rather it inscribes a minor hysteresis loop, reaching point *f* at zero current. If the current is then varied between zero and $-i_d$, the *B-H* characteristic operating point traces out the minor loop shown in figure 32.16c. Unlike soft magnetic material, the absence/removal of an external magnetic field does not lead to demagnetization.

The *B-H* trajectory between points *d* and *f* can be represented by a straight line, termed the *recoil line*, with a slope $\mu_o \mu_{rc}$, where μ_{rc} is defined as the relative recoil permeability. At the vertex of the minor hysteresis loop, point *d*, the material has been partially demagnetized, with the effective remanent magnetization of the magnetic material having been reduced to that represented by point *f*, which is less than the remanent magnetization B_r, point *c*. If the demagnetization is increased past point *d*, to point *e* of figure 32.16c, a new minor loop will be created, with a new recoil line but with a similar recoil permeability (slope $\mu_o \mu_{rc}$). If the demagnetizing field is increased beyond point *g*, H_c, the operating point of the magnet now moves into the third quadrant of the normal curve. Recoil still results in a positive remanence flux density. Before the intrinsic coercivity H_{ci} is reached, which is show in figure 32.16b, the magnet becomes completely demagnetized, since recoil is back to the origin, point *a*. When H_{ci} is reached and exceeded, the recoil flux density is negative, below point *a*. Intrinsic coercivity H_{ci} is therefore a measure of a magnet's ability to resist demagnetization.

The demagnetization effects of negative current excitation are equivalent to the introduction of an air gap into the magnetic circuit (up to an operating point, H_{ci}, 0 on the intrinsic curve). If the magnetized material were removed from the core, this is equivalent to creating a large air gap in the magnetic circuit, therein demagnetizing the hard magnetic material. The magnet is effectively weakened, since if it were re-inserted into the magnetic core, it would follow a recoil line and return to a remanent magnetization operating point (to point *f*) less than B_r. Hard magnetic materials such as Alnico materials, often do not operate stably with varying mmf and geometry conditions, since they can be significantly demagnetize due to improper operation. An advantage of magnetic materials such as ceramic ferrite, samarium-cobalt, and neodymium-iron-boron is that, because of their 'straight-line' characteristic in the second quadrant (with slope close to μ_o), their recoil lines closely match their magnetization characteristic. As a result, demagnetization effects are reduced. At the expense of a modest reduction of the remanent magnetization, hard magnetic materials can be stabilized to operate over a specified field region.

32.5   Permanent magnet model

When a magnetic field is imposed on a permanent magnet, intrinsic induction J is created. The free poles establish a field potential $-H_d$ between free poles. The field potential is due to some of the magnetization J lost internally. The field potential $-H_d$ associated with a permanent magnet is a due to the magnetization J and is 180° opposed to J. The magnitude of $-H_d$ depends on the geometry of the magnet including the spacing of the poles. These relationships are shown pictorially in figure 32.17.

The behaviour of a permanent magnet is described with reference to the second quadrant of its *B-H* curve, termed the demagnetization curve. For reference, the *ideal* curves in figure 32.17 are shown in blue. A practical permanent magnet material neither achieves its theoretical intrinsic coercivity $-H_{ci}$, nor does the entire magnetization flip over exactly when a reverse field of $-H_{ci}$ is reached. The practical

intrinsic demagnetization curve, shown dashed red in figure 32.17 does not have an abrupt transition at -H_{ci}, but rather a *knee* in the curve represents a more gradual reversal of the material's magnetization. The actual normal demagnetization curve, shown solid red in figure 32.17 mirrors this *knee*. The coercivities -H_{ci} and -H_c are now defined as the intercepts of the practical intrinsic and normal curves with the *H*-axis.

The *B* from within the magnet is the flux density that can be delivered into the adjacent air gap, and the point at which a magnet operates on its demagnetization curve relates *B* to the experienced demagnetizing force -*H*. The demagnetization curve shows that as the magnitude of -*H* increases, the flux density produced by the magnet falls, ultimately at $H = -H_c$ to $B = 0$. However, before -H_{ci} is reached, the *knee* in the demagnetization curve signifies the onset of a reversal of the material's magnetisation *M*. It is therefore desirable that the operating point of a permanent magnet remain above any *knee* (Cunic point) in the demagnetization curve - at all operating temperatures.
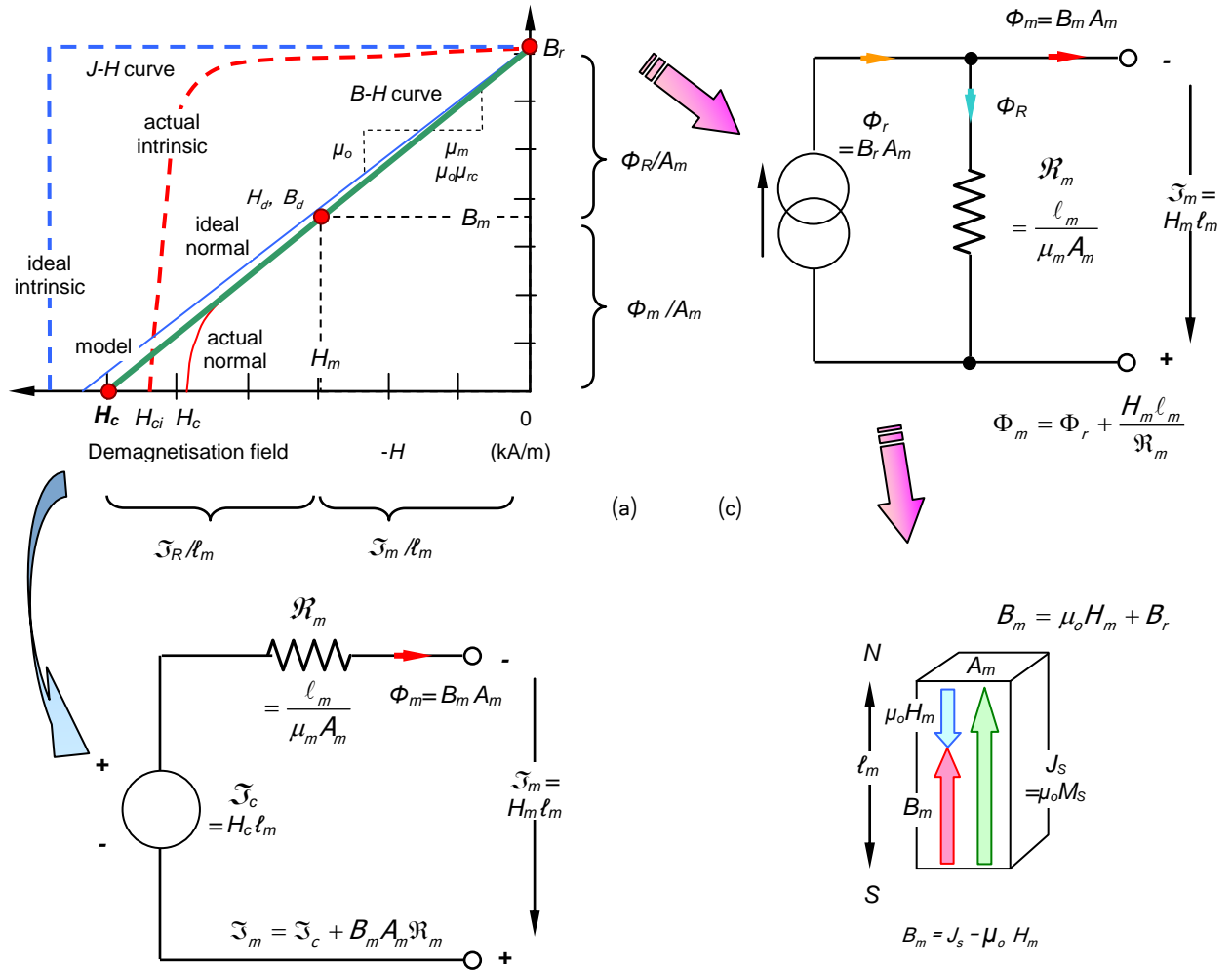

Figure 32.17. *Magnetic circuit models of a magnet based on:*
(a) a linear demagnetization curve, (b) mmf source equivalent series circuit, (c) flux source equivalent shunt circuit, and (d) magnet internal fluxes.

Consider a permanent magnet of uniform cross sectional area A_m and length ℓ_m. The demagnetization curve of the magnet is a straight line with a coercive force of H_c and a remanent flux density of B_r as shown in figure 32.17. A point H_d, B_d on a linear demagnetization B_m - H_m curve can be defined by

$$\boldsymbol{B_m} = B_r + \mu_m \boldsymbol{H_m} = \frac{B_r}{H_c}\left(H_c + \boldsymbol{H_m}\right) = \mu_m\left(H_c + \boldsymbol{H_m}\right) \tag{32.13}$$

where $\mu_m = B_r / H_c$ is the permeability of the permanent magnet, which is slightly greater than μ_o, the permeability of free space. For NdFeB and SmCo$_5$ sintered magnets, $\mu_m = 1.05\,\mu_o$, as listed in Table 32.5.

Equation (32.13) shows that the demagnetisation curve can be defined in terms of μ_m and either B_r or H_c. If H_c is used as a reference, the model will be based on an mmf source $H_c\ell_m$ in series with the magnet reluctance $\mathfrak{R}_m$. If B_r is used as a reference, the model will be based on a flux source $B_r A_m$ in parallel with the magnet reluctance $\mathfrak{R}_m$. The two models are equivalent, and in electrical circuit terms, behave as Thevenin and Norton equivalent circuits, as illustrated in figure 32.17.
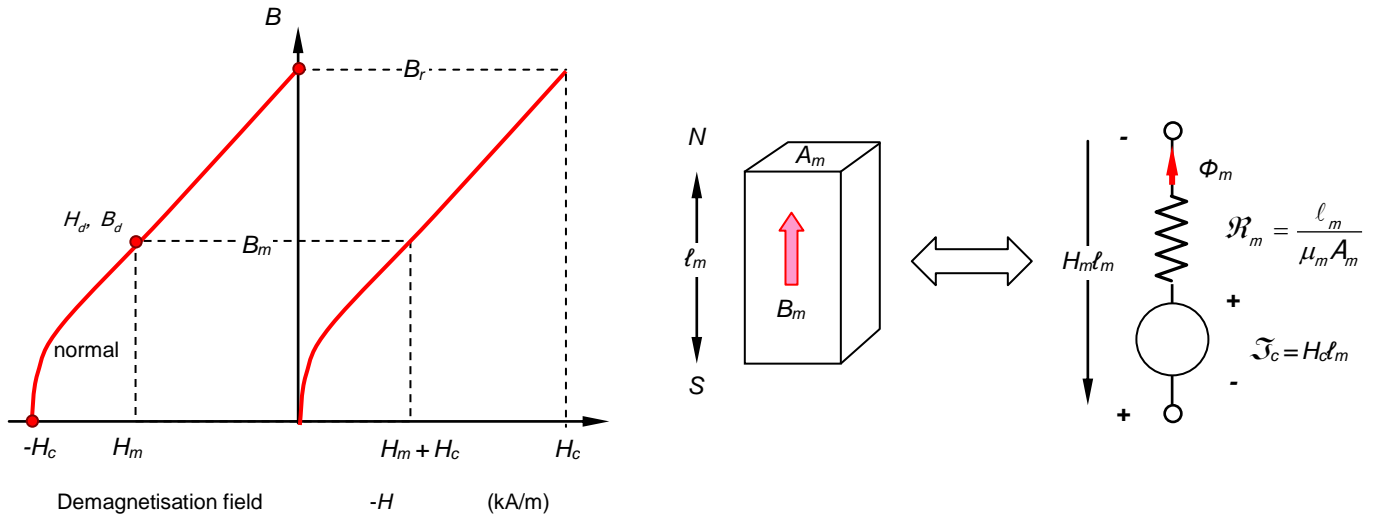
32.18. *Magnetic circuit Thevenin model of a magnet with nonlinear demagnetization curve.*

Thevenin equivalent magnetic circuit

The traditional, less intuitive modelling approach is based on an mmf source in series with the magnet reluctance. From equation (32.13) rearranged, the magnetic mmf across the magnet, using flux $\Phi_m = B_m A_m$, can be expressed as

$$H_m \ell_m = \left(\frac{B_m}{\mu_m} - H_c \right) \ell_m = \frac{\ell_m}{\mu_m A_m} \phi_m - H_c \ell_m = \mathfrak{R}_m \phi_m - \mathfrak{I}_c \qquad (32.14)$$

$\mathfrak{R}_m = \ell_m / \mu_m A_m$ is the magnet reluctance and $\mathfrak{I}_c = H_c \ell_m$ the magnetomotive force (energy source) of the magnet. In a magnet, B_m and H_m, being in the second quadrant, oppose. The series equivalent circuit satisfying the sum of mmf's around a closed loop summing to zero, is shown in figure 32.17b.

For a magnet with a nonlinear demagnetization curve, the magnetic circuit model in figure 32.17 remains valid, except that the magnetic permeability is

$$\mu_m = \frac{B_m}{H_m + H_c} \qquad (32.15)$$

which is a function of the magnetic field in the magnet. The magnetic circuit model derivation of a nonlinear magnet is illustrated graphically in figure 32.18.

The operating point (H_d, B_d) does not move along the nonlinear demagnetization curve if a small cyclic external magnetic field (such that the magnet will not be demagnetized) is applied to the magnet. Instead, the operating point moves along a minor loop or for simplicity, a straight line (centre line of the minor loop) as illustrated in figure 32.19.
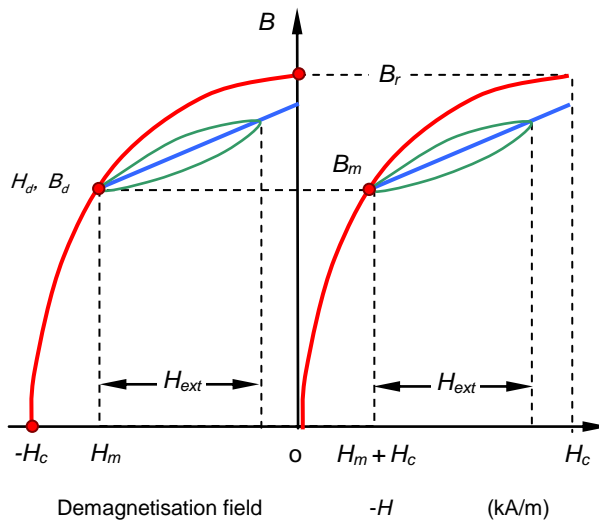

Figure 32.19. *Movement of operating point of a nonlinear magnet under an external field H_{ext}.*

Norton equivalent magnetic circuit

From equation (32.13) rearranged, the magnetic flux from magnet, using flux $\Phi_m = B_m A_m$, can be expressed as

$$\boldsymbol{B_m}A_m = B_rA_m + \mu_m\boldsymbol{H_m}A_m = B_rA_m + \frac{\mu_mA_m}{\ell_m}\boldsymbol{H_m}\ell_m = B_rA_m + \frac{1}{\mathscr{R}_m}\boldsymbol{H_m}\ell_m$$

$$\phi_m = \phi_r + \frac{\mathfrak{I}_m}{\mathscr{R}_m}$$

(32.16)

$\mathscr{R}_m = \ell_m / \mu_m A_m$ is the magnet reluctance, $\mathfrak{I}_m = H_m\ell_m$ the magnetomotive force across the magnet, and Φ_r is the energy source. In a magnet, B_m and H_m, being in the second quadrant, oppose. The equivalent circuit satisfying the three fluxes at a node summing to zero, is shown in figure 32.17c.
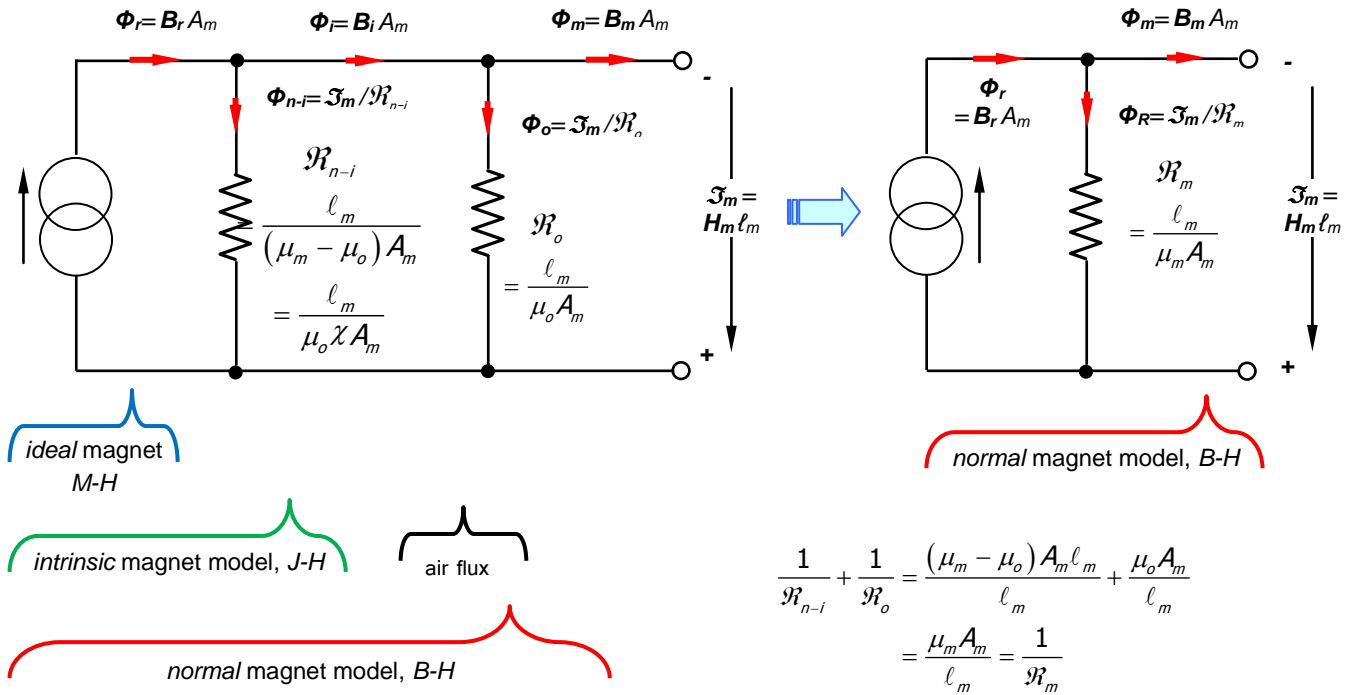

Figure 32.20. *Magnet internal model showing an intrinsic magnet model.*

In the case of NdFeB and SmCo magnets, there are several advantages in using a flux source model based on B_r rather than the series mmf model based on H_c.

- B_r is common to both the intrinsic and normal demagnetisation curves (H_c and H_{ci} differ).
- At a given temperature, the demagnetisation curve slope is near constant, $1/\mathscr{R}_m$, for an increasing reverse field, until a knee is reached. (With H_c as a reference, if a knee exists in the demagnetisation curve, the implied B_r is under estimated if a straight line demagnetising characteristic is used for modelling or analysis).
- A magnet is normally operated in the near linear region above any knee - B_r as a reference models this region independent of the existence and effects of any knee.
- The current source model in figure 32.20 clearly illustrates with two reluctances in parallel that the mmf, hence field intensity, must be the same value for the load operating point on the normal and intrinsic demagnetisation curves.

Both models yield the same mathematical solutions, since both yield the same demagnetisation load line equation, when using $B_r = \mu_m H_c$:

$$A_m\boldsymbol{B_m} = A_mB_r + \frac{1}{\mathscr{R}_m}\boldsymbol{H_m}\ell_m = \mu_mA_mH_c + \frac{1}{\mathscr{R}_m}\boldsymbol{H_m}\ell_m$$

or $\quad \boldsymbol{B_m} = B_r + \mu_m\boldsymbol{H_m}$

(32.17)

32.6 Load lines

One or more air gaps introduced into a magnetic circuit enable useful work to be exploited.

Magnet material can be designed to provide a specific air gap flux density, within a reasonable range. The exact flux density is determined by the magnetic circuit dimensions, particularly those of the permanent magnet and the air gap. The second quadrant of the magnet demagnetization *B-H* curve gives magnetic properties per unit magnet volume. The external magnetic circuit, termed the *magnetic load*, together with the demagnetization curve, specify the magnet's operating point on its demagnetisation curve.

Consider the magnetic circuit shown in figure 32.21a, where a permanent magnet, with magnetization M oriented as shown, drives flux clockwise into an air gap via two steel high permeability pole pieces. The steel high permeability, in conjunction with their shape, confines most of the magnetic flux from the magnet (area A_m, length ℓ_m) into the air gap (area A_g, length ℓ_g). The lines of magnetic flux are shown in figure 32.21b, and magnified in figure 32.21c, where leakage fluxes outside the air gap volume, termed fringing, are shown.
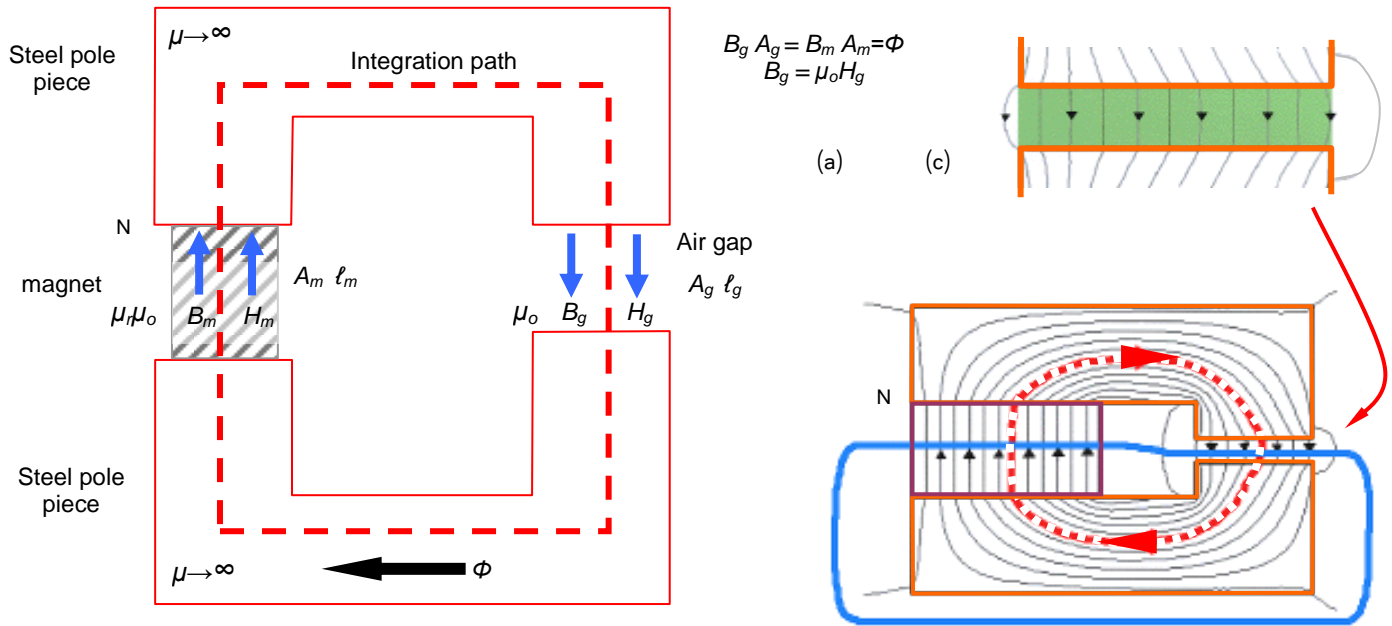

Figure 32.21. *Magnet in an iron circuit with an air gap:*
(a) magnetic circuit, (b) magnetic circuit flux lines, and (c) air gap flux and its leakage.

32.6.1 Magnetic Circuit Equations

Flux conservation gives the integral of flux density through a closed surface (equivalent to Kirchhoff's current law), while Ampère's law yields the integral of magnetizing force around a closed loop (equivalent to Kirchhoff's voltage law). These can be applied to the magnetic circuit shown in figure 32.21a, to derive its load line and hence find the flux density levels within the magnetic circuit. Any convenient surface and loop may be chosen to achieve these. The subscript m denotes the permanent magnet and g denotes the air gap, while s is for both steel pole pieces, and ℓ denotes the external regions into which some magnetic field leaks.

The magnetizing force $\boldsymbol{H}$ is integrated around the closed loop in the direction shown in red. No electrical currents passing through any surface spanning this loop, so $i = 0$. From figure 32.21a, as with Kirchhoff's voltage law around a closed loop, the closed integral has three series components:

$$\int_m H.d\ell + \int_s H.d\ell + \int_g H.d\ell = 0$$

$$\boldsymbol{H}_m \ell_m + \boldsymbol{H}_s \ell_s + \boldsymbol{H}_g \ell_g = 0$$

Since the steel pole pieces have a significantly higher permeability than either the magnet or the air gap, their mmf contribution is small, $\boldsymbol{H}_s \ell_s = 0$. It is therefore a simplification to either ignore this small component, $k_r = 1$ or to lump together the two external terms using a dimensionless *loss or reluctance factor* k_r, where $k_r > 1$. Outside the magnet, the magnetisation is zero, that is, $M = 0$. Each individual $\boldsymbol{H}\ell$ term is a magnetomotive force (mmf), $H_m \ell_m$ being the mmf across the permanent magnet and $\boldsymbol{H}_g \ell_g$ the mmf across the air gap.

$$\boldsymbol{H}_m \ell_m + k_r \boldsymbol{H}_g \ell_g = 0$$

Rearranging yields

$$\boldsymbol{H}_m = -k_r \frac{\boldsymbol{H}_g \ell_g}{\ell_m} \tag{32.18}$$

Integration of the flux density $\boldsymbol{B}$ through the closed surface shown in blue (Kirchhoff's current law), yields:

$$\boldsymbol{B}_m A_m - \boldsymbol{B}_\ell A_\ell - \boldsymbol{B}_g A_g = 0$$

Each term is the flux in the respective magnetic component, $B_m A_m$ being the flux from the permanent magnet, $B_g A_g$ the flux in the air gap, and $B_\ell A_\ell$ the total leakage flux. The magnet and air gap volumes are well defined, while the leakage regions are not. Because of the relatively high permeance of the steel, only a small percentage of the magnet flux does not pass directly through the air gap. A simplification is to incorporate the $B_\ell A_\ell$ leakage term into a dimensionless *leakage coefficient* k_ℓ, where $k_\ell > 1$, such that:

$$\boldsymbol{B}_m A_m - k_\ell \boldsymbol{B}_g A_g = 0$$

After lumping together the two fluxes external to the magnet, which are dominated by the gap flux, rearranging gives

$$\boldsymbol{B}_m = k_\ell \frac{\boldsymbol{B}_g A_g}{A_m} \tag{32.19}$$

The permanent magnet's demagnetization curve, shown in red in figure 32.22, gives its magnetic properties per unit volume as a characteristic relationship between B_m and H_m. The load line (in blue) gives the characteristics of the magnetic circuit, also in terms of B_m and H_m. The operating point (H_d, B_d) is the intersection of the two lines.

Since $\boldsymbol{B}_g = \mu_o \boldsymbol{H}_g$ in the air gap (where $M = 0$), equations (32.18) and (32.19) can be combined to give the load line (of slope $-\mu_o P_c = -S$) as:

$$\frac{\boldsymbol{B}_m}{\boldsymbol{H}_m} = -\mu_o \frac{k_\ell}{k_r} \frac{A_g \ell_m}{A_m \ell_g} = -\mu_o P_c = -S$$

where $P_c = \dfrac{A_g \ell_m}{A_m \ell_g}$ and k_ℓ / k_r is assumed to be unity.

That is

$$\boldsymbol{B}_m = -\mu_o \frac{A_g \ell_m}{A_m \ell_g} \boldsymbol{H}_m = -\mu_o P_c \boldsymbol{H}_m = -S \boldsymbol{H}_m \tag{32.20}$$
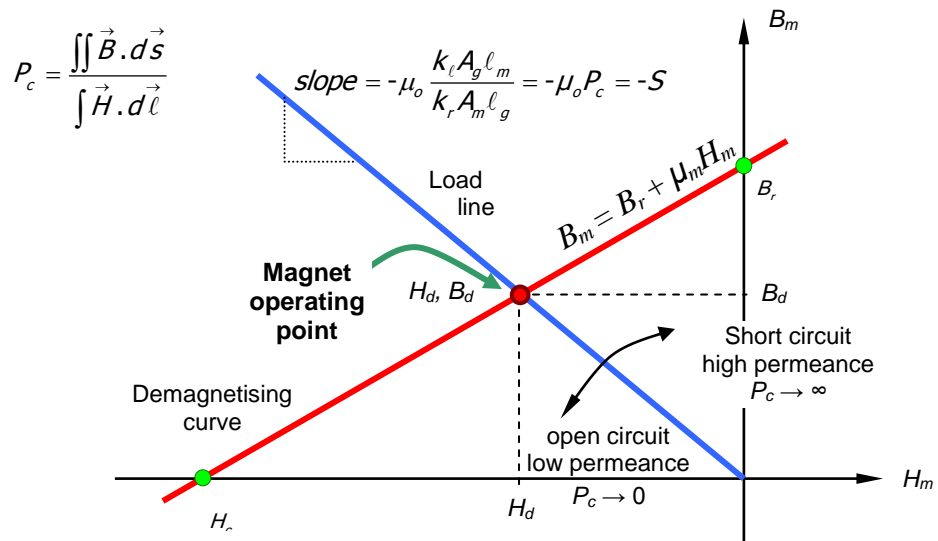

Figure 32.22. *Load line for a permanent magnet, air gap, and iron circuit.*

The intercept of the demagnetization curve ($B_m = B_r + \mu_m \boldsymbol{H}_m$) and the load line, equation (32.20), gives the magnet operating point B_d and H_d. The flux density and magnetizing force elsewhere in the magnetic circuit can then be derived from the foregoing equations, assuming $k_r = k_\ell = 1$.

$$\boldsymbol{B}_m = B_r + \mu_m \boldsymbol{H}_m = \mu_m H_c + \mu_m \boldsymbol{H}_m = -\mu_o \frac{A_g}{A_m} \frac{\ell_m}{\ell_g} \boldsymbol{H}_m = -S \boldsymbol{H}_m \tag{32.21}$$

$$\underbrace{\text{Second quadrant}}_{\text{demagnetising curve}} \qquad \underbrace{\text{Load line}}$$

The second and fifth equalities in equation (32.21) give

$$H_d = -\frac{B_r}{S + \mu_m} = -\frac{\mu_m H_c}{S + \mu_m} \tag{32.22}$$

From the first and last equalities in equation (32.21), on substitution of H_m from equation (32.22)

$$B_d = -SH_m = B_r \frac{S}{S + \mu_m} \tag{32.23}$$

From equation (32.19), the gap flux density $\boldsymbol{B_g}$, which can be used to calculate the gap energy, is

$$\boldsymbol{B}_g = \frac{A_m}{A_g} \boldsymbol{B}_m = \frac{A_m}{A_g} B_r \frac{S}{S + \mu_m} \tag{32.24}$$

As the gap closes to zero (soft magnetic material forms at least one closed path), $\ell_g \to 0$, with $A_g = A_m$ and $S \to \infty$:

$$H_m \to 0 \quad \text{and} \quad B_m \to B_r$$

As the gap goes to infinity (open circuit - no soft magnetic material), $\ell_g \to \infty$ and $S \to 0$:

$$H_m \to -H_c \quad \text{and} \quad B_m \to 0$$

The open circuit magnetic flux intensity specifies the Thevenin equivalent circuit mmf source, namely

$$\mathfrak{I}_c = H_c \ell_m$$

From the first and third equalities in equation (32.22), rearranged:

$$\boldsymbol{H}_m = -H_c + \frac{\boldsymbol{B}_m}{\mu_m} \tag{32.25}$$

Equation (32.18), in conjunction with the fact that the mmf's in the closed magnetic circuit loop are defined by multiply equation (32.25) by magnet length ℓ_m, gives

$$\boldsymbol{H}_m \ell_m = -H_c \ell_m + \frac{\boldsymbol{B}_m}{\mu_m} \ell_m$$

$$-\boldsymbol{H}_g \ell_g = -H_c \ell_m + \frac{\boldsymbol{B}_m}{\mu_m} \ell_m$$

Rearranging gives

$$H_c \ell_m = \boldsymbol{H}_g \ell_g + \frac{\boldsymbol{B}_m}{\mu_m} \ell_m \tag{32.26}$$

Assuming no leakage flux, then using $\boldsymbol{\Phi} = \boldsymbol{B_g} A_g = \boldsymbol{B_m} A_m$ this equation reduces to

$$\mathfrak{I}_c = H_c \ell_m = \phi \left(\mathfrak{R}_g + \mathfrak{R}_m \right)$$

where the gap (external magnetic load circuit) reluctance (whence gap permanence) is

$$\mathfrak{R}_g = \frac{\ell_g}{\mu_o A_g} = \frac{1}{P_g}$$

and the (Thevenin/Norton equivalent) reluctance (whence permanence) of the magnet, where $\mu_m = B_r / H_c$, is

$$\mathfrak{R}_m = \frac{\ell_m}{\mu_m A_m} = \frac{1}{P_m} \tag{32.27}$$

From equations (32.18) and (32.19), the magnet volume, V_m, is

$$V_m = \ell_m A_m = \frac{\ell_m \boldsymbol{H}_g^2 A_g}{B_m H_m}$$

Note: the magnet B_m-H_m curve intersects the general load line at the operating point H_d, B_d, and that BH_{max} will minimise the necessary magnet volume V_m.

32.6.2 Intrinsic permeance coefficient

From equation (32.20), the dimensionless permeance coefficient P_c is:

$$P_c = \frac{B_m}{\mu_o H_m} = \frac{A_g \ell_m}{A_m \ell_g} = \frac{\mu_m}{\mu_o} \frac{\mathfrak{R}_m}{\mathfrak{R}_g} = \frac{\mu_m}{\mu_o} \frac{P_g}{P_m} = \frac{1}{N_i}$$

$$S = \mu_o P_c = \frac{B_m}{H_m} = \mu_m \frac{\mathfrak{R}_m}{\mathfrak{R}_g} = \mu_m \frac{P_g}{P_m}$$

This permeance coefficient is also known as the *normal* permeance coefficient because it provides the slope for a line that originates at the origin and intersects the *normal* demagnetisation curve at the

magnet operating point (H_d, B_d). This operating condition point of the magnet also leads to the operating point on the *intrinsic* curve (provided current $i = 0$).

The intrinsic operating point (H_d, B_{di}), has an intrinsic permeance coefficient P_{ci} which is obtained by adding 1 to the P_c value, that is, $P_{ci} = P_c + 1$. This is because, from equation (32.12), $J = \mu_o (\mu_m - 1)H$. The intrinsic demagnetising factor N_i is defined as $N_i = 1/P_{ci}$, thus both factors are determined by the shape of the magnetic circuit.

The P_c and P_{ci} load lines are shown as positive on demagnetisation curves but arithmetically are negative slopes. Figure 32.23 shows the case of the P_c and P_{ci} plotted for a NdFeB magnet when $P_c = 1$ and $P_{ci} = P_c + 1 = 2$.
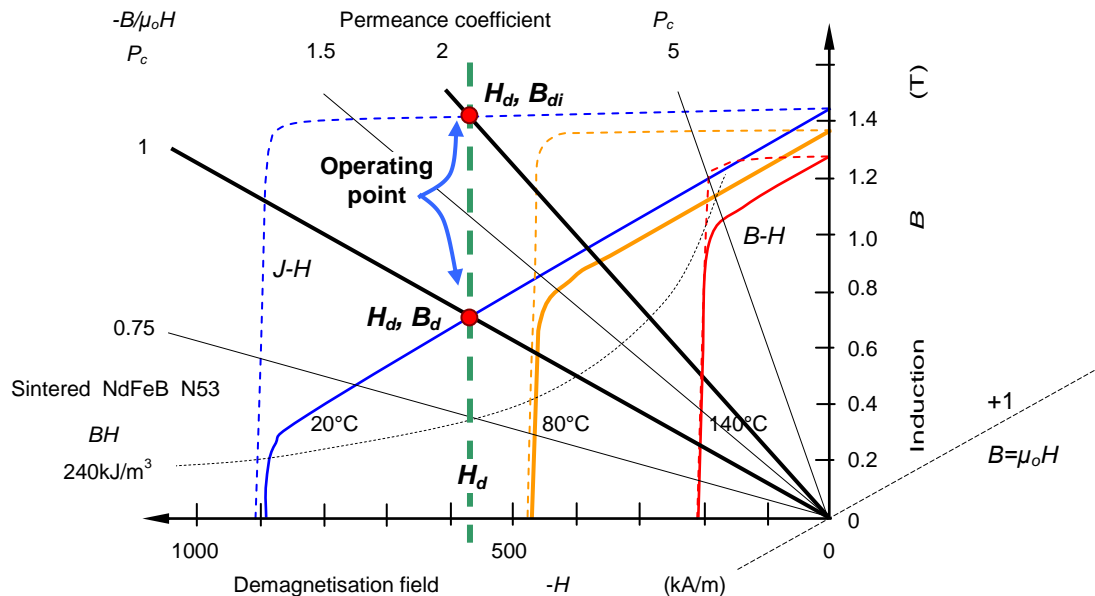

Figure 32.23. *Permanent magnet and gapped circuit load lines (constant energy contour shown).*

The P_{ci} and P_c straight load lines intersect the intrinsic and normal curves respectively with the same H_d value. This condition also occurs with an externally applied field (magnetising or demagnetizing influence) with or without air gap, which vertically shifts the common intersection origin of the P_{ci} and P_c lines by an amount related to the applied field (see section 32.6.3 and figure 32.28).

Example 32.1: *Magnet load dependant operating point*

Using an equivalent circuit approach, figure 32.17c; determine the magnet operating point, assuming a linear demagnetization characteristic, when:

    i.   A coil of *N* turns carries a demagnetising current *i*, wound on a core of infinite permeance, which is also the permeance seen by the magnet, and

    ii.   with zero coil current, an air gap of length ℓ_g is introduced.

Solution

From equation (32.21) the equation describing the magnet linear demagnetising characteristic in terms of three flux components, shown in figure 32.24, is given by

$$\boldsymbol{\phi_m} = \phi_r + \frac{\boldsymbol{\Im_m}}{\mathfrak{R}_m}$$

where $\boldsymbol{\Phi_m}$ is the intrinsic flux, $B_r A_m$. This three-term equation is common to any magnetic circuit loading the magnet. In order to obtain an operating point, the external magnetic loading circuit is expressed in terms of the magnet flux Φ_m and the magnet mmf $\Im_m$, that is, B_m and H_m respectively.

i. When the magnet is loaded by an external mmf *Ni*, which can tend to have either a remagnetisation or demagnetisation effect, the load circuit in terms of magnetic variables related to H_m and B_m is

$$\boldsymbol{\Im_m} = -\boldsymbol{Ni} \qquad\qquad \left(= \boldsymbol{H_m} \ell_m \right)$$

Substituting $\mathfrak{I}_m$ into the magnet load line equation yields magnet flux Φ_m:

$$\boldsymbol{\phi_m} = \phi_r - \frac{N\boldsymbol{i}}{\mathscr{R}_m} \qquad (= \boldsymbol{B_m A_m})$$

These two equations in terms of H_m and B_m give the operating point $H_d B_d$, specifically

$$\boldsymbol{H_m} = -\frac{N\boldsymbol{i}}{\ell_m} \tag{32.28}$$

and

$$\boldsymbol{B_m} = B_r - \mu_m \frac{N\boldsymbol{i}}{\ell_m} \tag{32.29}$$
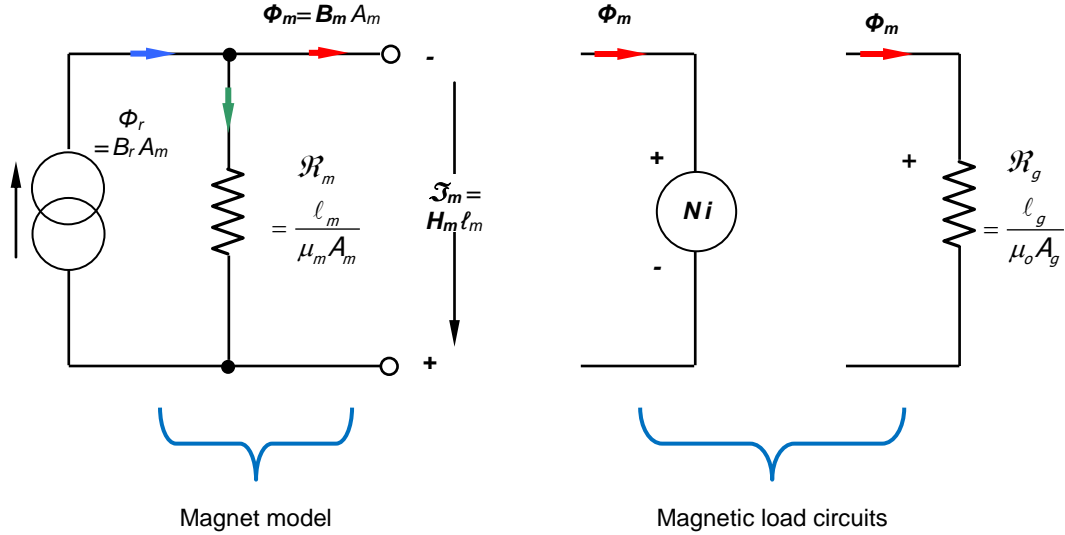

Figure 32.24. *Magnetic model for Example 29.1*

ii. When the magnet is loaded by the introduction of an air gap (progressively increased in length from initially zero to ℓ_g), the reluctance load circuit in terms of magnetic variables related to H_m and B_m is

$$\boldsymbol{\mathfrak{I}_m} = -\boldsymbol{\phi_m}\mathscr{R}_g$$

Solving the magnet load line equation and the load equation for magnet flux Φ_m and magnet mmf $\mathfrak{I}_m$ yields:

$$\phi_m = \frac{\phi_r}{1 + \dfrac{\mathscr{R}_g}{\mathscr{R}_m}} = \phi_r \frac{\mathscr{R}_m}{\mathscr{R}_g + \mathscr{R}_m}$$

(This is the same concept as a current (flux) dividing between two parallel-connected resistors (reluctances)).

Next, the magnet mmf is given by

$$\mathfrak{I}_m = -\phi_r \frac{\mathscr{R}_m \mathscr{R}_g}{\mathscr{R}_g + \mathscr{R}_m} = -\phi_r \frac{1}{\dfrac{1}{\mathscr{R}_g} + \dfrac{1}{\mathscr{R}_m}}$$

The two operating point expressions in terms of the specific operating point H_d and B_d are

$$B_d = \frac{B_r}{1 + \dfrac{\mathscr{R}_g}{\mathscr{R}_m}}$$

and

$$H_d = \frac{-B_r A_m}{\ell_m} \frac{\mathscr{R}_m \mathscr{R}_g}{\mathscr{R}_m + \mathscr{R}_g} = -H_c \frac{\mathscr{R}_g}{\mathscr{R}_m + \mathscr{R}_g} = -H_c \frac{1}{1 + \dfrac{\mathscr{R}_m}{\mathscr{R}_g}}$$

H_b and B_b can be rearranged, using $S = \mu_m \mathscr{R}_m / \mathscr{R}_g$, to yield equations (32.22) and (32.23).

For a given *B-H* demagnetisation characteristic, the operating point is determined solely by the ratio of the air gap reluctance and magnet reluctance.

The load line solutions are shown in figure 32.25. The operating point on the *B-H* characteristics will yield energy change per unit volume, $B \times H$, while the operating point on the BA_m versus $H\ell_m$ axes yields energy, $B \times H \times A_m \ell_m = B \times H \times Volume_m$.
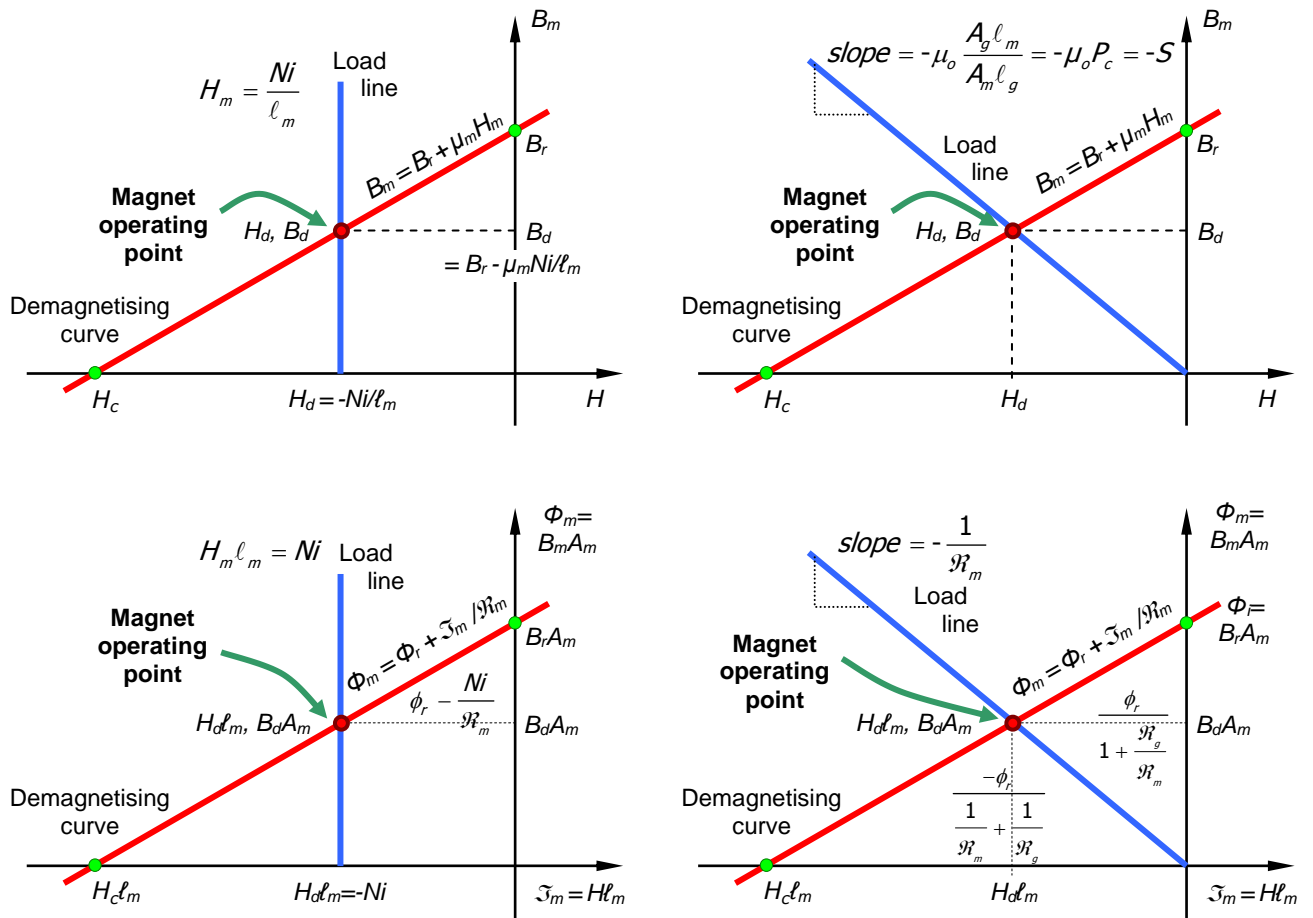

Figure 32.25. *Magnetic load line characteristics for problem 32.1.*

♣

32.6.3 Demagnetizing field

When a permanent magnet provides flux to a single air gap via two steel pole pieces, the specific dimensions of the magnet and air gap yield a unique load line, as shown in blue on figure 32.22. The permanent magnet material is characterized by its demagnetization curve (in red), the intercept between the two giving an operating point with a unique combination of B_d and H_d for the magnet in this condition. If the air gap length ℓ_g increases, the permeance, whence permeance coefficient, decrease, and the slope of the load line decreases and the magnet's operating point changes, moving down the curve.

Figure 32.26 shows the magnetic circuit in figure 32.21 with the addition of a coil of N turns carrying current i, with a direction that opposes (tending to demagnetise) the magnet (of area A_m, length ℓ_m) from delivering flux into the air gap (of area A_g, length ℓ_g). By integrating the magnetizing force H around the closed loop shown in red (Ampère's Law), where the loop is linked N times by the current i, the derived magnetic circuit equations are

$$\int H.d\ell = Ni$$

$$\boldsymbol{H}_m\ell_m + k_r\boldsymbol{H}_g\ell_g = N\boldsymbol{i} \tag{32.30}$$

Since

$$\boldsymbol{B_m}A_m = k_\ell\boldsymbol{B_g}A_g = k_\ell\mu_o\boldsymbol{H_g}A_g$$

Then, assuming $k_\ell/k_m = 1$:

$$\boldsymbol{B_m} = -\mu_o\frac{A_g\ell_m}{A_m\ell_g}\left(\boldsymbol{H_m} - \frac{Ni}{\ell_m}\right)$$

$$\boldsymbol{B_m} = -S\left(\boldsymbol{H_m} - \frac{Ni}{\ell_m}\right) = -\mu_oP_c\left(\boldsymbol{H_m} - \frac{Ni}{\ell_m}\right) \tag{32.31}$$
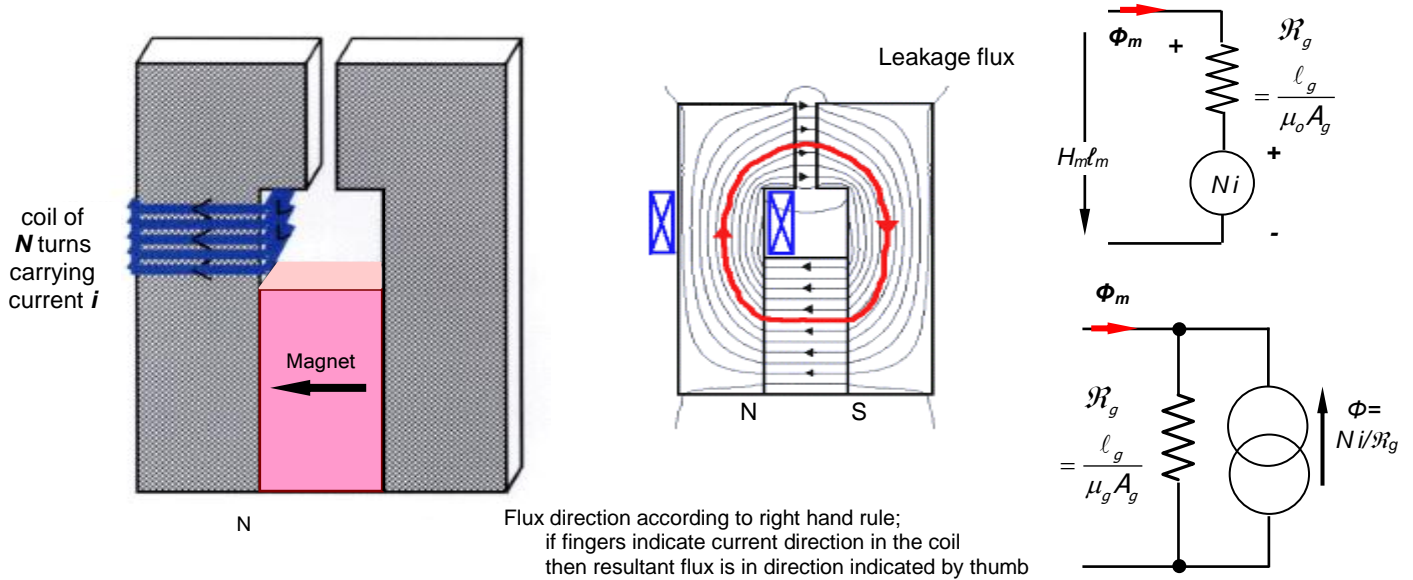
Figure 32.26. *Magnetic circuit with a permanent magnet, an air gap, and an excitation coil.*

When $i = 0$, this equation reduces to equation (32.20).

The load line expression now contains an additional term (the last term) representing the demagnetizing field produced by the coil current. The slope $B_m/\mu_o H_m$, namely P_c, of the load line is unchanged, but its parallel position is determined by the coil excitation term Ni/ℓ_m (H_m when $B_m = 0$ in equation (32.31)) as shown in figure 32.27.

Notice that the demagnetising field, H, is dependant on the magnet length, ℓ_m. Consequently, the dimensionless B-H operating point characteristics become dimension dependant when an external demagnetising field is introduced.

The induction at the load line operating point is given

$$\boldsymbol{B_m} = B_r + \mu_m \boldsymbol{H_m} \tag{32.32}$$

Substituting the magnet demagnetising field, H_m from equation (32.31) for H_d gives

$$B_m = B_r + \mu_m \left(\frac{Ni}{\ell_m} - \frac{B_m}{S} \right) \tag{32.33}$$
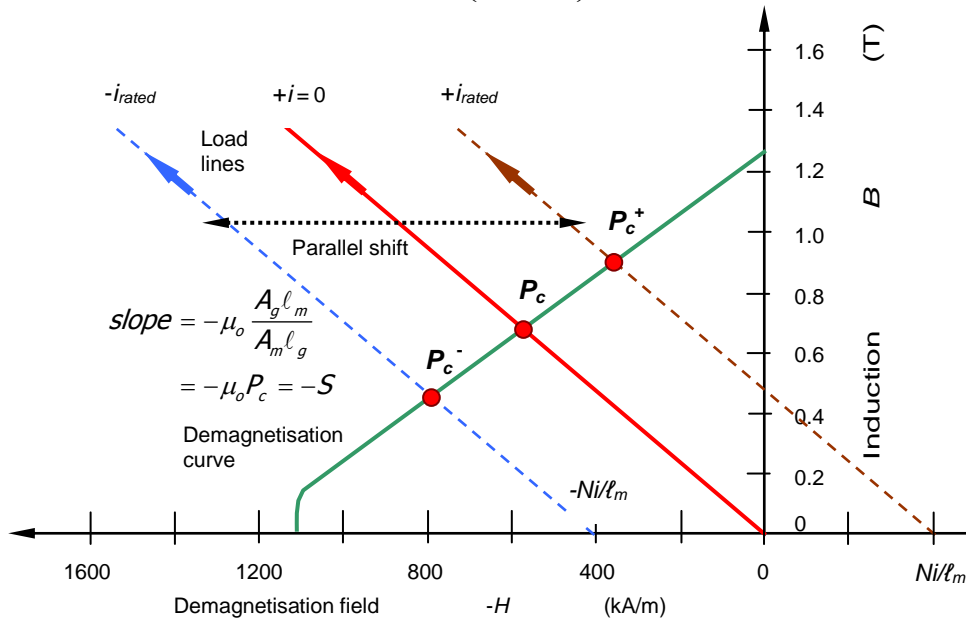

Figure 32.27. *Magnetic circuit operating point shift due to coil excitation.*

Isolating B_m and H_m gives the operating point H_d, B_d:

$$B_d = \frac{B_r + \mu_m \dfrac{Ni}{\ell_m}}{1 + \dfrac{\mu_m}{S}} = \frac{SB_r + \mu_m S \dfrac{Ni}{\ell_m}}{S + \mu_m} \tag{32.34}$$

$$H_d = -\frac{B_r + S\dfrac{Ni}{\ell_m}}{S + \mu_m} = -\frac{B_r + \mu_o P_c \dfrac{Ni}{\ell_m}}{\mu_o P_c + \mu_m} \tag{32.35}$$

Since linear models are used, by superposition, the operating point given by equations (32.34) and (32.35) reduce to:

- equations (32.29) and (32.28) when the air gap is reduced to zero such that $\ell_g = 0$ and $S \to \infty$.
- equations (32.23) and (32.22) when the current is reduced to zero such that $Ni = 0$.

Operating point based on the intrinsic demagnetization curve

Applying a magnetising field H (a demagnetizing or magnetising influence) creates a shift in the load line equal to the applied field, as shown in figure 32.27. A common unnecessary practice is to use the intrinsic magnetisation curve J as the basis for operating point analysis. The intrinsic curve related load line has a slope $P_{ci} = P_c + 1$, but the H axis intercept is not coincident with the normal load line, unless $i = 0$, as is highlighted in the characteristics in figure 32.28. But the B and J axis intercepts are coincident.

Applying an H field creates a horizontal shift of the normal and intrinsic load lines. The horizontal shift of both load lines is related not only to the external Ni, but also magnetic circuit physical dimensions. The intrinsic operating point H_{mi}, J_m is defined in terms the normal curve operating point related equations, namely equations (32.32) and (32.31), except μ_m is replace by $\mu_m - \mu_o$ in the magnet equation and P_c is replace by $P_c + 1$ for the slope in the load equation (the load line equation constant term, that is, the B axis intercept, is unchanged). That is, from the magnet equation, equation (32.32)

$$\boldsymbol{J_m} = B_r + (\mu_m - \mu_o)\boldsymbol{H_{mi}} \tag{32.36}$$

and from equation (32.31) the load line is

$$\boldsymbol{B_m} = -\mu_o P_c\left(\boldsymbol{H_m} - \frac{Ni}{\ell_m}\right) = -\mu_o P_c \boldsymbol{H_m} + \mu_o P_c \frac{Ni}{\ell_m}$$

$$\boldsymbol{J_m} \qquad\qquad = -\mu_o(P_c + 1)\boldsymbol{H_{mi}} + \mu_o P_c \frac{Ni}{\ell_m} \tag{32.37}$$

In the load line equations (32.31) and (32.37), $B_m(H_m = 0) = J_m(H_{mi} = 0) = SNi/\ell_m$. That is, both load line equations have the same flux density axis intercept, as illustrated in figure 32.28. Also, from the load line equations, the magnetising field H axis intercepts are Ni/ℓ_m and $P_c Ni/\ell_m P_{c+1}$, respectively, again shown in figure 32.28.
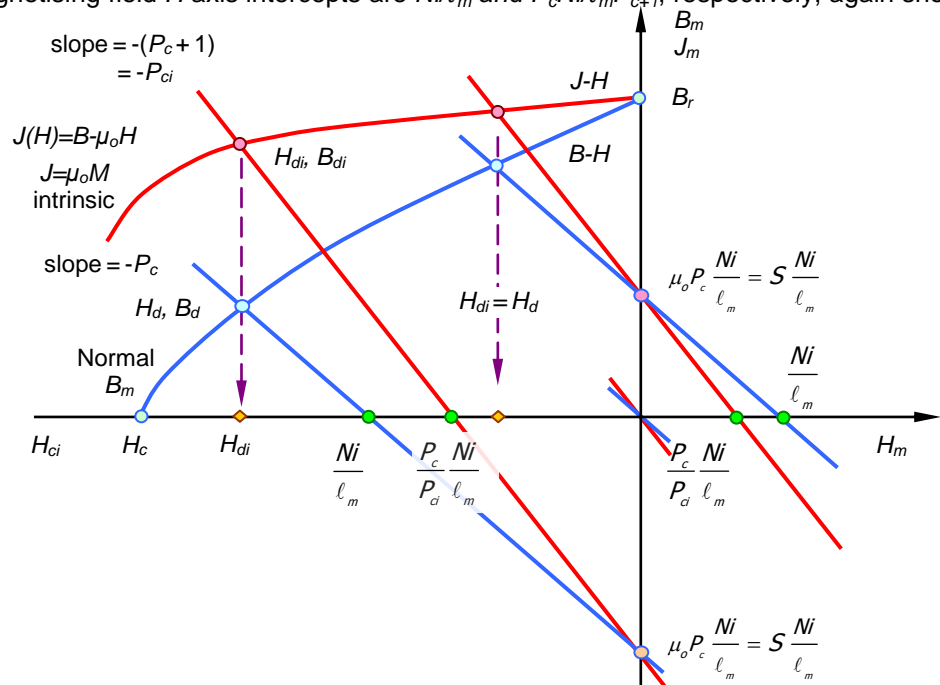

Figure 32.28. *Intrinsic demagnetisation characteristic and load lines for a magnet experiencing coil excitation Ampere turns bias.*

Solving for the operating point H_{mi}, J_m

$$J_m = B_r - \frac{\mu_m - \mu_o}{S + \mu_m}\left(S\frac{Ni}{\ell_m} + B_r\right) = \frac{(\mu_m + S)B_r - (\mu_m - \mu_o)S\dfrac{Ni}{\ell_m}}{S + \mu_m} \tag{32.38}$$

$$H_{mi} = -\frac{B_r + S \dfrac{Ni}{\ell_m}}{S + \mu_m} = H_m \qquad\qquad (32.39)$$

where, comparing equations (32.35) and (32.39), as expected $H_m = H_{mi}$, since $\boldsymbol{B_m} = \boldsymbol{J_m} + \mu_o \boldsymbol{H_m}$. This equation can be confirmed by substitution of B_m from equation (32.34) and H_m from equation (32.35), with the resulting equation for $\boldsymbol{J_m}$ being confirmed by equation (32.38).
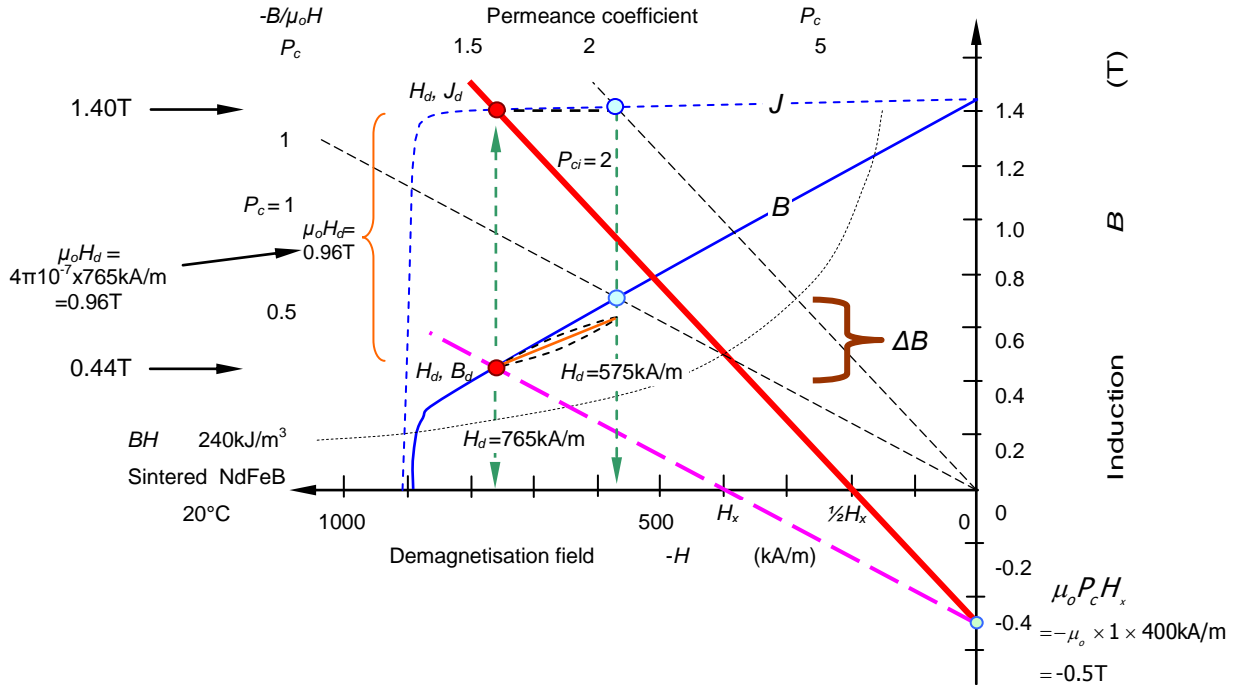

Figure 32.29. *Magnetic circuit operating point shift and flux density loss ΔB due to coil excitation (240kJ/m³ constant energy contour shown).*

Figure 32.28 shows load lines for positive and negative coil currents. The intrinsic (magnetization) curve operating point can be used to find the normal curve operating point, and vice versa, since $\boldsymbol{B_m} = \boldsymbol{J_m} + \mu_o \boldsymbol{H_m}$; where $\boldsymbol{H_m}$ is negative in the second quadrant). These load line and operating point characteristics are illustrated numerically in figure 32.29.

The commonality condition of the *J/B* axis intercept to both the normal and intrinsic related load lines is readily extracted (confirmed) using an equivalent circuit approach with $H_m\ell_m=0$, as shown in figure 32.29. Analysis is based on the fact that since the mmf is zero on the Y axis, then the two model current sources must be of equal magnitudes, with one sourcing flux - the other sinking the same flux.
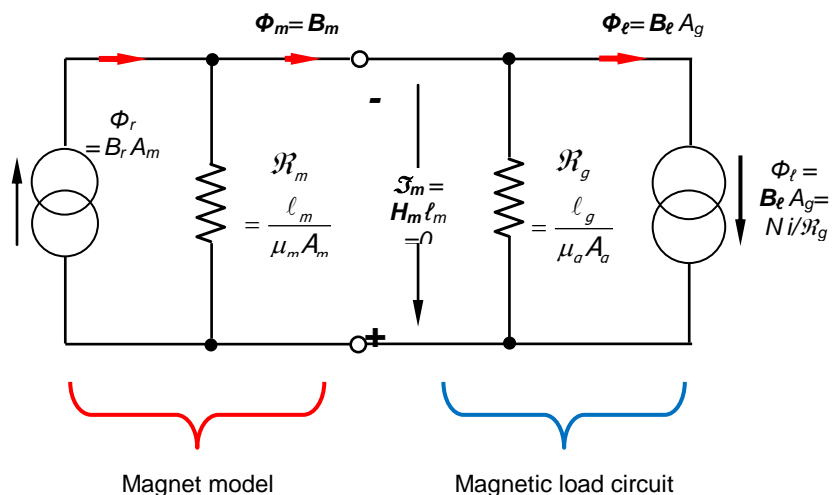

Figure 32.30. *Magnetic circuit for demagnetisation and load line characteristic of a magnet experiencing an air gap and coil excitation Ampere turns bias.*

That is, with zero net flux $\Phi_r = \Phi_m$, (the intrinsic and normal characteristics merge)

$$\text{when } H = 0 \text{ then } \phi_m = \phi_\ell \text{ thus } B_m A_m = B_\ell A_g$$

$$B_m(H = 0) = \frac{B_\ell A_g}{A_m} = \frac{Ni / \mathfrak{R}_g}{A_m} = S\frac{Ni}{\ell_g}$$

The operating point analysis approach adopted for externally applied fields H, highlights that use of the intrinsic demagnetising curve J is redundant. This is expected since J is artificially generated from the normal demagnetising curve B by adding $\mu_o H_m$. However, use of J-H does offer two features:

- All practical load line analysis can be performed in the second quadrant. Inspection of the B-H characteristics in figures 32.39 and 32.40 show that the demagnetising curves project into the third quadrant, down to $B_m = \mu_o H_m$, and figure 32.38 shows operating point analysis in the third quadrant.
- The slope of the intrinsic characteristic gives a better visual indication of recoil and thermal properties – the closer to horizontal, the better the magnet. On the other hand, visualising how close the normal characteristic slope is to μ_o is more subjective.

32.7 Generalising equivalent magnetic circuits in terms of permeances

The magnetic circuits considered thus far are simple circuits comprising a permanent magnet, a single air gap, and a coil - real magnetic circuits are generally more complex. For example, the effect of leakage flux was accounted for by the correction factor k_ℓ, but this is an important effect, which normally requires calculation using estimates of leakage gap areas and lengths. Leakage flux follows paths in parallel with the main air gap in a magnetic circuit, which complicates the calculation of the load line slope thus A_g and ℓ_g, must represent the net load experience by the magnet. While it is convenient to find the operating point of a magnet by the intersection of its load line with its demagnetization characteristic, determination of the effective load line for a complex magnetic circuit may be convoluted. Rather than resorting to a finite element CAD approach, an approach is to defining a characteristic equivalent magnetic circuit involving at most two parameters for each circuit component - its permeance and possibly an mmf source, A flux source and its permeance can be converted into an equivalent mmf source and the same permeance, and vice versa.

A magnetic circuit model represents each component in terms of its dimensions and material properties. Unity k_r and k_ℓ correction factors are assumed so the load line in equation (32.31) can be rearranged, in terms of flux $\boldsymbol{\Phi_m}$, gap permanence $P_g = \mu_o A_g / \ell_g$, and the magnets mmf $\boldsymbol{\mathfrak{F}_m} = H_m \ell_m$, as

$$\phi_m = \boldsymbol{B_m} A_m = -P_g(\boldsymbol{\mathfrak{F}_m} - N\boldsymbol{i}) \tag{32.40}$$

This linear relationship is a *load line* with a slope based on the air gap load. By defining the mmf across the gap as $\boldsymbol{\mathfrak{F}_g} = H_g \ell_g$, using the magnetic equivalent to Ohms law, the gap mmf $\boldsymbol{\mathfrak{F}_g}$ is obtained from

$$\phi_m = P_g \boldsymbol{\mathfrak{F}_g} \tag{32.41}$$

The gap permeance P_g is the slope of a flux versus mmf load line related either to the air gap or to the magnet. Hence in terms of the magnet's permeance:

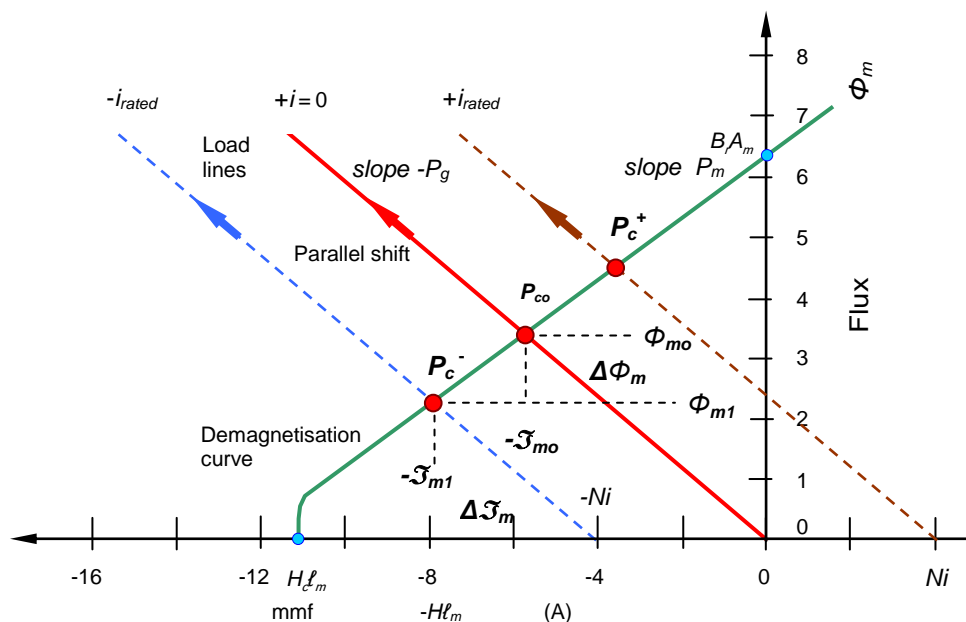$$\phi_m = P_m(\boldsymbol{\mathfrak{F}_m} + B_r \ell_m / \mu_o) \tag{32.42}$$

Figure 32.31. *Demagnetisation curve and load line for a magnet, expressed as permeances.*

Equations (32.40) and (32.42) are plotted in Figure 32.31, which is equivalent to Figure 32.27. The original demagnetization characteristic is scaled, the coercivity being multiplied by magnet length to give the equivalent mmf $H_c \ell_m$. The new load line is laterally displaced by the actual coil excitation Ni.

A coil current $-i$ moves the magnet's operating point from $-\Im_{mo}$, Φ_{mo} to $-\Im_{m1}$, Φ_{m1}, and the following relationships can be deduced from the geometry of Figure 32.31:

$$P_m = \frac{\phi_{m1} - \phi_{mo}}{\Im_{m1} - \Im_{mo}} = \frac{\Delta\phi_m}{\Delta\Im_m}$$

$$P_g = -\frac{\phi_{mo}}{\Im_{mo}} \tag{32.43}$$

$$Ni = \Im_{m1} + \phi_{m1}/P_g$$

The change in magnet flux due to coil excitation Ni can be found by rearranging the equalities in equation (32.43):

$$\Delta\phi_m = \phi_{m1} - \phi_{mo} = \frac{Ni}{P_m^{-1} + P_g^{-1}} \tag{32.44}$$

The magnetic circuit flux $\Delta\Phi_m$ can be decreased by decreasing either of the slopes P_m or P_g, which can be achieved by raising ℓ_m or ℓ_g respectively – with the advantage that additional magnet length also stabilizes temperature incurred permanent flux changes in the magnet.

In some applications, it is desired to maximise the flux change for a given excitation, which requires increasing P_m and/or P_g. This can be achieved not by reducing ℓ_m or ℓ_g, but by raising the permeability of the component materials since the magnet operates on a recoil line of slope $\mu_o\mu_{rc}$, the definition of P_m is changed to include μ_{rc}, thus equations (32.27) and (32.42) become

$$P_m = \frac{\mu_o\mu_{rc}A_m}{\ell_m} \tag{32.45}$$

$$\phi_m = P_m\left(\Im_m + \frac{B_r\ell_m}{\mu_o\mu_{rc}}\right) \tag{32.46}$$

A magnet with a *high* recoil permeability $\mu_o\mu_{rc}$, such as one of the alnico materials can be used to improve $\Delta\Phi_m$, equation (32.44). Similarly, a soft magnetic material of relative permeability μ can be considered for the *air* gap. The load line equation (32.40) is unchanged provided the gap component is defined by

$$B_g = \mu_o\mu H_g \tag{32.47}$$

$$P_g = \frac{\mu_o\mu A_g}{\ell_g} \tag{32.48}$$

These equations are more general versions of the equations for air, for which $\mu = 1$.

The alternative to plotting the two intersecting lines, is to solve equations (32.40) and (32.42) for Φ_m and $\Im_m$

$$\phi_m = \frac{Ni + B_r\ell_m/\mu_o}{\Re_m + \Re_g} \tag{32.49}$$

The load circuit may comprise a number of parallel-connected components, such as a leakage path around a main gap, and because these are in parallel with the same mmf, equation (32.41) shows that the permeance P_g used as the slope of the load line will be the sum of the parallel component permeances.

$$P_g = P_1 + P_2 + ...$$

That is, parallel connected reluctance components

$$P_g = \frac{1}{\Re_g} = \frac{1}{\Re_1} + \frac{1}{\Re_2} + ...$$

The magnetic load circuit may also comprise a number of series connected components, such as pole pieces and the main air gap, and because these experience the same flux, the net load line slope will be the sum of the series component reluctances

$$\Re_g = \Re_1 + \Re_2 + ...$$

or

$$\frac{1}{P_g} = \frac{1}{P_1} + \frac{1}{P_2} + ...   \quad P_g^{-1} = P_1^{-1} + P_2^{-1} + ..$$

Note the analogy of magnetic flux, mmf, reluctance, and permeance to electrical current, emf, resistance, and conductance, respectively. Kirchhoff's voltage and current laws are analogous to mmfs around a closed loop and fluxes at a node, both summing to zero.

The electrical equivalent approach involves reducing the magnetic load circuit to a Thevenin or Norton equivalent. With a graphical approach based on fluxes and mmfs, swept areas are energy, in Joules.

Also, magnetic flux density, *B*, magnetic induction, and magnetic field are generally interchangeable, as are magnetic field intensity, *H*, magnetic field strength, and magnetizing/demagnetising field.

32.8 Permanent magnet stability - loss of magnetism

The ability of a permanent magnet to support an external magnetic field results from small magnetic domains *locked* in position by crystal anisotropy within the magnet material. Once established by initial magnetization, these positions are maintained until acted upon by forces exceeding those that retain the domains. The energy required to disturb the magnetic field produced by a magnet varies with material type. Permanent magnets can be produced with extremely high coercive forces H_c that maintains domain alignment in the presence of high external magnetic fields. Stability is described as the repeated magnetic performance of a material under specific conditions over the magnet's operational life.

Factors affecting magnet stability include time, temperature, reluctance changes, adverse fields, radiation, shock, stress, strain, and vibration.
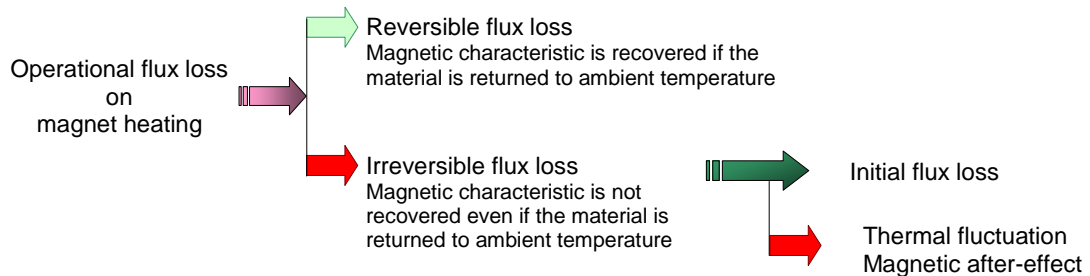

Operational flux loss on magnet heating

Reversible flux loss
Magnetic characteristic is recovered if the material is returned to ambient temperature

Irreversible flux loss
Magnetic characteristic is not recovered even if the material is returned to ambient temperature

Initial flux loss

Thermal fluctuation
Magnetic after-effect

Figure 32.32. *Types of magnetic output loss.*

There are three types of loss in magnetic output due to temperature effects:

• **Reversible**: Flux output increases or decreases as temperature or mechanical stress changes. When the temperature returns to room temperature, the original flux output is observed. That is, there is no permanent change in the flux output of the magnet. If the magnetic properties vary with temperature without causing the magnet to operate at a *B-H* point below any *knee*, then the magnet only experiences a reversible loss, since the original operating condition is restored when the temperature returns to its normal level.

It is because the temperature coefficients of B_r and H_{ci} (and H_c) are significantly different that the demagnetization curve develops a *knee* at elevated temperatures. Reversible losses cannot be eliminated by magnet stabilization and are described by the Reversible Temperature Coefficients *α* and *β*, shown in Table 32.2 and expressed as %/°C. To accommodate exposure to temperatures at which mild de-magnetization occurs, magnets can be *pre-stabilized*, that is, partially de-magnetized.

• **Irreversible, Recoverable**: With material temperature change (high or low), a critical operating parameter is reached resulting in the magnet being partially demagnetized. These losses are only recoverable to the original flux level by re-magnetization, and are not recovered when the temperature returns to its original value. These losses occur when the operating point of the magnet falls below the *knee* on the demagnetization curve. An efficient permanent magnet design should have a magnetic circuit in which the magnet operates at a permeance coefficient above the *knee* of the demagnetization curve at expected elevated temperatures. This will prevent performance variations at elevated temperatures.

• **Irreversible, Unrecoverable**: The magnet is exposed to high temperature or corrosion conditions that result in a permanent metallurgical degrading microstructural change. Table 32.2 shows critical temperatures for the various materials, where:

T_C is the Curie temperature at which the elementary magnetic moments are randomized and the material is demagnetized; and

T_{op} is the maximum practical operating temperature in air.

Different grades of each material exhibit values differing slightly from the values shown in Table 32.2. The maximum practical operating temperature is dependent on the operating point of the magnet in the magnetic circuit. The higher the operating point on the demagnetization curve, the higher the magnet allowable operating temperature.

Partially demagnetizing a loaded magnet by exposure to elevated temperatures in a controlled manner stabilizes the magnet with respect to temperature. The slight reduction in flux density improves a magnet's stability because domains with low commitment to orientation are the first to lose their orientation. A magnet thus *stabilized* will exhibit constant flux, with smaller variation between magnets, when exposed to equivalent or lower temperatures.
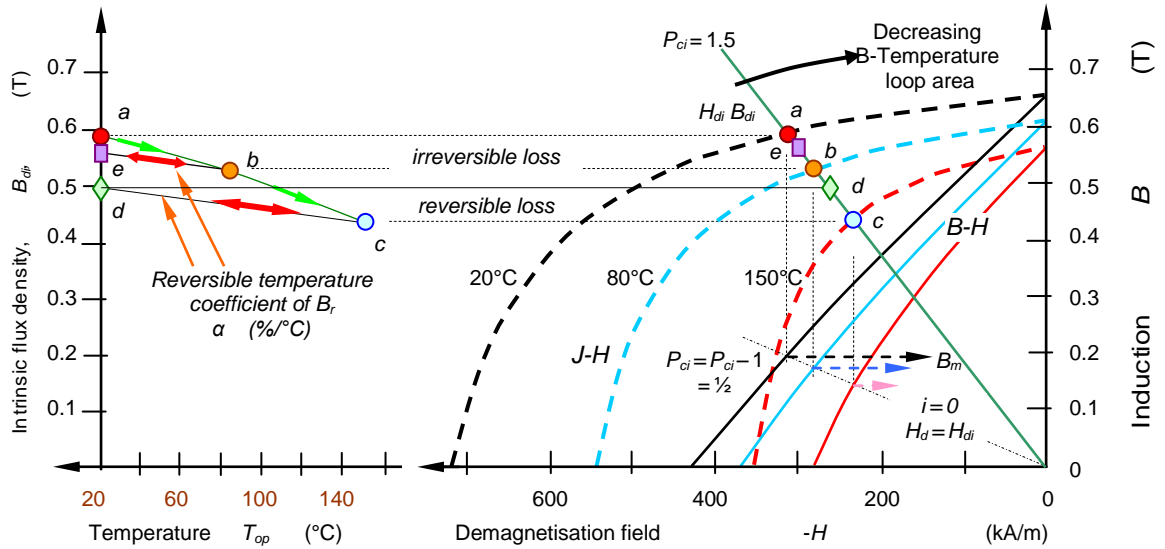

Figure 32.33. *Induction reversible and irreversible losses of a bonded magnet after a temperature increase.*

Flux losses in a magnet, due to increasing temperature, can be separated into irreversible and reversible loss components.

In figure 32.33, the reversible loss is the portion of loss at the elevated temperature which is recovered when the magnet returns to its initial temperature. The irreversible loss is the part of the flux loss at the elevated temperature that is not recovered when the magnet returns to its initial temperature. To regain the *reversible* portion of the lost flux, the magnet will have to be remagnetized. The irreversible loss in an application can be minimized by cycling the magnet above the expected operating temperature or by magnetically stabilizing (by approximately 1.5 to 2 times the expected irreversible loss).

For a given load condition, P_{ci} =1.5 in figure 32.33, the flux change is partially reversible up to 80°C, although point b represents reduced magnet energy. On cooling to 20°C from 80°C, the operating point flux density is reduced to point e. If the temperature is then increased to 150°C, the magnet operating point shifts from point e through 'b' to point c, well below the characteristic knee, and the reversible change on subsequent cooling to 20°C is to operating point d, as determined by the reversible temperature coefficient, α, independent of the load line slope. The reversible flux density is the difference between the flux at the operating points c and d. Irreversible loss is the flux density at the operating point 'a' minus the flux density at point 'd'. Continued cycling between 20°C and 150°C will incur minimal additional irreversible (recoverable) loss. The flux-density temperature-dependant loop-area in figure 32.33 decreases as the load line permeance increases.

Characteristic parameters B_r, H_c, H_{ci}, and μ_{rc} (recoil relative permeability) specify the second quadrant of the hysteresis loop.

Changes in temperature affect both flux output, which is proportional to B_r, and resistance to demagnetization, which is proportional to H_{ci}. The amount to which these change are called the *reversible temperature coefficient of induction B_r*, namely α or the *reversible temperature coefficient of coercivity H_{ci}*, namely β. These are sometimes referred to as α (alpha) or β (beta) respectively and typical values for different hard magnetic material are shown in Table 32.2. Temperature variation of maximum energy product BH_{max} and intrinsic coercivity H_{ci} are shown on figure 32.34. The changes in B_r and H_{ci} as a function of temperature are not linear. A negative value indicates a loss of B_r or H_{ci} with an increase in temperature. Note that intrinsic coercivity for ferrites increases with temperature.

Irreversible-Recoverable loss occurs when the combination of: temperature extreme, H_{ci}, reversible temperature coefficient, and applied demagnetizing field exceeds the magnet's ability to remain fully magnetized. This occurs when the magnet is at an operating point below the *knee* of the curve.

In addition to the change in B_r and H_{ci} values, the demagnetization curve undergoes a subtle temperature induced change. The recoil slope of all magnetic materials increases, to varying extents, with increased temperature. For example, the recoil slope for SmCo increases from 1.082 at room temperature by 4%, up to 1.210 at 200°C.
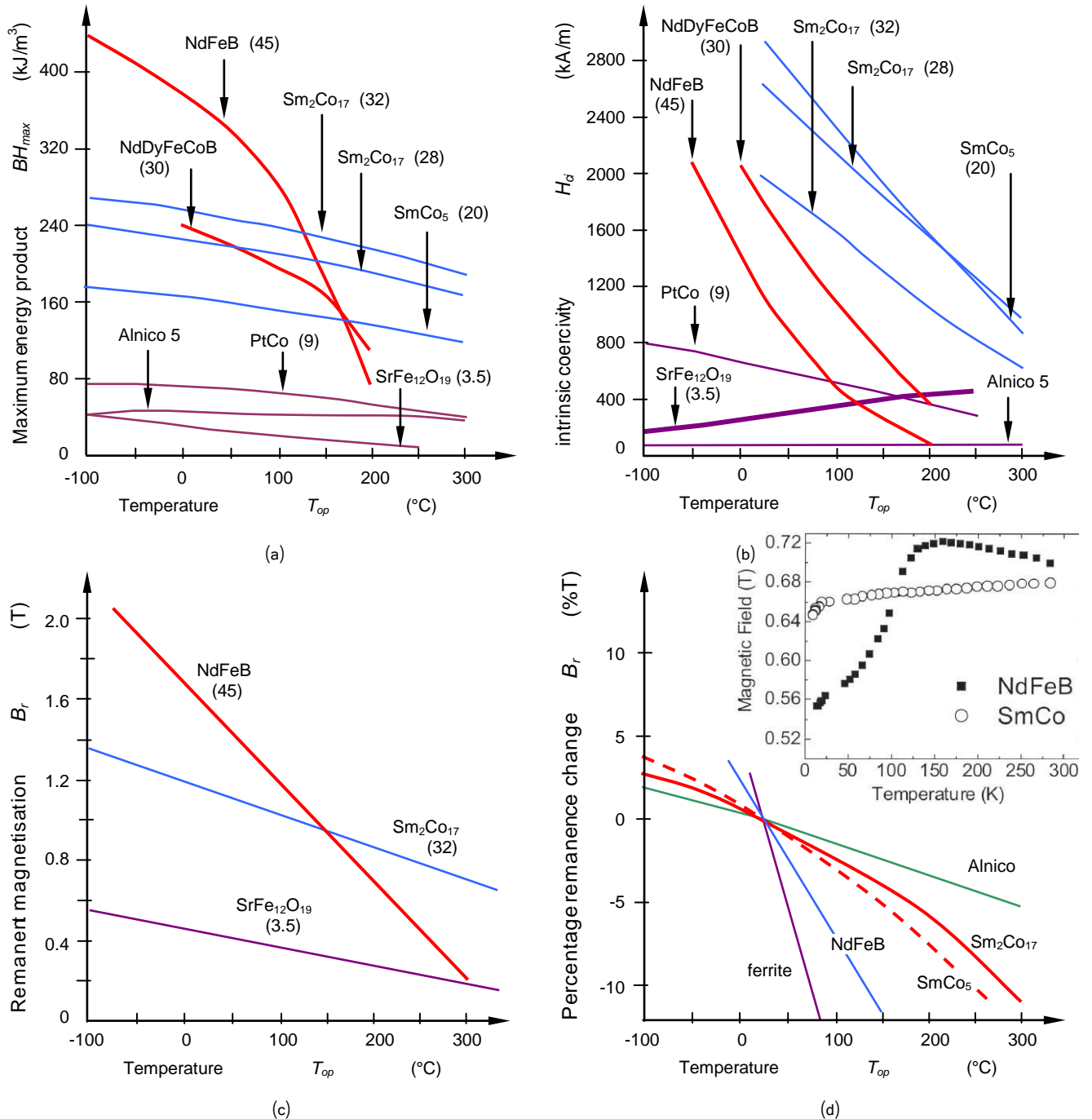
Figure 32.34. *Temperature effects on: (a) maximum energy BH_{max}, (b) intrinsic coercivity H_{ci}, (c) remanence B_r, where material room temperature maximum energy product is shown in brackets, and (d) percentage reversible changes in remanence.*

Time

The effect of time on permanent magnets is minimal. These changes, known as *magnetic creep*, occur as less stable domains are affected by fluctuations in thermal or magnetic energy, even in a thermally stable environment. This variation is reduced as the number of unstable domains decreases. Rare Earth magnets are not as likely to experience this effect because of their extremely high coercivities. Irreversible aging losses increase with increasing temperature and decreasing permeance, with the vast majority of the decrease occurring within the first year after magnetisation. Below 50°C, irreversible loss for magnets over a ten-year period is less than ½% for low permeance coefficients, ranging from virtually zero for Samarium Cobalt materials to less than 3% for Alnico 5 materials.

Radiation

SmCo materials, and especially Sm_2Co_{17}, withstand radiation up to 40 times better than NdFeB materials. SmCo exhibits significant demagnetization when irradiated with a proton beam of 10^9 to 10^{10} rads. NdFeB will lose all of it magnetization at a dose of 7×10^7 rads, and 50% at a dose of 4×10^6 rads. Magnet materials with high H_{ci} values, operated at high permeance coefficients, P_c, should be used in radiation environments, and then shielded from direct heavy particle irradiation. Similar to temperature effects, stabilization can be achieved by pre-exposure to expected radiation levels.

Shock, stress, and vibration
Rigid magnet materials are brittle in nature, and can easily be damaged or chipped by improper handling. Samarium Cobalt in particular is a fragile material. Thermal shock when ferrites and Samarium Cobalt magnets exposed to high temperature gradients can fracture within the material.

32.9   Recoil operation and associated magnetisation losses

32.9.1 Losses due to reverse magnetic fields

i. Increased reverse field – increased air gap
For dynamic systems with changing operating straight lines (for example, motors) shearing should be selected so that the permanent magnet's working point remains within the straight-line range of the demagnetization curve. The reason is to ensure stability from outside field and temperature influences, as shown in figure 32.35. The working point shifts to a larger opposing field strength, for example, from P_1 to P_2, if the air gap in a magnet system is increased. If the gap change is reversed, the original operating point P_1 can only be recovered if P_2 is within the linear section of the demagnetization curve, as in figure 32.35a. At room temperature, +20°C, the magnetic material suffers no apparent irreversible loss of its magnetization, even if continuously cycled between P_1 and P_2.
Provided the demagnetization curve is linear and M is constant, there are no irreversible losses and the operating point traverses the same characteristic *reversibly* as implied by:

$$\text{from } B_m = \mu_o \left(H_m + M \right)$$

$$\frac{dB_m}{dH_m} = \mu_o \left(1 + \frac{dM}{dH_m} \right)$$

$$M = \text{constant} \rightarrow \frac{dB_m}{dH_m} = \mu_o$$

However, as the air gap is further increased past P_2, to operating point P_3, as shown in figure 32.35b, to below the knee of the demagnetization curve, irreversible losses arise. On reducing the air gap, the working point shifts to P_4 on an inner recoil return path with a correspondingly lower flux density. The slope of this return path is referred to as permanent permeability. If the demagnetization exceeds the intrinsic coercivity $-H_{ci}$, then the reversal of M is complete. An irreversible loss has occurred, and the magnet can only be returned to its original condition if it is fully remagnetised.
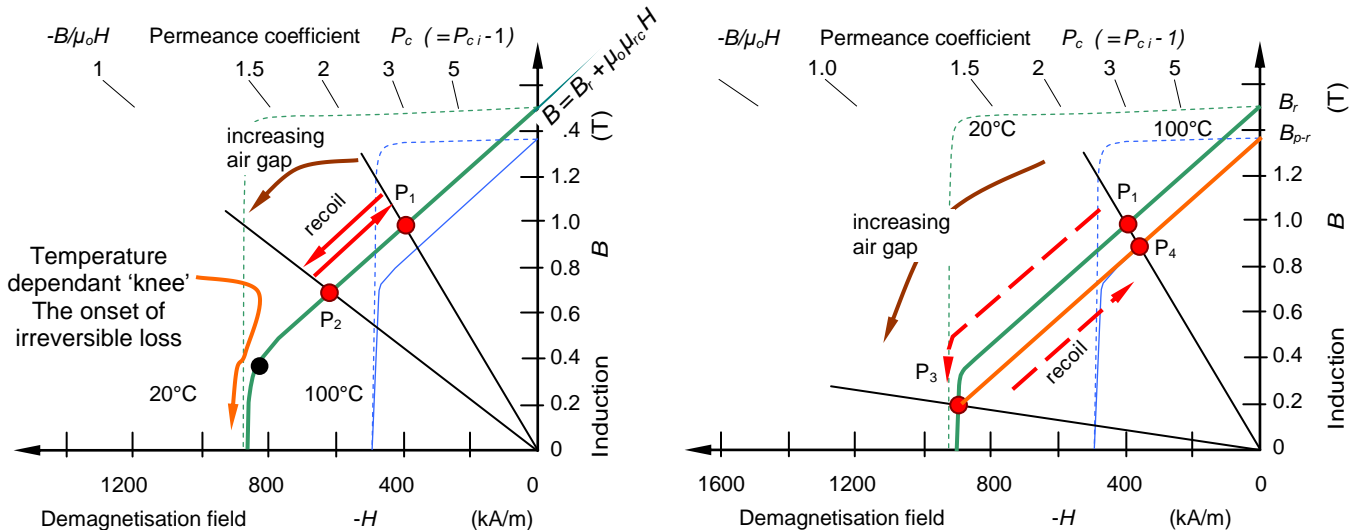
Figure 32.35. *Demagnetisation operation for varying air gap.*

Remagnetisation is not practical for a magnet installed in a magnetic circuit (a motor), but if the loss of magnetization is minimal, the device can be designed to operate within its *major* demagnetization curve at a lower flux level. In figure 32.35b, the orange line from P_3 that the operating point follows to P_4, on the original load line, is called a *recoil line*, which is actually part of a *minor* magnetization curve. The excursion of the operating point in recoil does not traverse a line, but a narrow hysteresis loop, as shown in figure 32.16, although a line of slope $\mu_o\mu_{rc}$ is assumed for calculation purposes. All recoil lines have approximately the same slope, termed *recoil relative permeability*, μ_{rc}. In many magnetic materials the slope is near constant whatever the point of origin and is approximated by the slope of the major

hysteresis loop at point $H = 0$ where $B = B_r$. If a recoil line is projected to intercept the B_m axis at a reduced 'remanence' of $B_{p-r} = \mu_o M_r$, then the equation (similar to that for the demagnetization curve) describing it is:

$$\boldsymbol{B_m} = \mu_o \left(\mu_{rc} \boldsymbol{H_m} + M_r \right)$$

A permanent magnet's uniform magnetization M produces a magnetizing force H which establishes a flux density B. For operation in recoil, it is the recoil line (rather than the demagnetization curve) and the load line which are the two characteristic equations describing the magnet in a particular magnetic circuit, their intercept giving a unique magnet operating point with a specific B_m and H_m for the magnet. In terms of the B_m versus H_m graph in figure 32.35b, the recoil line replaces the demagnetization curve.

ii. Reverse applied field - Ampere turns bias

Irreversible loss caused by the same effect as an excessive air gap, can result if an excessive demagnetizing field is applied to a magnet via current in a coil wound as shown in figure 32.26. When a coil biasing current flows, creating -400kA/m, the operating point moves from P_1 under zero current to P_2, as shown in figure 32.36a. When the current ceases the operating point recoils, without magnetisation losses to the original operating point P_1. As shown, a higher current, equivalent to -800kA/m, causes the operating point to move past P_2, around the *knee*, down to the working point P_3. On winding current cessation, recoil to point P_4 results, such that the magnet has suffered irreversible loss of its magnetisation, with the remanence flux density decreasing from B_r to B_{r-p} on figure 32.36a.

Since $H=Ni/\ell_m$, the H axis excursion of the load line is proportional to the coil's excitation i and is also inversely proportional to the magnet's length ℓ_m. Additional magnet length ℓ_m, hence additional magnet material volume, can be used to stabilize a magnet against irreversible loss in two ways:
- it raises the slope of the load line, so the magnet's operating point at any temperature or ampere turns bias, is further away from the *knee*; and
- for a given coil excitation, it reduces the rate at which the load line approaches the *knee* (with its associated loss of magnetization).

The penalty of such temperature stability mechanisms is the use of additional magnet material.

Since an irreversible loss has occurred in operating at point P_3, the magnet can only be returned to its original condition if it is fully re-magnetized. Figure 32.36b show a *J-H* curve recoil calculation.
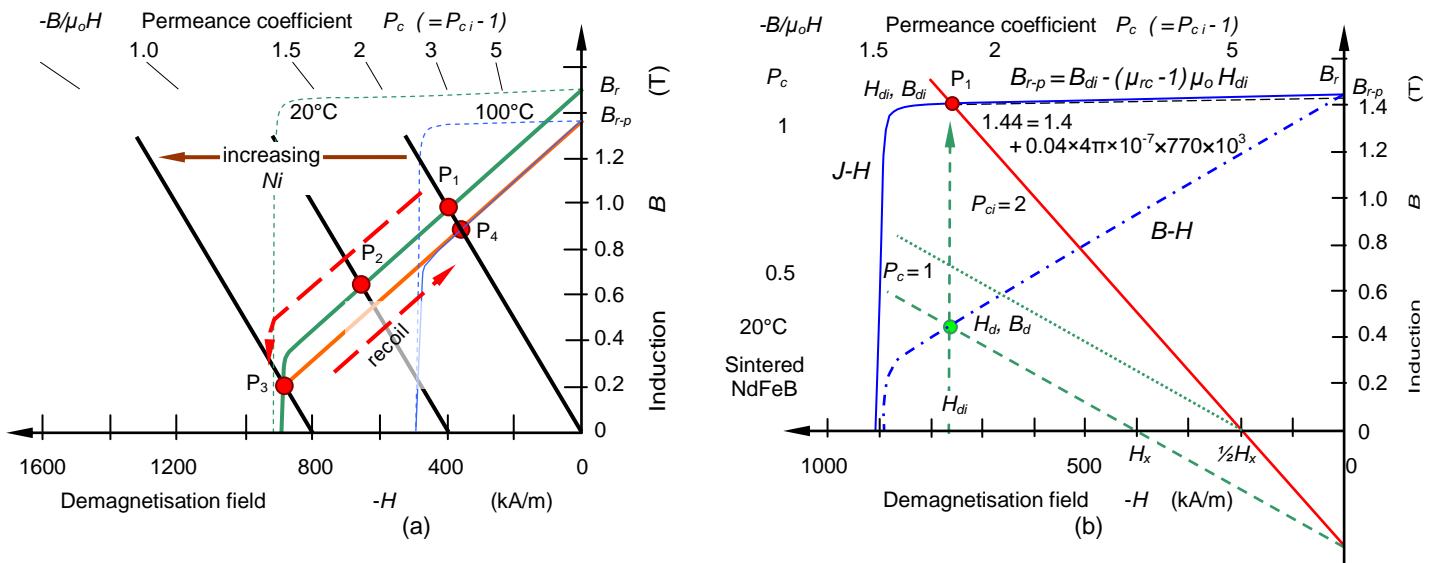

Figure 32.36. *Demagnetisation for varying Ampere turns demagnetising bias.*

32.9.2 Demagnetisation due to temperature increase

i. Increasing air gap – no external reverse field

Both induction B (and specifically remanent flux density B_r) and intrinsic coercivity H_{ci}, whence maximum energy product, are temperature (non-linear) dependant. Temperature variation of maximum energy product, remanence B_r, and intrinsic coercivity H_{ci} are shown in figure 32.34 for various hard magnetic materials. The relationships are referred to as the Reversible Temperature Coefficients, alpha α for B_r and beta, β for H_{ci}, in % change per °C, over a specified temperature range, as indicated by equations (32.3) and (32.4). Both coefficients are negative, except in the case of ferrite ($SrFe_{12}O_{19}$), where β is positive, as shown in figure 32.34b. Consequently, the demagnetization curves of permanent magnets are temperature dependent, as shown in figure 32.37. Notice that each diagonal magnet line has a bend in it, referred to as the *knee* in the curve, and the knee gets higher with increased temperature.

An increase in temperature causes the working point to shift along the load line radially towards the origin. In figure 32.37a, for a high permeance, P_{c1}, as the temperature increases the operating point progressively moves from point P_w, to P_x then to P_y and finally to P_z. Since the operating points stay within the linear region (above the *knee*) of each demagnetization curve, each reduction in flux density is reversible, that is, after cooling the flux density returns to its original value associated with operating point P_w. The magnet is operating in its safe linear region and performs as expected.
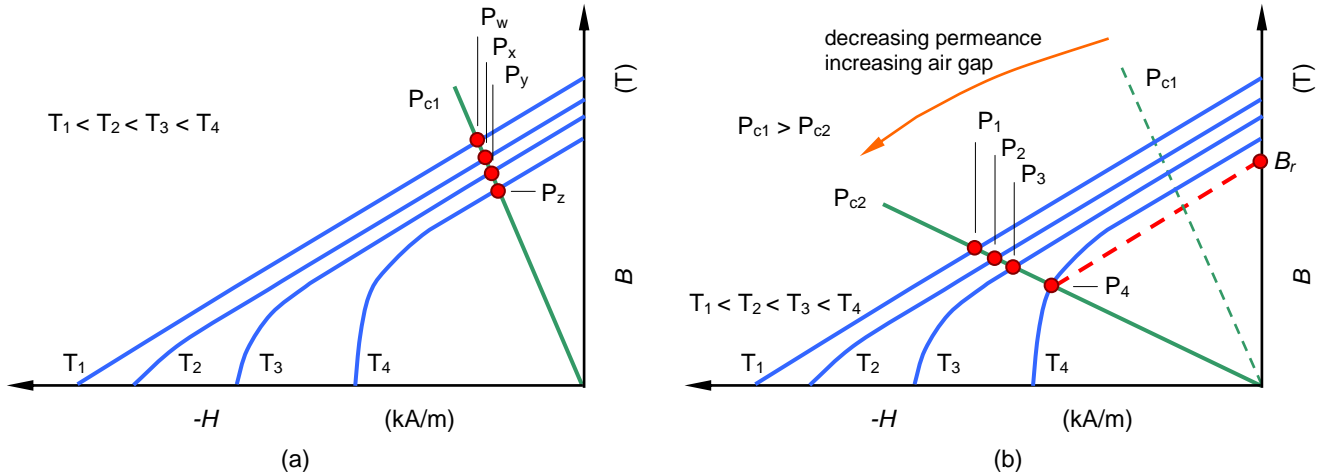

Figure 32.37. *Load line and operating point temperature dependence.*

In figure 32.37b, for the load line with decreased permeance P_{c2}, as the temperature increases the operating point moves towards the origin, from point P_1, to P_2 then to P_3 and finally to P_4. With an increased magnet temperature T_4, the operating point P_4 is below the *knee* of the demagnetization curve and the change in flux density is irreversible, that is, after cooling the flux density does not return to its original value associated with P_1. Only a portion of the magnetisation is reversible, as shown in figure 32.33. If the air gap is closed, the operating point recoils to a lower remanence flux density, B_r at T_4. As in figure 32.33, equation (32.3) can be used to estimate the remanence flux density for temperatures T_1, T_2, and T_3, based on the projected B_r for temperature T_4. With any operating point below the *knee* on the demagnetising curve, P_4, the irreversible component (demagnetisation - irreversible magnetic losses) and can only be recovered by remagnetisation. The knee flux density level increases with increasing temperature, reflecting the material's increasing vulnerability to demagnetization at higher temperatures.

To avoid irreversible changes in the flux density through temperature fluctuations, the operating point must remain within the upper linear section of the demagnetization curve over the entire temperature range in which the magnet is to operate. A permanent magnet can be completely demagnetized by heating to a temperature above the Curie temperature T_c. After cooling to the initial temperature, the initial state of magnetization can be reproduced by remagnetising, provided heating has not caused changes in the material microstructure.

ii. Reverse field – constant air gap
Consider a coil excitation that cycles the load line between zero and $H_x = -320\text{kAt/m}$, but with the magnet now operating at +150°C rather than +20°C. The diagram in figure 32.38b shows that, at higher demagnetizing fields, the operating point passes the *knee* and the magnet suffer an irreversible loss of magnetization. The operating point does return up along the major demagnetization curve, but follows a recoil path within (below) this characteristic. Since an irreversible loss has occurred, the magnet only returns to its original condition if it is fully remagnetized.

In figure 32.38a, N_o is the operating point on the *B-H* (normal) 20°C curve for the operating line $P_c = 1$ derived from the magnetic circuit and the corresponding point on the *J-H* (intrinsic) 20°C curve, with $P_{ci} = P_c + 1 = 2$, is point I_o. Both operating points have the same magnet field co-ordinate, $H_{io} = H_o$, when no external bias field is applied, that is, $i = 0$ in any coil.

When a demagnetizing field $H_x = -320\text{kAt/m}$ is applied to the magnet (via current in a coil), at 20°C, the operating point moves from I_o to the operating line $P_{ci} = 2$ at point I_1 on the *J-H* curve, equivalent to point N_1 on the *B-H* curve. The field intensities for the normal and intrinsic operating points remain the same even when $i \neq 0$. The operating points shift (virtually) back to I_o and N_o as the demagnetizing (current) field is reduced to zero, that is, $i = 0$. The projected remanence flux density decreases slightly during what is effectively a stabilisation process.
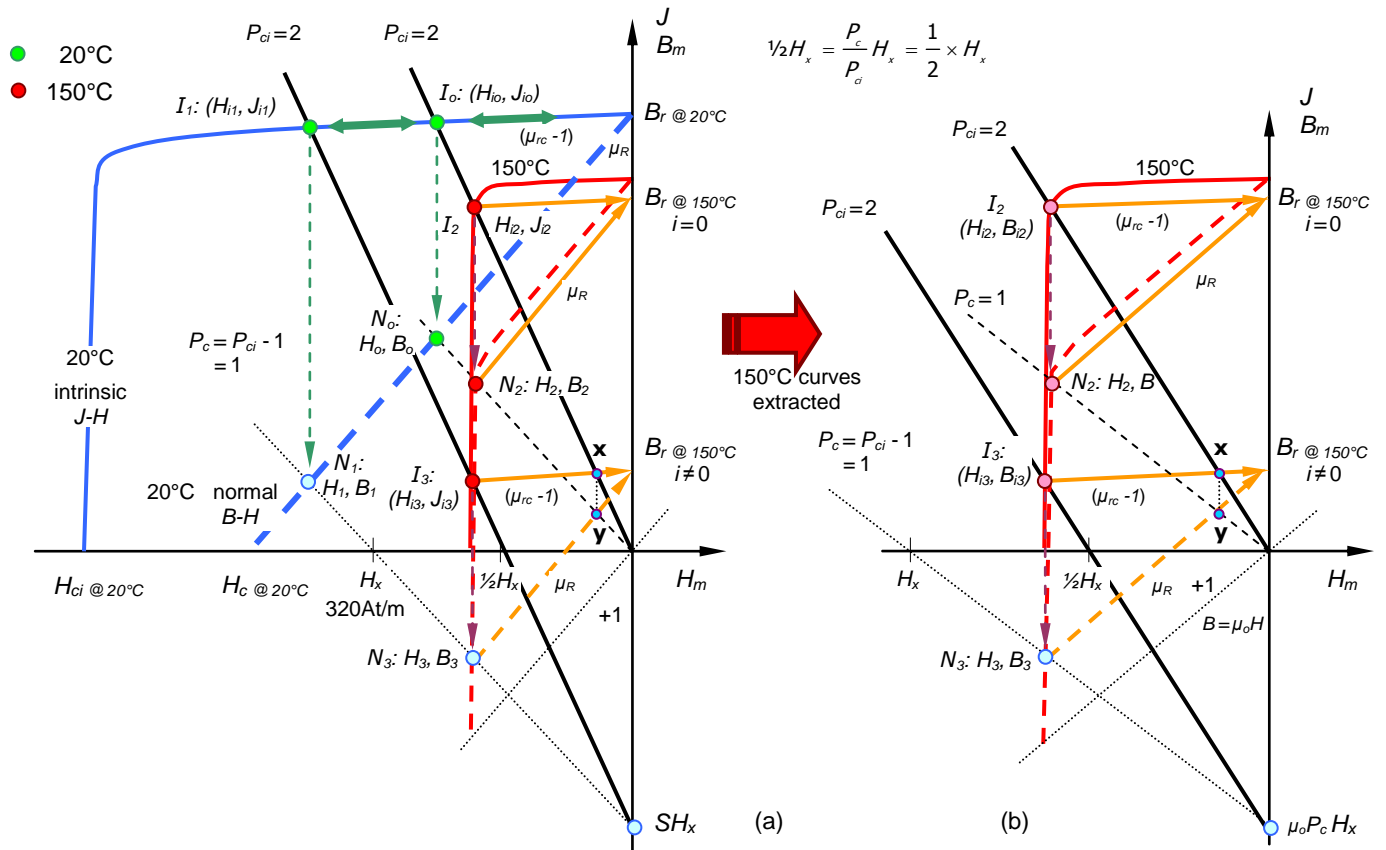
Figure 32.38. *Losses at elevated temperatures with demagnetisation in an external field at:*
(a) 20°C and 150°C with (b) 150°C operation extracted and expanded.

Figure 32.38b shows the operating point trajectories at a higher temperature, 150°C, where coil excitation causes the operating points to locate well below the knee, in fact in the third quadrant. With no field bias, $i = 0$, operation at points $I_2 : N_2$ results in a small reduction in B_r. Having applied a coil current corresponding to $H_x = -320\text{kAt/m}$, removal of the demagnetising bias field leaves the magnet with severe irreversible loss, with the operating points having reduced from $I_3 : N_3$ to x : y, respectively. When a bias field is applied, either the intrinsic or normal demagnetising curves readily illustrate the loss.

Magnet Stability: irreversible thermal losses
The variation in a magnet's remanence B_r, in figure 32.34c is approximately linear with increasing temperature and reversible up to its specific transition temperature. Once the change becomes non-linear, an irreversible loss of B_r occurs. This transition is associated with the onset of a reversal of the material's magnetization, and is represented by a *knee* in the demagnetization curve. The load line intersection with the demagnetization curve identifies the operating point (B_d, H_d) for the magnet supplying flux to a given magnetic circuit. As with the remanence, if the operating point is above the demagnetization curve *knee*, changes in the magnet's condition are reversible, but if the operating point falls below the *knee*, irreversible loss of part of B_r occurs.

The position of the *knee*, that is, the threshold for a irreversible loss component arising, depends on temperature, and as the temperature increases, the operating point may readily fall below the *knee* of the applicable demagnetization curve.

Example 32.2: *Magnet load and temperature dependant operating point*

Consider the following two magnets to be operating in a magnetic circuit with a load line as specified:

iii.   A fully dense anisotropic neodymium-iron-boron magnet with demagnetization curves as shown in figure 32.39, is temperature cycled between 20°C and 120°C. Determine the subsequent remanence flux density at 20°C and 120°C, if the load line slope is -1.5; and

iv.   A ceramic ferrite magnet with demagnetization curves as shown in figure 32.40, is temperature cycled between -60°C and 60°C. Determine the subsequent remanence flux density at -60°C and 60°C, if the load line slope is -1.

Solution

i. Sintered NdFeB

a. Reversible loss:- magnet operating temperature is cycled between $+20^{o}C$ and $+80^{o}C$.

The second quadrant demagnetization *B-H* curves in figure 32.39 develop a *knee* in the second quadrant above about $0^{o}C$, with a knee apparent for a temperature of $+20^{o}C$. The magnet's operating point at the intersection of the load line, P_{ci} = -1.5, and the $+80^{o}C$ curve is above the *knee*, so no irreversible loss occurs for temperatures up to about $85^{o}C$. This reversible change is illustrated on the right of the *B*-axis, with magnet flux cycling between point ′a′ at $20^{o}C$, to point ′b′ at $+60^{o}C$ and point ′c′ at $+80^{o}C$.

b. Irreversible loss:- magnet operating temperature is cycled between $+20^{o}C$ and $+120^{o}C$.

The magnet begins again at $20^{o}C$, point ′a′, is heated first to $+60^{o}C$, point ′b′, then to $+80^{o}C$, point ′c′, and then up to $+100^{o}C$ - point ′d′. However, the intersection of the load line and the $+100^{o}C$ demagnetisation curve is now below the *knee*, and an irreversible loss of magnet flux occurs (starting just above $+80^{o}C$). When the magnet is cooled to $20^{o}C$, the magnet's operating point on the load line, point ′d*′, is no longer on the $20^{o}C$ demagnetization curve, but at some point within the major *B-H* curve in the second quadrant. If rather than cooling from $100^{o}C$, the magnet is heated to $120^{o}C$, the operating point moves to point ′e′. Now when the magnet is cooled to $20^{o}C$, operating point ′e*′ results. The magnet is no longer fully magnetised, having suffered irreversible loss. Operation up to 120C is stabilised but it must be re-magnetized to saturate the material's magnetization once again, and to regain operation on the major *B-H* curve.

In summary:

  ′a′ to ′b′ to ′c′ is a linear change and is reversible, as described in part a.

  ′c′ to ′d′ then to ′e′ are non-linear changes and represent partial irreversible loss.

  ′e′ to ′e*′ is a linear change and is reversible, but with reduced magnetic properties.

  ′e*′ to ′a′ illustrates restoration of full magnetic properties after re-magnetizing the magnet.

The recoil lines in figure 32.39 from ′e′ and ′e*′ predict remanence fluxes of 0.87T and 1.06T at $+120^{o}C$ and $+20^{o}C$, respectively. The magnet is now temperature stabilised for operation up to $120^{o}C$.

As the load line slope is increased, given the shape of these demagnetization curves, the transition temperature to an irreversible loss also progressively increases. A greater load line slope raises the flux produced by the magnet to the magnetic circuit and helps to stabilize the magnet against irreversible loss thermal effects.
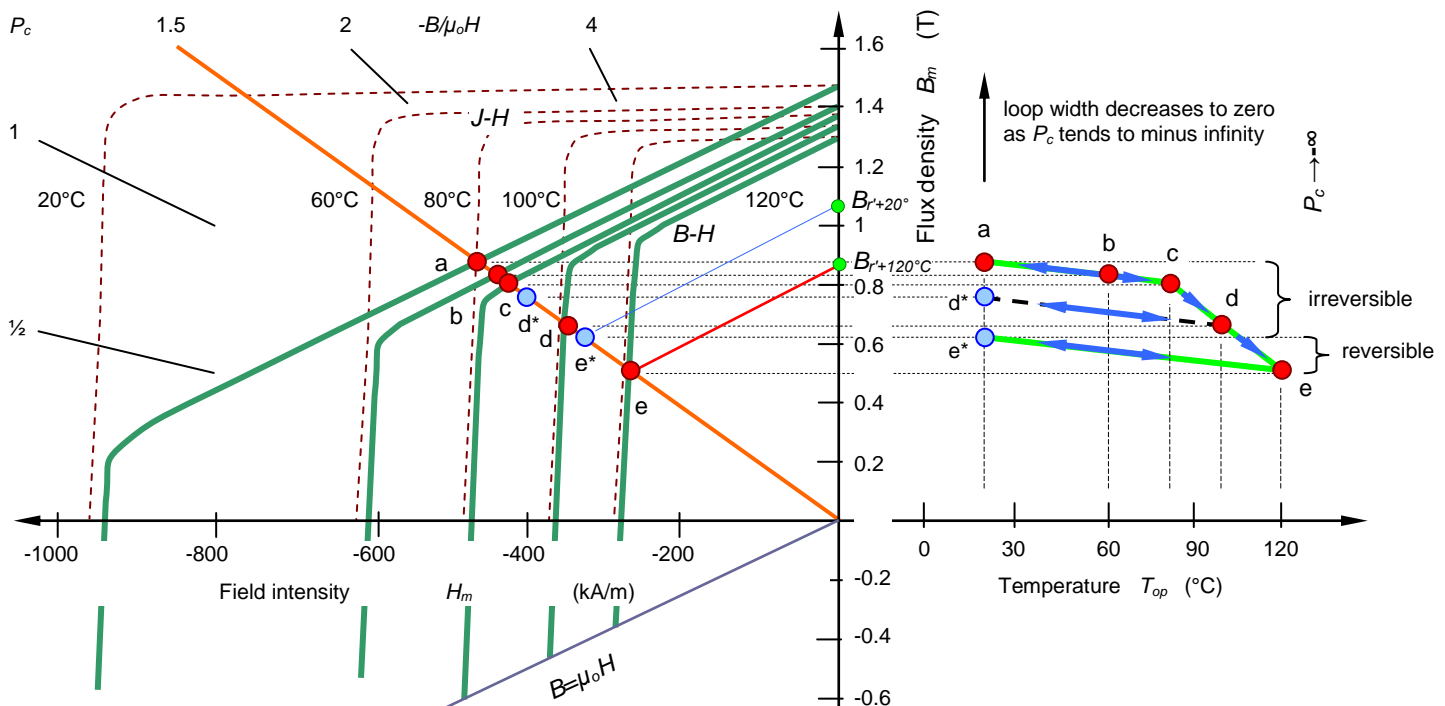

Figure 32.39. *Interpretation of irreversible and reversible temperature losses for a NdFeB magnet.*

ii. Ferrite

When considering the change in coercivity, H_{ci} decreases with temperature both for samarium-cobalt and for neodymium-iron-boron magnets; H_{ci} increases with temperature in the case of ceramic ferrites (being based only on magneto-crystalline anisotropy). This means that the *knee* of the demagnetization curve can arise as the temperature *falls*. The magnet is cycled from $+20^{o}C$ to $-60^{o}C$ and back again. Figure 32.40 illustrates that, with a load line slope of -1, the transition to an irreversible loss occurs when the temperature falls below about $-20^{o}C$.
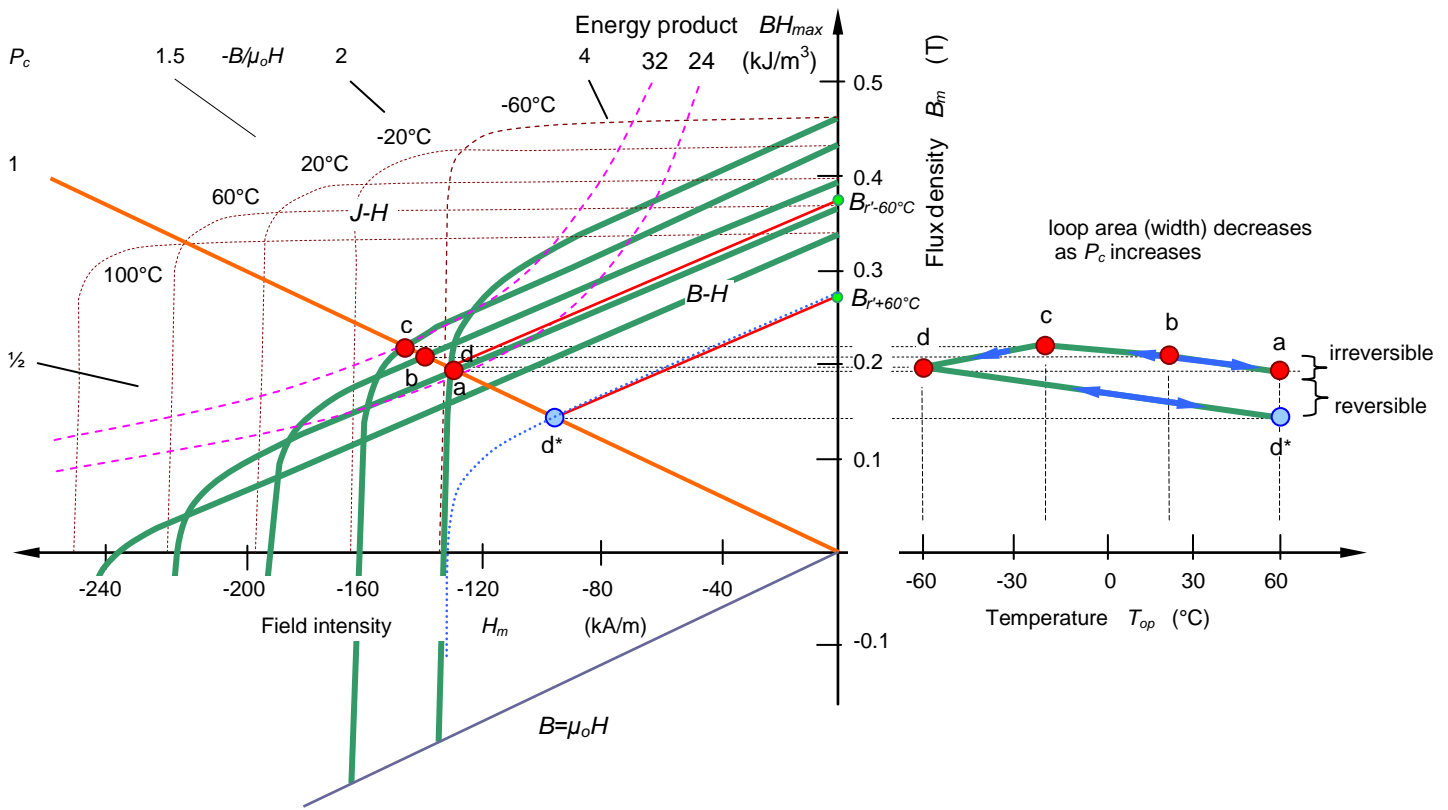
Figure 32.40. *Interpretation of irreversible and reversible temperature losses for a ferrite magnet.*

The sequence of thermal events is:
  a to b to c is a *linear* reversible change between +60°C and -20°C.
  c to d is a *non-linear* irreversible change from -20°C down to -60°C.
  c to d to d* is a *linear* reversible change from -60°C back to +60°C, but with reduced magnetism.

The recoil lines in figure 32.40 from 'd' and 'd*' predict remanence fluxes of 0.38T (reduced from 0.46T) and 0.275T (reduced from 0.37T) at -60°C and +60°C, respectively.

♣

If operation of a magnet over its working temperature range is predicted to introduce unacceptable irreversible loss, then the magnet application should be reassessed to increase the load line slope and stabilize its operation without degrading the properties.

32.10 Energy transfer

One or more air gaps introduced into a magnetic circuit enable useful work to be performed. The mechanical energy used to separate a magnet from soft iron, there-in creating an air gap, is stored as potential energy within that air gap and the magnet. This moves the point of operation on the intrinsic curve in the second quadrant. The normal curve in the second quadrant represents the energy output of the magnet and is used during magnet design. If the iron in the circuit is completely removed, the air gap becomes large and the operating point of the curve approaches H_c (the normal coercivity) in the second quadrant and the induction B approaches zero.

If the air gap is closed again, the stored potential energy is used to perform the work of bringing the magnet and the iron together. However, the operating point does not return to B_r. The magnet recoils along a so-called minor hysteresis loop to a point below B_r, figure 32.16c.
Repeated opening and closing of the air gap will result in the magnet cycling along this minor hysteresis loop. The average slope of the minor loop is the recoil permeability, $\mu_o\mu_{rc}$.

Section 32.6 presented the method for determining a magnet's operating point (B_m, H_m), with which is associated stored energy, that may be instrumental in the conversion of electrical and mechanical work. In figure 32.41, the energy stored in volume V_m of a magnet, leading to the change in energy is:

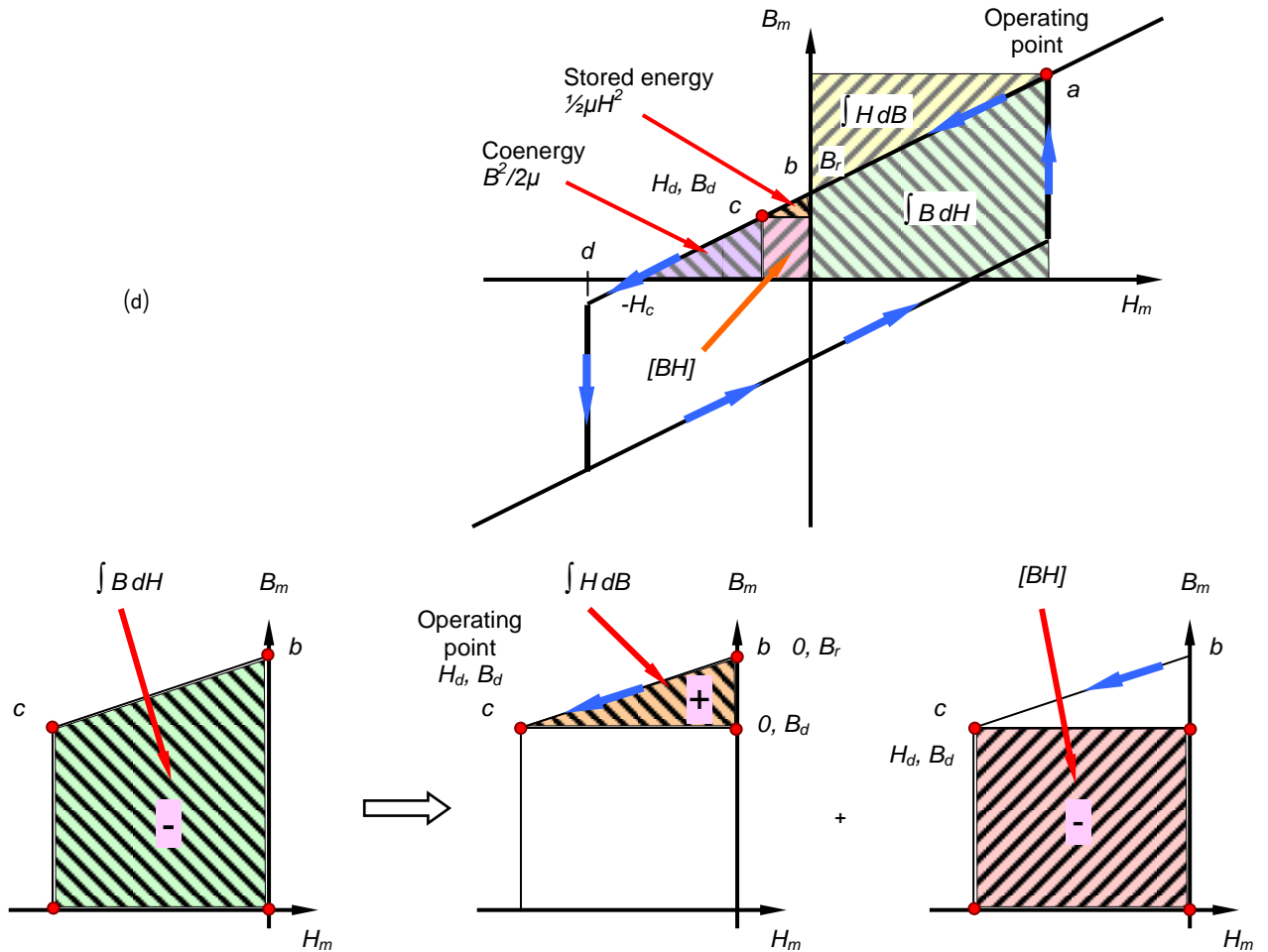$$-\int_a^b BdH - \int_a^b HdB = -\left[BH\right]_a^b \tag{32.50}$$

Figure 32.41. *Graphical demagnetisation change per unit volume: (a) applied field energy, (b) magnet kinetic energy, (c) total potential energy, and energy changes around the B-H loop.*

The first term is the work done (energy) by the applied field, the second is the internal kinetic energy stored, and the sum equals the total potential energy per unit magnet material volume.

After being magnetized to saturation, point a, the potential energy is reduced to zero at remanence $(H_m = 0$ at point b); the magnet conditions must move into the second quadrant to deliver its stored energy. Figure 32.41 shows how the three energy density components of equation (32.50) develop as the magnet moves from point *b* to point c. Considering the direction of integration, the three areas sum according to equation (32.50), namely, the work done as a result of the applied field $\int BdH$ equalling the change in potential energy [*BH*] plus the release of kinetic energy from the magnet $\int HdB$. The higher the potential energy of a permanent magnet, the greater the release of its kinetic energy in establishing an external field. While magnet developments have focussed on improving the available (potential) energy density, it also requires a corresponding increase in the work to change the operating condition of the material. Consequently, the basis of most devices using high-energy magnets is a design that keeps the magnet close to a unique operating point with a minimum of dynamic operation.

The kinetic energy released by a magnet of volume V_m, which is operating at a typical point c, (H_d, B_d), in figure 32.41, is

$$W = V_m \int H\, dB \quad \left(= \int F\, d\ell \right) \tag{32.51}$$

This triangular area in figure 32.41b, the kinetic energy being released by the magnet, is the magnetic energy stored in the magnet reluctance, equivalent to $w = \tfrac{1}{2}LI^2$. For a given operating point, (H_d, B_d), this energy can be derived from the Thevenin or Norton equivalent circuits, specifically the magnetic energy in the magnet reluctance:

$$w = \tfrac{1}{2}\phi_m^2 \Re_m = \tfrac{1}{2}\Im_r^2 / \Re_m$$

Energy being delivered, is readily derived from the Norton equivalent circuit in figure 32.17c, where

$$w = \tfrac{1}{2}\phi_m^2 \Re_m = \tfrac{1}{2}\left(B_m A_m\right)^2 \frac{\ell_m}{\mu_m A_m} = \tfrac{1}{2}\frac{B_m^2}{\mu_m} A_m \ell_m = \tfrac{1}{2}B_m H_m \times volume$$

This energy is only released if work is done, that is, power is released or absorbed. Mechanically this could be an air gap change or electrically a voltage developed across a current carrying coil. Note coil current alone is insufficient, the voltage component can only be produced by a changing flux, from $v = N \times d\Phi/dt$, which implies a magnet operating point flux change, $d\Phi$.

Energy delivered to an air gap

The following equation may be applied to the field in any volume, even an air gap V_g, where $B_g = \mu_o H_g$, that is:

$$
\begin{aligned}
W_g &= V_g \int \frac{B_g}{\mu_o} dB \\
&= \tfrac{1}{2} \frac{B_g^2}{\mu_o} V_g = \tfrac{1}{2} B_g H_g V_g = \tfrac{1}{2} \mu_o H_g^2 V_g
\end{aligned}
\tag{32.52}
$$

If this is the air gap in the magnetic circuit of figure 32.21, then equations (32.18) and (32.19) may be used in equation (32.52) to show that all the energy released from the magnet is delivered into the gap:

$$
W_g = \tfrac{1}{2} B_g H_g V_g = -\tfrac{1}{2} B_m H_m V_m
\tag{32.53}
$$

Note the energy density delivered to the gap is half the magnet's energy product. The work done by the externally applied field in establishing the air gap energy has two components as shown in figure 32.42a. The first component is the pu volume energy released into the air gap, equation (32.53), the second is the pu volume energy associated with establishing the operating point, namely the energy associated with increasing the air gap from zero at point b to length ℓ_g at point c.

Once the magnet operates on a recoil line of relative permeability u_R and recoil remanence B_r, this equation is modified by $B_m = \mu_o \mu_{rc} H_m + B_r$ to

$$
W_g = \tfrac{1}{2} B_m H_m V_g = \tfrac{1}{2} \left(-\mu_o \mu_{rc} H_m - B_r \right) H_m V_g = \tfrac{1}{2} \left(-\mu_o \mu_{rc} H_m^2 - B_r H_m \right) V_g
\tag{32.54}
$$

The further down its demagnetization curve a magnet is driven, the greater the area swept by the load line, by which the applied field within the magnet does more work. This energy is recaptured by the magnet if the gap is re-closed and the load line returns to its original position. However, if this cycle includes driving the magnet beyond a *knee* in its characteristic, a return to the original load line along a recoil line involves the irreversible loss of magnet field energy, as shown in figure 32.42. Large dynamic excursions of a high-energy magnet can be restricted by increasing ℓ_g during magnet installation. Subsequent cycling along the recoil line incurs no further irreversible loss, only reversible energy changes.

While BH_{max} is the most common figure of merit for a permanent magnet, operation at this point maximizes the release of magnet energy into the gap, namely $-\tfrac{1}{2} V_m BH_{max}$. If the magnetization M is constant and the linear demagnetization characteristic is represented by $B_m = \mu_o (H_m + M)$, then the air gap energy, equation (32.53), may be written as

$$
W_g = -\tfrac{1}{2} \mu_o V_m \left(H_m^2 + M H_m \right)
\tag{32.55}
$$

Differentiating, BH_{max} occurs at $B_m = \tfrac{1}{2} \mu_o M$, $-H_m = \tfrac{1}{2} M$, for which

$$
W_g^{max} = \tfrac{1}{2} \mu_o V_m \left(\tfrac{1}{2} M \right)^2 \approx \tfrac{1}{2} \mu_o V_m \left(\tfrac{1}{2} B_r \right)^2
$$

The magnet energy released is lower either side of the BH_{max} point on the major demagnetization characteristic, and by virtue of a reduced alignment of the magnetization M, W_g is also smaller for operation on recoil lines within the major B versus H curve. The superimposed constant energy contours on the characteristic in figure 32.42 illustrate the energy penalty of non-optimal operation. Convention is to express these as constant energy product $B_m H_m$ (as also seen in figures 32.8, 32.11, and 32.15, amongst others), rather than the actual energy density $\tfrac{1}{2} BH_{max}$.

A more realistic representation of the soft iron pole pieces requires the inclusion of the flux leakage coefficient k_ℓ and mmf loss factor k_r via equations (32.19) and (32.18) within equation (32.52). Both loss factors reduce the amount of magnet energy delivered in to the gap

$$
W_g = \tfrac{1}{2} B_g H_g V_g = -\tfrac{1}{2} \frac{B_m H_m}{k_\ell k_r} V_m
$$

By adding a coil of N turns with current i, as in figure 32.26, and using equation (32.30), the air gap energy becomes

$$
W_g = -\tfrac{1}{2} \frac{V_m B_m}{k_\ell k_r} \left(H_m - \frac{Ni}{\ell_m} \right)
$$

The last term represents the energy contribution from the coil. Since the flux in the circuit is $\Phi = B_m A_m$, and the total flux linkage with the coil is defined as $\lambda = N\Phi$, the gap energy can be written as:

$$
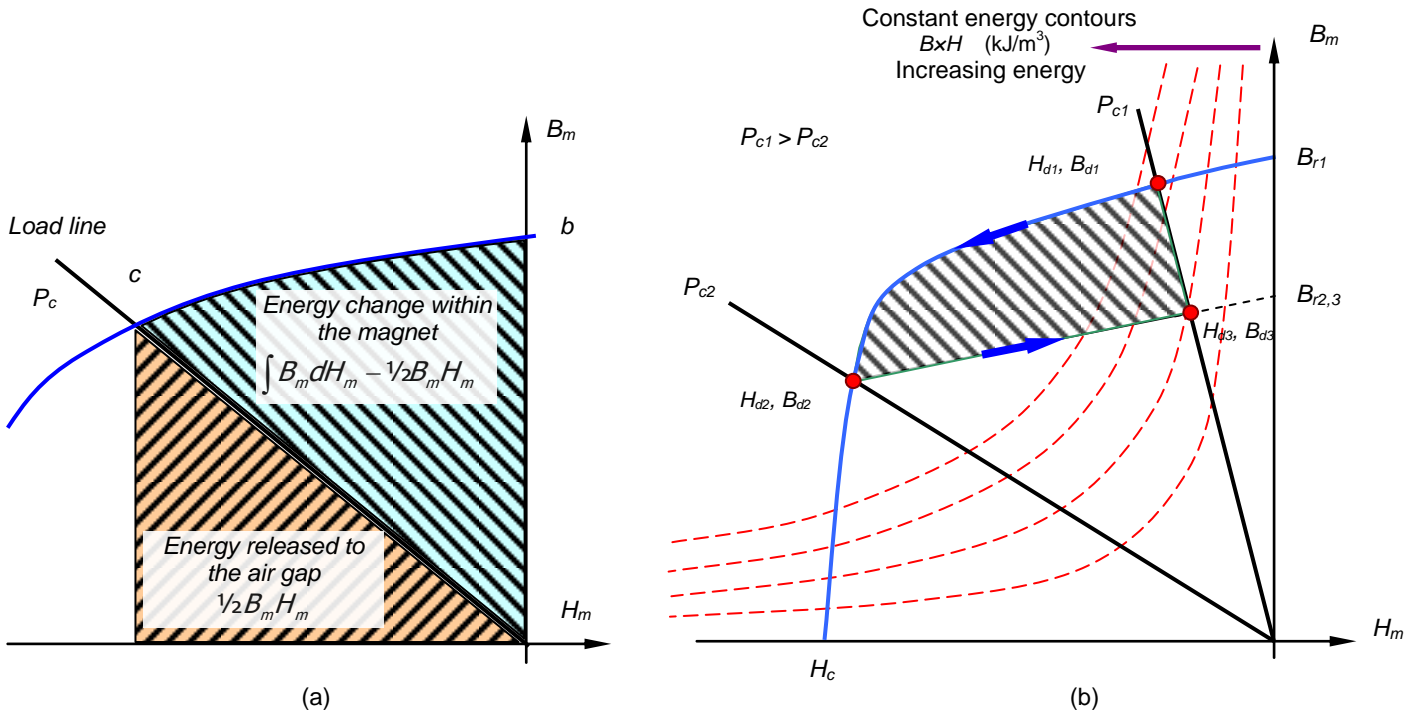W_g = \tfrac{1}{2} \frac{1}{k_\ell k_r} \left(-V_m B_m H_m + \lambda i \right)
$$

Figure 32.42. *Per unit volume change:*
(a) of the magnet's applied field energy and (b) magnetic field energy with load line slope.

Coenergy

Coenergy can be considered a dual of stored energy that is often used to compute forces on electromechanical systems with permanent magnets and current-carrying coils. Force and torque can be deduced by changes in energy with respect to position, but the process is complicated by the need to compute the energy that is sunk or sourced by the supplies driving the coils over the change in position. Conversely, computing the change in coenergy for constant currents directly yields the mechanical work done on the system.

An expedient lower bounds for coenergy computation, for the integral is $H_o = -H_c$. The coenergy density in the magnet w_m' is, for the case in which the flux density is aligned with the magnetization:

$$w_m' = \int_{-H_c}^{H} B(H)\,dH = B_r H + \tfrac{1}{2}\mu H^2 \Big|_{-H_c}^{H} = \tfrac{1}{2}\mu\left(H + H_c\right)^2$$

The definition of magnet flux density B from equation (32.11) yields a simpler definition of coenergy within the magnet:

$$w_m' = \frac{B^2}{2\mu}$$

Stored energy and coenergy can be shown as regions associated to the demagnetization curve as shown in figure 32.43.
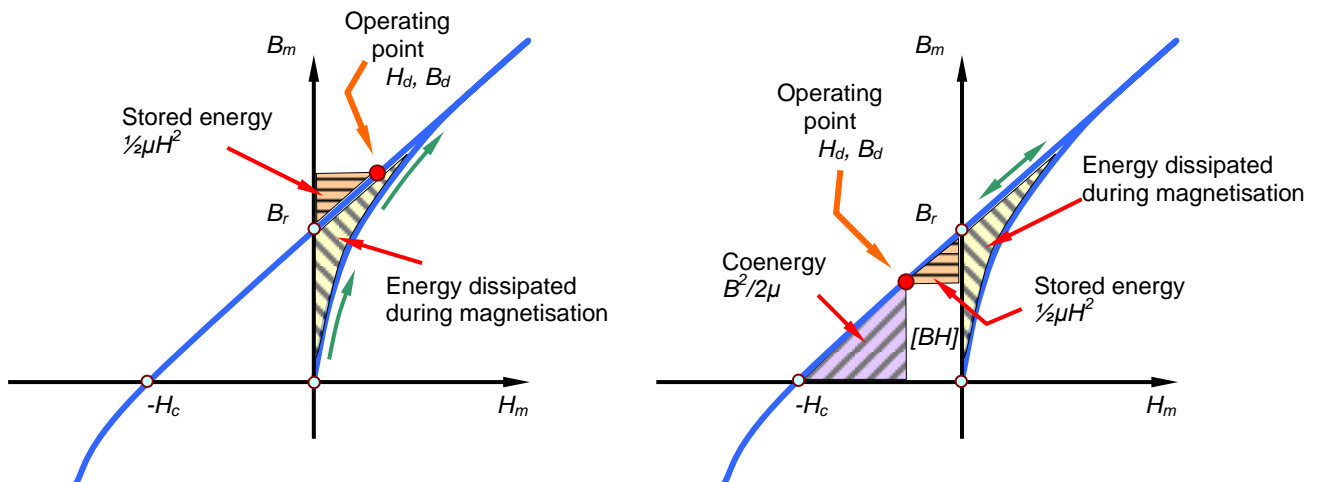

Figure 32.43. *Graphical representation of permanent magnetic energy components:*
(a) with applied bias $+H_d$ to enable operation in the first quadrant and
(b) demagnetisation quadrant operation energy components.

As shown, the area swept in the first quadrant represents the energy per unit volume (the integral of *H(B) dB*) that was needed to magnetize the material. This energy can never be recovered, even if a large field intensity is applied to the magnet to push its operating point back into the first quadrant, as indicated in both parts of Figure 32.43. Remagnetisation only stores energy ($\frac{1}{2}\mu H^2$) in the magnet without possibility of extracting the energy associated with the magnet's magnetisation.

32.11   Force of attraction within an air gap

The equation *F = -dW/dx* can be used to calculate the force of attraction between two pole faces bounding the air gap of figure 32.21 (figure 32.44) of area A_g and length ℓ_g. The energy in this gap is given by equation (32.52), which, with $B_g = \mu_o H_g$, becomes

$$W_g = \frac{1}{2}\frac{B_g^2}{\mu_o}V_g = \frac{1}{2}\frac{B_g^2}{\mu_o}A_g\ell_g \qquad (32.56)$$

Using Cartesian axes in the air gap, with flux along the gap length ℓ_g being in the x-direction, force is calculated by differentiating equation (32.56) with respect to ℓ_g, which yields

$$F_x = -\frac{dW_g}{d\ell_g} = -\frac{1}{2}\frac{A_g B_g^2}{\mu_o} = -\frac{1}{2}\frac{\phi^2}{\mu_o A_g} \qquad (32.57)$$

The definition of -F_x acting into the air gap confirms this as a force of attraction, which will increase as the gap closes. Although ℓ_g, is not a parameter in equation (32.57), F_x is proportional to Φ^2, where a flux increase results from decreasing ℓ_g, which causes an increase in load line slope as the magnet's operating point moves up its demagnetization characteristic. Similarly, there are forces acting to retard the lateral displacement of one pole piece with respect to the other (F_y, F_x), which may also be determined from equation (32.56) by splitting A_g into its *y* and *z* components and differentiating with respect to the appropriate axis.
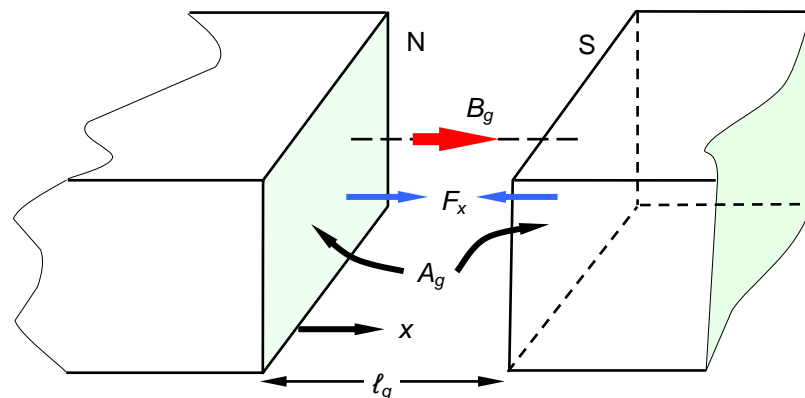
Figure 32.44. *Force of attraction between opposite pole faces bordering a uniform air gap.*

27.12   Appendix: Magnet processing and properties

Permanent magnet manufacturing Process

Sintered / fully dense, anisotropic magnets - maximum output: (Rare Earths, Ceramics, and Alnicos)
- Maximum energy product for magnet size and weight
- Restricted to simple geometries
- Brittle thus requires careful handling
- No dilution effect due to non-magnetic phase

Injection moulded - shape flexibility: (Rare Earths and Ceramics)
- Complex geometries
- Tight geometric tolerancing without finishing operations
- Relatively robust, resistant to chippage
- Insert and over moulding to reduce assembly costs
- Variety of pole configurations are possible
- Multistep and multi-component moulding to produce assemblies
- Dilution of magnetic phase produces lower energy product
- Anisotropic and isotropic powders offer a wide range of magnetic alignment and output options
- Relatively high tooling costs make them suited to high volume manufacturing

Compression bonded - low cost manufacturing: (Rare Earths and Ceramics)
- Higher loading than injection moulded, but lower than fully dense creates a compromise in energy product
- Limited to simple geometries: rectangles, cylinders, arcs – thin walled cylindrical shape possible
- Tight geometric tolerancing except in pressed thickness
- Brittle thus requires careful handling
- Isotropic powder allows complex magnetizing patterns

Casting: (Alnico)

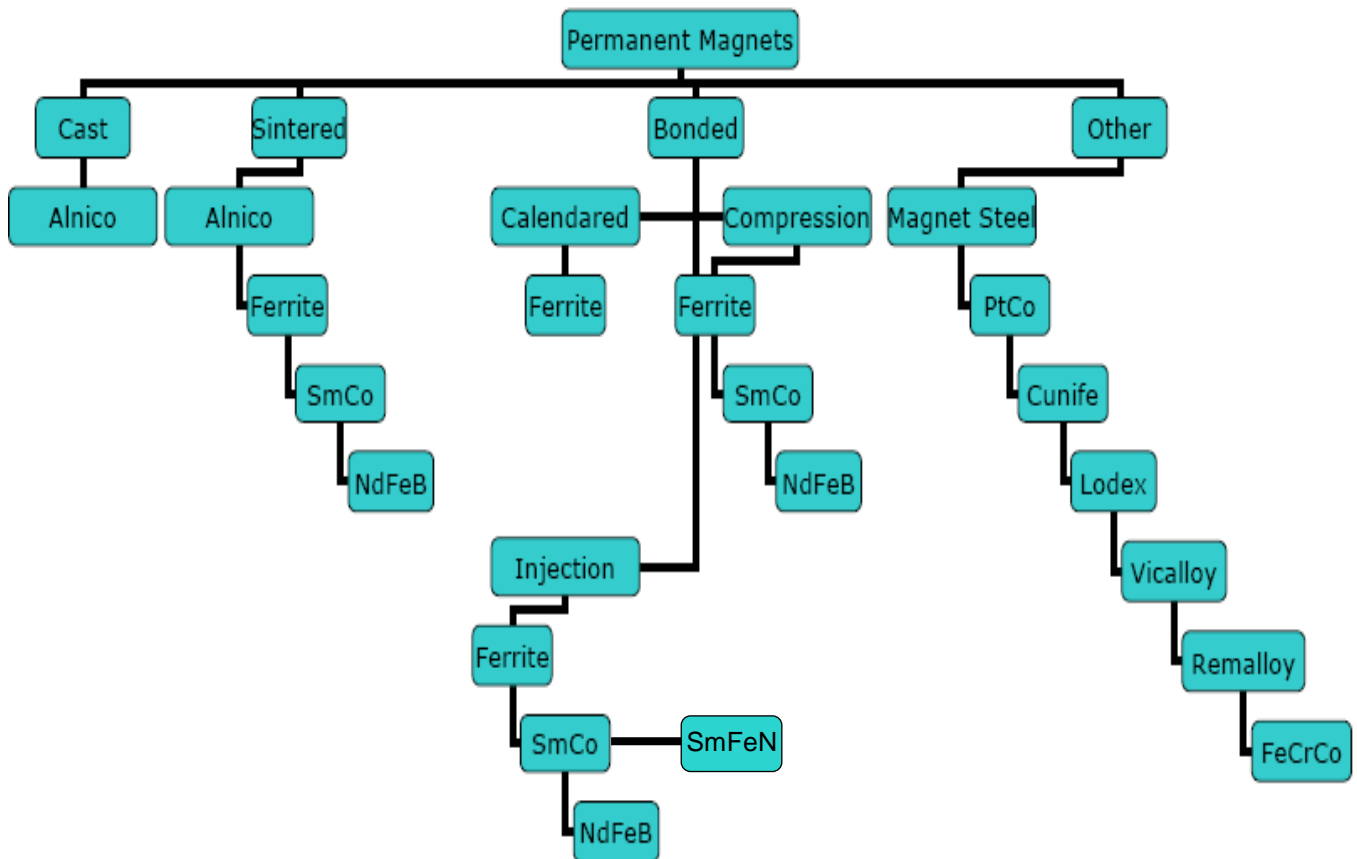Extruded: (Bonded NdFeB and Flexible)

Calendering: (Flexible)

Table 32.6. Physical and mechanical properties of AlNiCo, FeCrCo, FeCoVCr, SmCo, NdFeB, and hard ferrite

Material and production method			Physical properties				Mechanical properties			
Material	isotropic or anisotropic	Production method	Coefficient of thermal expansion	Thermal conductivity	Resistivity	Density	Tensile strength	Compressive strength	Young's modulus	Hardness
			10^{-6}/K	W/m.K	μΩ×m	g/cc	MPa	MPa	MPa	HV
AlNiCo	i or a	casting or sintering	11	10 - 15	0.45 - 0.55		80 - 300	300 - 400	100 - 200	300 - 400
FeCrCo	i or a		10	10 - 13	0.7 - 0.8		1200 - 1400 600 - 700			300 - 350 400 - 500
FeCoVCr	a	casting	11.5		0.55 - 0.65		2000 - 5000 2500 - 3500			
$SmCo_5$	a	sintering	//6 ⊥13	10 -13	0.5 - 0.6	8.2	30 -40	900 - 1000	100 - 150	500 - 600
Sm_2Co_{17}	a		//8 ⊥11	10 -13	0.75 - 0.85	8.4	40 - 50	800 - 900	150 - 200	600 - 700
NdFeB	a		//3.4 ⊥-5	8 - 10	1.4 - 1.6	7.4	80 - 90	1000 - 1100	150 - 200	500 - 600
hard ferrite	i or a		9, 12, 11	4	> 10^4	4.9	50 - 60	600 - 700	15 - 200	500 - 600

NdFeB: Temperature Coefficient of resistivity 2×10^{-4} /K, specific heat capacity 0.12 kg.K, Poisson's ratio 0.24

Magnet Material

Neodymium-Iron-Boron - high energy
- Relatively abundant resource with large proven reserves
- Refining costs are moderate
- Manufacturing technology is established
- Highest energy product output of all commercially available PM materials
- High temperature, > 150ºC, applications require a compromise in energy product
- Tendency to corrode requires protective coating, chips, cracks, and brittle
- PrFeB variant for temperatures between a few degrees Kelvin and 135K

Samarium Cobalt - stable
- Relatively abundant resource with large proven reserves
- Manufacturing technology is established; dominated by 2-17 grades
- Second to NdFeB in magnetic output – high energy product and coercive force
- Excellent high temperature performance with grades available for use to 550ºC
- Corrosion resistance superior to NdFeB, but coatings generally advisable
- Brittle, chips, cracks easily, and hard to machine
- Refining costs are higher than for NdFeB

Ferrite (Ceramic) - low cost
- Abundant, low cost raw material
- Magnets are lowest cost option
- Manufacturing technology is well-established
- Lower magnetic output than the rare earth materials, but high coercive force
- Excellent high temperature performance with grades available for use to 250ºC
- Limited low temperature performance, generally to -40ºC
- Corrosion resistance is outstanding, but brittle and chips easily

Alnico – stable properties
- High corrosion resistance
- High mechanical strength, tough but brittle
- High temperature stability
- High cost
- Low coercive force and energy product

32.13 Appendix: Magnetic basics

$$B = \mu_o H$$
B = magnetic flux density or magnetic induction, Vs/m^2, 1 Tesla
μ_o = magnetic permeability of a vacuum = $4\pi \times 10^{-7}$ Vs/Am
H = magnetic field strength, A/m

If a material is present, the relation between magnetic field strength and magnetic flux density becomes
$$B = \mu_o \mu_r H$$
B can be split into the flux density in the vacuum plus the material part according to
$$B = \mu_o H + J$$
$$J = \mu_o M$$
This gives
$$B = \mu_o (H+M)$$
The definition of B yields
$$M = (\mu_r - 1)H = \chi_{mag} H$$

with $\chi_{mag} = (\mu_r - 1)$ = magnetic susceptibility. With superconductors (= ideal diamagnets), $\chi_{SC} = -1$.

32.14 Appendix: Magnetic properties for sintered NdFeB and SmCo magnets

Neodymium magnets are graded by the material they are made of. The higher the grade (the BH_{max}, following the 'N' in Table 32.3), the stronger the magnet.

Table 32.7 can be used to determine whether it is better to use sintered Neodymium Iron Boron or sintered Samarium Cobalt in a particular application.

Table 32.7. Typical magnetic properties for NdFeB and SmCo

	Neodymium Iron Boron (NdFeB)	Samarium Cobalt (SmCo)
High temperature applications	Higher H_{ci} materials can be used up to 200°C, moderate H_{ci} materials used up to 150°C. Low H_{ci} materials limited to 100°C	SmCo can be used at substantially higher temperatures than NdFeB. Continuous operation at temperatures above 250°C Also significantly better at temperatures below 100K
Loss of flux density at elevated temperatures	Loses 0.11% of B_r/°C. See NdFeB temperature effects on B_r & H_{ci}	Loses about 0.03% of B_r/°C
General environmental conditions	Neodymium Iron Boron is highly reactive to environmental conditions, while Samarium Cobalt magnets are very corrosion resistant.	
Humid environments	Surface treatment advisable, due to oxidation Options are nickel, IVD or polymer coatings.	Surface treatment is not required. Does not oxidize.
Hydrogen rich atmosphere	Not recommended, hydrogenation occurs, causing the magnet material to disintegrate	No known adverse effects
Cost of part	Lower cost generally	Higher cost than NdFeB because of Co content
Radiation environment	Damaged by radiation, mainly gamma rays	Higher grades are stable to radiation
Mechanical strength	Mechanically strong, not as brittle as SmCo	Brittle. Both alloys require diamond tooling, EDM, or abrasive grinding when machining.
Clean room environments	Surface treatment recommended	Surface treatment not required
Vacuum applications	Needs to be coated, with nickel or IVD recommended (metallic - do not outgas). Polymer coatings can be used, but not in an ultra high vacuum or high temperatures in a vacuum, due to outgassing.	Surface treatment is not required. However, fairly porous; parts may outgas for a limited duration before high vacuums can be achieved
High field requirements	Higher fields achievable, higher energy products (up to 440kJ/m^3)	Highest energy product is 240kJ/m^3, difficult to obtain higher.
Cryogenic temperatures	Only special formulation grades	Operates well in cryogenic temperatures.
Aerospace applications	Gaining use in aerospace applications, optionally with surface treatments. Used in aircrafts, missiles, and satellites.	Established in aerospace, military, and defence applications.
Salt, open seas, and salt spray environments	Surface treatment essential, limited life	Stable in this environment
Acid and alkaline environments	Surface treatment is necessary, limited life	Stable in this environment, however, qualification tests recommended
Thin walled, thin cross-section applications (a dimension below 1mm)	Mechanically stable, parts as thin as $\frac{1}{5}$mm	Poor in thin cross-sections. Under ½mm is not recommended
Single piece large parts	Better than SmCo, larger blocks can be sintered	Larger blocks (over 75mm in any dimension) are challenging
Nickel plating as per military specifications	Not available – proprietary plating to specifications, only electrolytic nickel	Electroless and electrolytic nickel plating
Plating as per military specifications	Not available. Plating as per proprietary specifications.	Not typically used.
Radial ring (for true radially oriented field)	Possible.	Not available
Sensitivity of flux density, B_r, and coercivity, H_c, to temperature changes	Temperature coefficient of B_r ranges from, negative, 0.11%/°C to 0.13%/°C. Higher coercivity materials (>160kA/m) are closer to negative, 0.11%/°C Temperature coefficient of H_c ranges from, negative, ½%/°C to ¾%/°C. The higher the intrinsic coercivity, the lower the temperature coefficient of H_c	Temperature coefficient of B_r ranges from negative, 0.03%/°C to 0.04%/°C. Series Sm_2Co_{17} less sensitive to temperature changes (about negative 0.03%/°C) than $SmCo_5$ (about negative 0.04%/°C) Temperature coefficient of H_c ranges from negative, 0.15%/°C to ¼%/°C. Series Sm_2Co_{17} less sensitive to temperature changes (about negative 0.15) than $SmCo_5$ (about negative ¼)

Based on Table 32.7, in summary, do *NOT* use Neodymium Iron Boron magnets under the following conditions:

- In an acidic, alkaline, or organic solvent (unless the magnet is hermetically sealed)
- In water or oil (unless hermetically sealed, or a limited life results)
- In an electrically conductive liquid, such as electrolyte containing water
- In a hydrogen-containing atmosphere, especially at elevated temperatures. Hydrogenation, a process where the H_2 molecule reacts with the NdFeB, causing rapidly deteriorate
- Environments containing corrosive gasses, such as $C\ell_2$, NH_3, $N0_X$, etc.
- In the path of radioactive rays

32.15   Appendix: Magnetic axioms

1. Flux lines, like electrical currents, follow the path of least resistance. In magnetic terms, this means that flux lines will follow the path of greatest permeance (lowest reluctance). Flux lines will always follow the shortest path through any medium. They therefore can only travel in straight lines or curved paths, and they can never take true right-angle turns.
2. Flux lines repel each other, hence never cross, if their direction of flow is the same.
3. For unsaturated ferromagnetic materials, flux lines will always leave and enter at right angles.
4. All ferromagnetic materials have a limited ability to carry flux. When saturated, they behave as though they do not exist (like air, aluminium and so on). Below the level of saturation, a ferromagnetic material will substantially contain the flux lines passing through it. As saturation is approached, because of axioms one [1] and two [2], the flux lines may travel as readily through the air as through the material (which appear like air when saturated).
5. Flux lines will always travel from the nearest north pole to the nearest south pole in a path that forms a closed loop. They need not travel to their own opposite pole; although they ultimately do if poles of another magnet are closer and/or there is a path of lower reluctance (greater permeance) between them.
6. Magnetic poles are not unit poles. In a magnetic circuit, any two points equidistant from the neutral axis function as poles, so that flux will flow between them (assuring that they meet the other conditions stated above).

Table 32.8. The relationship between magnetic parameters in cgs and SI units.

Quantity	symbol	Gaussian	Gaussian (cgs units)	S.I.	S.I. Units	Conversion factor (cgs to S.I.)
Magnetic Induction	B	gauss	G		Tesla, T	$1G = 10^{-4}$ T
Applied Field strength	H	Oersted	Oe		Am^{-1}	$10^{-3} / 4\pi$
Magnetisation	M		emu cm^{-3}		Am^{-1}	10^3
Magnetisation	$4\pi M$		G		-	-
Magnetic Polarisation	J		-		T	-
Specific Magnetisation	s		emu g^{-1}		JT^{-1} kg^{-1}	1
Induction in free space		$B = H$	G	$B = \mu_o H$	T	$1G = 10^{-4}$ T
Induction in medium		$B=H+4\pi M$	G	$B = B_o + \mu_o M$	$B = \mu_o (H + M)$	$1G = 10^{-4}$ T
Permeability of free space	μ_o	unity	Dimensionless	$4\pi \, 10^{-7}$	H m^{-1}	$4\pi . 10^{-7}$
Relative Permeability	μ_r		-		Dimensionless	-
Susceptibility	χ		emu cm^{-3} Oe^{-1}		Dimensionless	4π
Maximum Energy Product	BH_{max}		M G Oe		kJ m^{-3}	1 MGOe $=10^2 / 4\pi$
G = Gauss, Oe = Oersted, T = Tesla						

Reading list

http://www.magnets.bham.ac.uk/magnetic_materials/
http://www.mceproducts.com/
http://www.dextermag.com/Permanent-Magnet-Materials.aspx
http://www.arnoldmagnetics.com/
http://www.intemag.com/magnet_materials.html
http://www.magnetweb.com/
http://www.femm.info/wiki/PMEnergy

Quadrant-II Demagnetizing Normal Operation; Quadrant-I Magnetizing; Normal (B, H) (Total, Measurable); Air Flux $B = \mu_0 H$; Intrinsic (B_i, H_i); B_r; Intrinsic Flux B_i; Normal Flux $B = B_i + \mu_0 H$; H_{ci}; H_c; Recoil Line; $\mu_{rm} = \dfrac{\Delta B}{\Delta H}$; Recoil Point; Quadrant-III Magnetizing; Quadrant-IV Demagnetizing Normal Operation